AFWL-TR-65-175

AFWL-TR
65-175

LABORATORY TESTING AND THEORETICAL STUDIES IN TRANSIENT RADIATION EFFECTS ON MICROELECTRONICS

W. W. Grannemann, et al.

University of New Mexico
Bureau of Engineering Research
Albuquerque, New Mexico

Contract AF 29(601)-6637

TECHNICAL REPORT NO. AFWL-TR-65-175

May 1966

AIR FORCE WEAPONS LABORATORY
Research and Technology Division
Air Force Systems Command
Kirtland Air Force Base
New Mexico

DISCLAIMER NOTICE

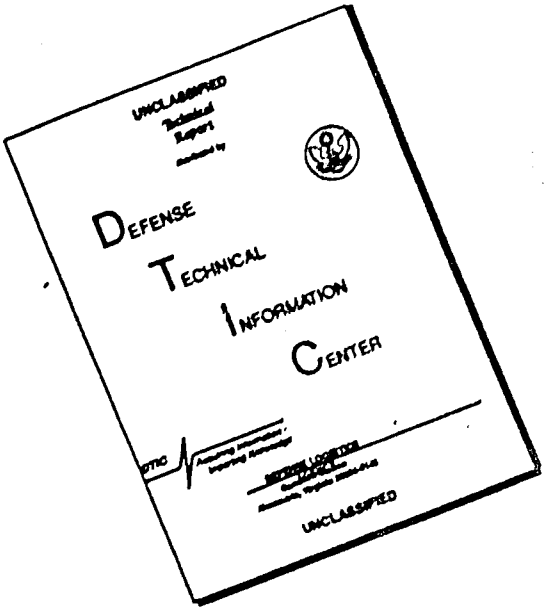

THIS DOCUMENT IS BEST QUALITY AVAILABLE. THE COPY FURNISHED TO DTIC CONTAINED A SIGNIFICANT NUMBER OF PAGES WHICH DO NOT REPRODUCE LEGIBLY.

AFWL-TR-65-175

LABORATORY TESTING AND THEORETICAL STUDIES IN TRANSIENT RADIATION EFFECTS ON MICROELECTRONICS

W. W. Grannemann, et al.

University of New Mexico
Bureau of Engineering Research
Albuquerque, New Mexico
Contract AF29(601)-6637

TECHNICAL REPORT NO. AFWL-TR-65-175

FOREWORD

This report was prepared by the University of New Mexico Bureau of Engineering Research, Albuquerque, New Mexico, under Contract AF29(601)-6637. The research was performed under Program Element 7.60.06.01.D, Project 5710, Subtask 16.015, and was funded by the Defense Atomic Support Agency (DASA).

Inclusive dates of research were 1 September 1964 to 31 July 1965. The report was submitted 14 January 1966 by the AFWL Project Officer, Lieutenant John L. Mullis, (WLRE).

This report covers approximately the second half of the project. The first half was covered in a report entitled, "Directional Effects of Transient Radiation on Semiconductor Devices," by W. W. Grannemann, Goebel Davis, Jr., and Arthur C. Golubiewski (AFWL-TR-65-69). In addition, the results of radiation testing of the Westinghouse WS-106 and Philco PL-903 integrated circuits were presented in an informal report to Lt John L. Mullis dated 30 June 1965.

The principal investigator on the contract was Dr. W. W. Grannemann. Other investigators were Dr. Harold D. Southward, Dr. William J. Byatt, Dr. Lewellyn Boatwright, Mr. Harold Cates, Mr. Goebel Davis, Jr., Mr. LeRoy Meyer, and Mr. Robert Schnurr. Mr. Raymond H. Gore worked on the project without compensation in the area of engineering models for thin film devices.

The authors wish to acknowledge the assistance of TSgt F. W. Fisher and AlC A. H. Hoffland in operating the flash X-ray system.

This report has been reviewed and is approved.

John L. Mullis

JOHN L. MULLIS
1Lt USAF
Project Officer

Edgar M. Munyon

EDGAR M. MUNYON
Colonel USAF
Chief, Effects Branch

William H. Stephens

WILLIAM H. STEPHENS
Colonel USAF
Chief, Research Division

ABSTRACT

A series of experimental studies has been conducted on transistor elements suitable for microcircuits. A relationship of transient radiation effects to active volume and other parameters has been made. The experimental and theoretical method developed offers a way of obtaining minority carrier lifetimes, depletion layer width, junction area, diffusion length, and active volume when the absorbed dose and the ionization efficiency are known in the transistor element of a microcircuit. Conversely, given the above parameters it is possible to determine the primary photocurrent of the microcircuit junction under a variety of radiation conditions. Developments have been made on the Boltzmann equation. It has been shown that the fundamental Boltzmann equation describing charge transport in semiconductors can be used to modify the usual continuity equation to obtain a more accurate circuit model for transistor elements in microcircuits. This should result in changes in the Ebers-Moll model, charge control model, and the Linvill model to take into account the thin layers used in microcircuit diffusion processes. The oxide-isolated microcircuits have been tested and compared with the usual back-biased isolation junction diode type. Circuits used were the same except for the type of isolation. Several mock-up circuits were used, and it was determined that the mock-up technique was reasonably accurate for radiation effects studies. Proper elements must be included for the parasitic elements that are inherent in microcircuits.

CONTENTS

ILLUSTRATIONS

ILLUSTRATIONS
(con't)

LIST OF TABLES

SECTION I

TRANSIENT X-RAY RADIATION EFFECTS ON p-n JUNCTIONS SUITABLE FOR MICROCIRCUITS

1. Introduction

Basic radiation effects phenomena near a p-n junction are reviewed with the desire to relate them to microcircuit design and the transient radiation environment. Experiments were performed to substantiate theoretical predictions and relating dose to primary photocurrents, secondary photocurrents, and active volume. Theoretical calculations which are applicable to junctions of different active volumes were made on the time-dependent primary photocurrent. The theory, together with the experimental data, offers a method of obtaining minority carrier lifetime, depletion layer width, junction area, diffusion length, and active volume when the absorbed dose and the ionization efficiency are known. Conversely, given the above parameters, it is shown that it is possible to predict the primary photocurrent of a p-n junction suitable for microcircuit design.

2. Initial Interaction of X Rays with Matter

a. Ionization of Electrons

When X rays interact with matter there are three predominant mechanisms of interaction. They are the photoelectric, Compton, and pair production effects. The relative importance of each of these depends on the X-ray energy and the atomic number of the absorbing material.

For low energies ($\leq$ 100 kev) and large atomic numbers the photoelectric effect is the predominant process. The photoelectric effect is the process whereby the energy of the incident photon is totally absorbed in ejecting an electron from an atom and imparting kinetic energy to it.

For energies between 100 kev and 4 mev the Compton process becomes important. It represents an interaction with an orbital electron of an atom to produce an energy-degraded photon and a recoil electron.

At higher energies, above 1.02 mev, the pair production process becomes increasingly important with increase in photon energy. It is an absorption process for X rays in which the incident photon is annihilated in the vicinity of the nucleus of an atom, and an electron-hole pair is produced (reference 1).

When an X ray hits the semiconductor, electron-hole pairs are produced through direct ionization by photons or by the slowing down of electrons and positrons. In most materials an amount of energy equal to two to four times the ionization potential of the material would be expended per ionization produced.

In gases approximately 30 ev are dissipated per electron-ion pair. Gamma rays deposit most of their energy via secondary electrons. Hole-electron production is directly proportional to the amount of energy per unit volume deposited by both primary and secondary radiation.

The energy spectrum of secondary electrons due to X-ray interaction depends upon the type of processes involved in their generation (photoelectric, Compton, or pair production). The first generation of electrons will have predominantly high energies. The next generation of high-energy secondary electrons results again in a $1/(\text{Energy})^2$ electron spectrum. If this spectrum still has some high-energy components, these components are capable of producing further ionization. These electrons will then continue to lose their energy by further inelastic scattering until finally they are trapped or recombined (reference 2).

Ionization within a semiconductor, therefore, results in the production of electron-hole pairs. Both hole and electron pairs may carry current either by diffusion, when there is a carrier concentration gradient, or by drift when there is an

electric field. The free electron will be attracted towards the positive terminal, and the hole moves towards the negative terminal in the presence of an applied electric field (reference 3).

If the air surrounding the semiconductor is ionized, the positive ion produced can move. But the positive ion moves with a much smaller mobility than the free electron of the air, and it does not add much to the flow of current. The electrons produced by ionization of gases around a semiconductor device often contribute significantly to the results of transient radiation measurements unless preventive steps are taken (references 4 and 5).

b. Immobilization of Electrons

Sooner or later the excess electron-hole pairs produced by radiation are captured and can no longer contribute to the transient effects of the circuit. One method of immobilization would be by direct recombination of the electron and positive ions. But this process happens very rarely as the probability of an electron coming within range of attraction of the positive ion is very small. Instead, more complicated multistep processes (trapping, attachment, and defect centers) are responsible for electron capture. The carriers in insulators can combine rapidly (10^{-12} to 10^{-10} sec), or one or both types of carriers may become trapped for a longer period of time at a crystal defect site.

In solids, where the freed electron occupies a state in the conduction band, the electron returns to a valence band state in several sequential transitions by means of a recombination center. These recombination centers are discrete levels located near the center of the forbidden-energy gap, and are so called because they aid the recombination between electrons and holes. This process simply amounts to the center first capturing an electron and subsequently capturing a hole. A recombination center thus has a large capture cross section (probability that any localized level can capture an excess

carrier) for both electrons and holes. In some cases, depending upon the atomic origin of the level, the level has a high capture cross section for one of the mobile carriers, but an extremely small cross section for its mate. This level is called a trap, because it tends to trap the carrier for which it has the larger capture cross section without capturing the other kind of carrier. Some trapping phenomena have been observed in which excess mobile carriers have been held for hours, or days, as in the formation of F centers in alkali halides (reference 4).

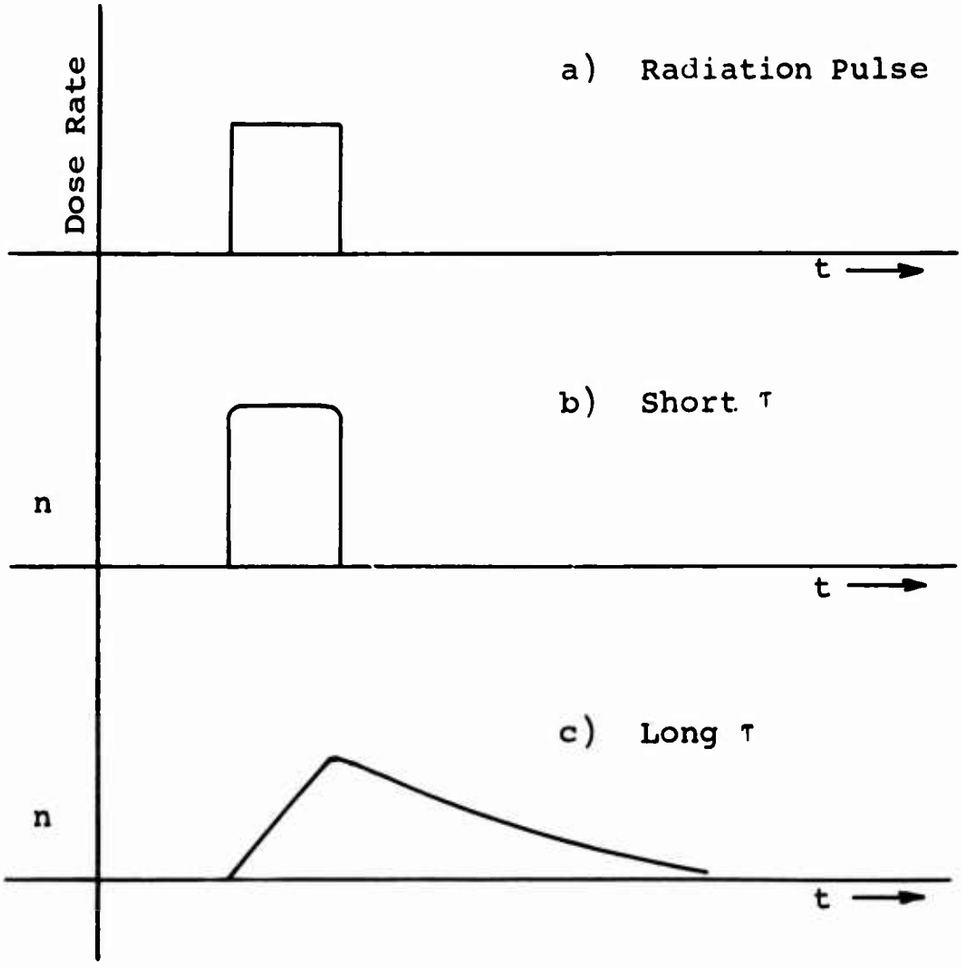

Figure 1. Time Dependence of Ionized Electron Concentration

Figure 1 shows the characteristic shapes of the signal that would be observed for ionizing-radiation pulse lengths

which are short or long compared with the electron lifetime. If the electronic lifetime τ is short compared with the duration and rise and fall of the radiation pulse, one would expect the electron concentration n to follow the radiation pulse as in figure 1b. But if the electron lifetime is long compared with the duration of the radiation pulse, the characteristic shape should be as shown in figure 1c.

In a typical germanium or silicon transistor the recombination time is usually of the order of a few nanoseconds to a few microseconds. The recombination occurs indirectly by use of a recombination center. The rate of recombination is a function of the concentration of these recombination centers. The purer the material the longer is the lifetime of excess carriers. The maximum experimental value for very pure single crystal silicon is about 500 microseconds.

c. Processes of Current Flow in a Semiconductor

There are two different kinds of mobile carriers present in a semiconductor device and each kind can carry current either by drift in a potential gradient or by diffusion in a density gradient. The two different kinds of mobile carriers are the negatively charged electrons and positively charged holes.

The drift component results from a movement of carriers due to the force of an electric field on a charge. Since opposite charges attract, the electrons drift towards the positive potential and the holes drift towards the negative potential.

The diffusion of carriers results from a density gradient, i.e., the tendency of particles to move from a region of high concentration to a lower concentration. Intuitively, one can see that the shorter the distance in which the electron density changes (i.e., the greater the gradient of electron density) the greater will be the diffusion current (reference 6).

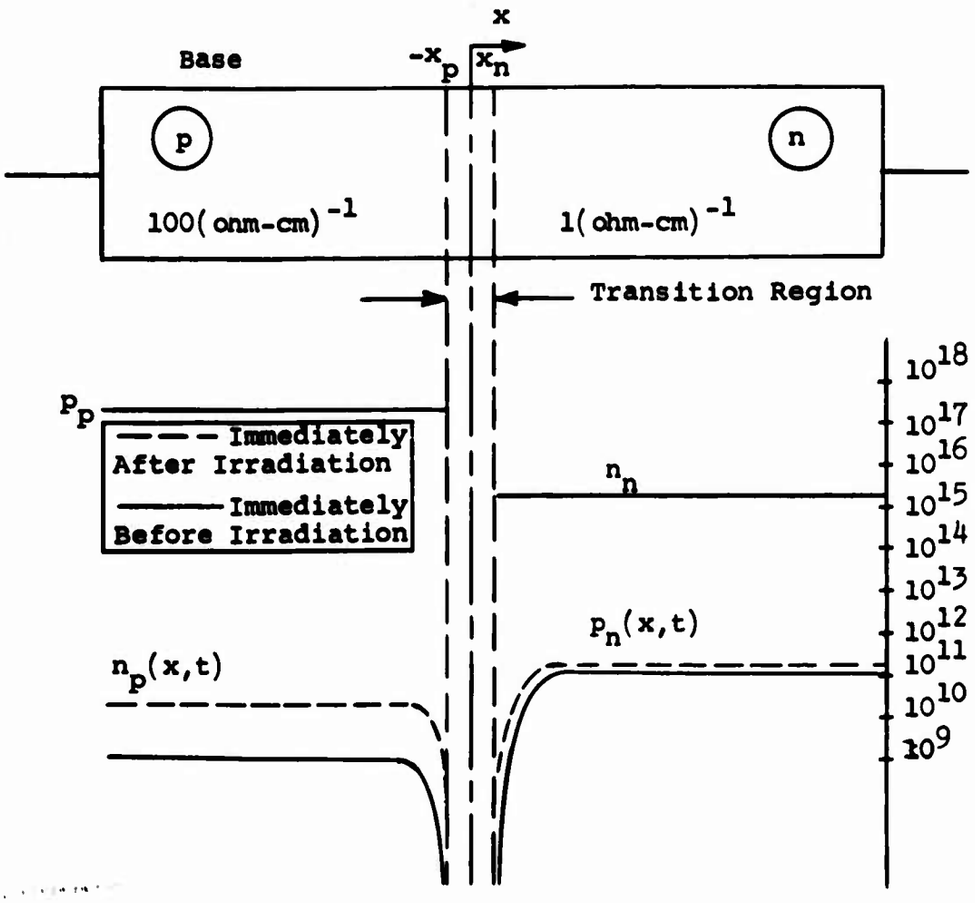

a. Reverse Biased

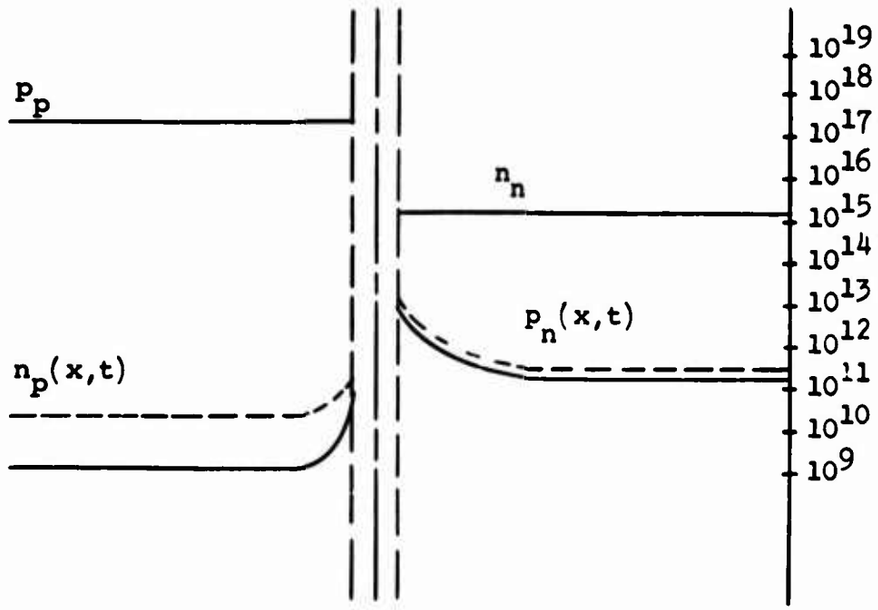

b. Forward Biased

Figure 2. Approximate Minority and Majority Carrier Densities in a p-n Diode Before and Immediately After Irradiation

d. Effect of Ionizing Radiation on a p-n Junction

Irradiation of a semiconductor p-n junction produces an excess carrier concentration. With constant voltage applied to the junction, the resulting current pulse depends on the radiation pulse width, the pulse shape, and the recombination time of the minority carriers. When the recombination time is long compared to the radiation pulse width, the concentration increases at a rate proportional to the radiation dose rate until the pulse is shut off. Then the semiconductor relaxes to its preirradiation steady-state value within some characteristic time. But if the recombination time is short compared to radiation pulse width, then the excess-carrier concentration is proportional to the dose rate at any particular time and follows the shape of the radiation pulse.

The variation of majority and minority carriers in the vicinity of a one-dimensional p-n junction is shown in figure 2. Solid lines indicate the equilibrium carrier concentration under bias before irradiation, and dotted lines indicate a typical carrier concentration immediately after irradiation (reference 7). In a reverse bias condition the minority carriers constitute the reverse leakage current (see figure 2a). Because the holes in the n-region are injected into the p-region and electrons are injected into the n-region, the direction of current flow is from the n-region to the p-region.

When the diode is irradiated by a pulse of ionizing radiation, electron hole pairs are generated uniformly throughout the device. Since there is a built-in electric field in and near the junction transition region, the carriers generated in this region will be swept across the junction and collected in less than a few nanoseconds. If the radiation pulse is much wider than a few nanoseconds, these carriers constitute a current which has essentially no time delay relative to the radiation pulse. For this reason this current is referred to as the prompt photocurrent component.

In the regions outside of the junction transition region there is a transient increase in the minority carrier densities as shown by the dotted lines in figure 2a. As indicated by the dotted lines, the minority carrier density gradients at the edges of the junction have increased. This would increase the minority carrier diffusion tendency (i.e., density gradient) in the vicinity of the junction and more carriers would diffuse towards the junction. Most of the excess minority carriers which are within a diffusion length of the junction diffuse to the junction and contribute to a transient current. On the average, excess minority carriers greater than one diffusion length from the p-n junction generated in the p- and n-regions do not reach the junction before they recombine. Therefore, they do not contribute significantly to the transient current.

The diffusion component of current generally takes a time which is large compared to the duration of the radiation pulse to diffuse to the junction. It is therefore referred to as a delayed photocurrent component. The excess holes in the n-region diffuse towards the p-region, so that the radiation-induced delayed component of current is from the n- to the p-region. Since the depletion and diffusion photocurrent is in the same direction as conventional current flow in a reverse biased diode, the net result is a transient photocurrent superimposed on the steady-state leakage current.

A forward biased junction can be regarded as a short circuit in most instances. The voltage drop due to applied voltage across the junction will be small and normally will not completely cancel out the built-in junction potential. Thus an electric field will still exist in the same direction as in a reverse biased junction. Carriers which are generated in the junction transition region will, as before, be swept across the junction by this field and collected within a few nanoseconds. This current will be in opposition to the normal forward bias current. As indicated by the dotted lines in figure 2, the majority carrier densities immediately after irradiation will not be altered appreciably, but the minority carrier

density gradient will decrease. The net effect of pulsed X rays on a forward biased junction is a transient photocurrent opposite in direction to the normal steady-state current.

The derivation of the junction transient current is given in appendix I. This is the same type of result given by Brown, van Lint, Caldwell, Keister, et al.(references 8, 9, 10, and 11). The photocurrent derived is for a radiation pulse of magnitude g and duration t_o as given by the equation

$$i_{pp}(t) = qAg\left[W_t + L_n \operatorname{erf}\sqrt{\frac{t}{\tau_n}} + L_p \operatorname{erf}\sqrt{\frac{T}{\tau_p}}\right] \quad 0 \le t \le t_o \qquad (1a)$$

$$i_{pp}(t) = qAg\left[L_n \operatorname{erf}\sqrt{\frac{t}{\tau_n}} - \operatorname{erf}\sqrt{\frac{t - t_o}{\tau_n}} + L_p \operatorname{erf}\sqrt{\frac{t}{\tau_p}} - \operatorname{erf}\sqrt{\frac{t - t_o}{\tau_p}}\right] \quad t > t_o \qquad (1b)$$

In appendix II it is shown that the width of the depletion region is a function of the bias voltage (reference 12). Thus the primary photocurrent consists of the following two components: (1) A voltage insensitive diffusion component that is contributed to by the p and n regions; and (2) a voltage sensitive drift component that is contributed to by the depletion layer. Usually the voltage insensitive diffusion component is much greater than the voltage sensitive drift component (reference 13). The primary photocurrent can be considered as a constant-current generator connected across the junction as shown in figure 3.

If the collector-base region of a planar, discrete, or integrated circuit transistor is used as a diode, then most of the primary photocurrent usually originates in the collector region. With the above approximations of neglecting the depletion region and the base diffusion component, the transient photocurrent response to a radiation pulse is of the form

$$i_{pp}(t) = gA_c qL_c \left[u(t)\ \text{erf}\sqrt{\frac{t}{\tau_c}} - u(t - t_o)\ \text{erf}\sqrt{\frac{t - t_o}{\tau_c}} \right] \quad t>0 \qquad (2)$$

where

q = electron charge = 1.6×10^{-19} coulombs
A_c = collector-to-base junction area
g = electron-hole pair generation/cm^3-sec
L_c = collector minority carriers diffusion length
τ_c = lifetime of minority carriers in the collector
t_o = X-ray pulse width
$u(t)$ = unit step function starting at $t = 0$
$u(t - t_o)$ = unit step function starting at $t = t_o$

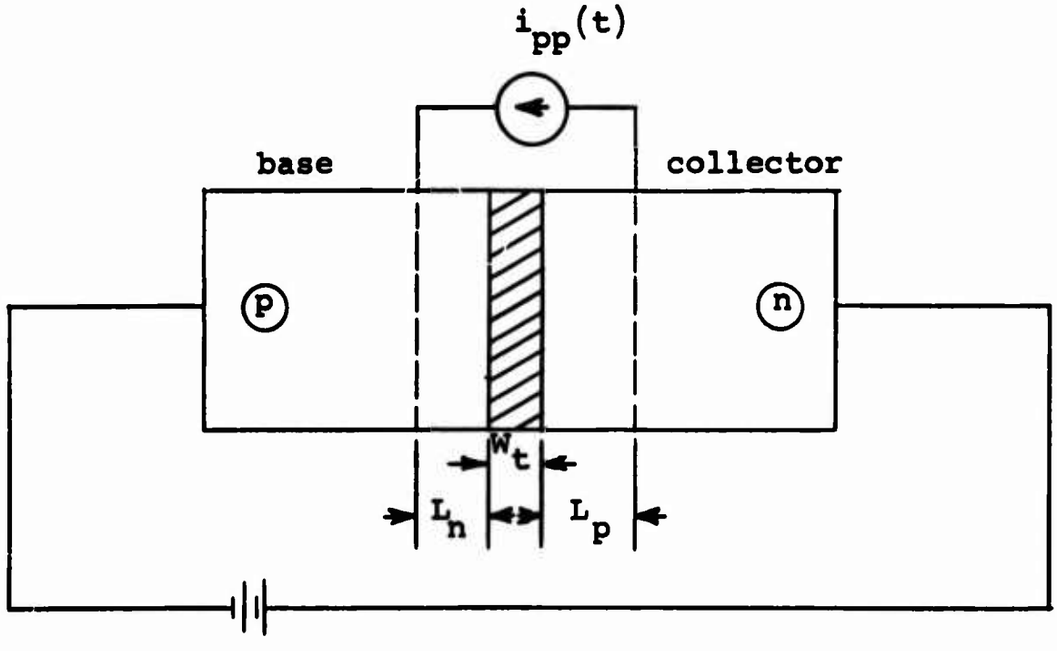

Figure 3. Simulation of Primary Photocurrent in a p-n Junction

The generation rate, g, for a silicon transistor can be calculated from (references 14 and 15)

$$g = \frac{(100)\rho}{(\overline{E}\ 1.6 \times 10^{-12})}\ \dot{\gamma} = 4.2 \times 10^{13}\ \dot{\gamma}\ \text{pairs/cm}^3\text{-sec} \qquad (3)$$

where

ρ = density of silicon = 2.42 g/cm^3

$\overline{E}$ = average energy in electron volts to produce an electron hole pair $\approx$ 3.6 ev for silicon

$\dot{\gamma}$ = dose rate in rads/sec (Si)

e. Effect of Ionizing Radiation on a Transistor

Consider an n-p-n transistor connected in the open base configuration and biased as shown in figure 4. When the transistor is irradiated by a short pulse of ionizing radiation, electron-hole pairs are created uniformly through the volume. Just as before in the case of the diode, the radiation generated electrons and holes will drift across the junction and diffuse to the junction. This will result again in a prompt photocurrent component from the transition region and a delayed component from the diffusion of minority carriers from one region to another. With an n-p-n transistor the electrons in the base will diffuse to the collector-base junction, and they will be collected as a component of the delayed photocurrent.

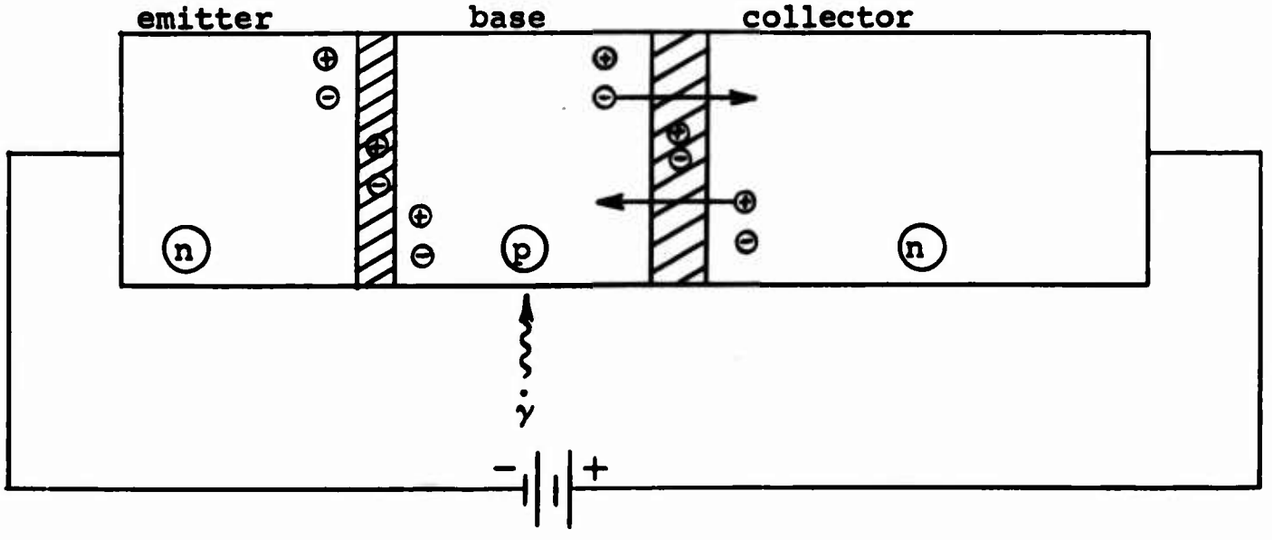

Figure 4. Open Base Transistor Under Irradiation

In the absence of these electrons, the holes left behind form an excess positive charge in the base. At the time the electrons are diffusing from the base, holes are diffusing

from the collector to the collector-base junction, and they are swept into the base region. These holes will further increase the excess positive charge in the base. The excess majority carriers (holes) in the base will increase the forward bias of the emitter-base junction, which causes more electrons from the emitter to flow into the base. The electron current entering the base from the emitter is determined by the current gain of the device as well as the radiation-induced charge in the base. It results in a collector current transient (secondary photocurrent) in addition to the collector component of the primary photocurrent. These injected minority carriers (electrons from the emitter into the base) will continue to diffuse to the collector-base junction and drift across the junction as long as an excess positive charge remains stored in the base region (references 7 and 10).

From the above it is seen that the photocurrent consists of the following contributions: (1) A voltage-sensitive depletion layer component contributed by the emitter-base and collector-base junction, and (2) a voltage-insensitive diffusion component contributed by the emitter, base, and collector regions.

In planar and mesa transistors most of the primary photocurrent usually originates in the collector region (reference 16). The collector diffusion length, L_c, is much greater than the base width and the depletion width. This means that the number of holes available from the diffusion of holes from the collector to base is much greater than the diffusion of electrons from the base to collector. Thus, after the termination of the radiation pulse, holes generated in the collector region within one diffusion length of the junction will diffuse into the base. The charge accumulated in the base due to diffusion of carriers from the collector will therefore not reach a maximum until approximately a time equal to one to two times the lifetime of minority carrier in the collector (τ_c).

It is postulated that the substrate collector junction will contribute only primary photocurrent to the total photocurrent. The substrate to base dimension is wider than a diffusion length so that the substrate-collector-base transistor has a very low current gain and poor transistor action. It will then follow that the secondary photocurrent will be small.

3. Instrumentation and Equipment

a. General Layout

Figure 5 shows the layout of the flash X-ray facilities at Kirtland Air Force Base. The controls for the flash X-ray system are situated outside of the screen room. The test equipment and the test sample are enclosed in a double-walled rf shield room. Inside the room the rf noise level is reduced by 120 db. See appendix III for a more detailed discussion of the flash X-ray system.

b. Test Circuit

The test circuit is shown in figure 6. Preliminary testing showed that in order to keep the circuit time constant small compared to the transistor response, the viewing resistor had to be less than 200 ohms. It was decided to use a viewing resistor which would properly terminate the coaxial cable with its characteristic impedance of 50 ohms.

In order to minimize the cable length, and hence the constant of the viewing circuit, an amplifier was used. This allowed the leads to be shortened to approximately 2 feet. The amplifier and power supply were shielded from incident radiation by a wall made of 2-inch thick lead bricks.

Air ionization will cause a shunt leakage path on the order of 10 megohms (reference 5). Since the viewing resistor is very much smaller than the shunt resistance due to air ionization, the effect of air ionization was neglected. In order to eliminate any effect of radiation on the cable or resistors, a 1-inch thick lead block was placed between the

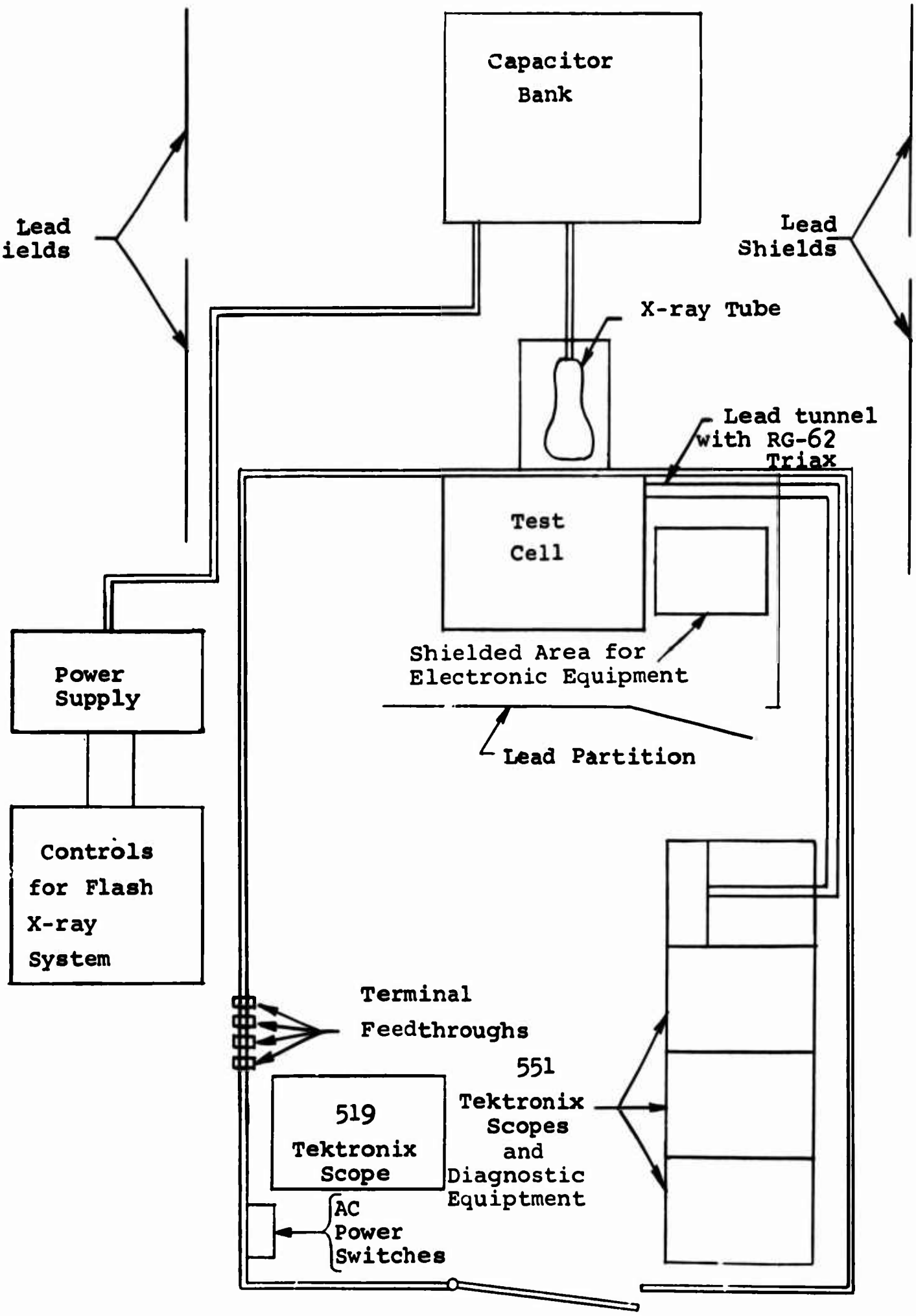

Figure 5. AFWL 600-KV Flash X-ray Facility

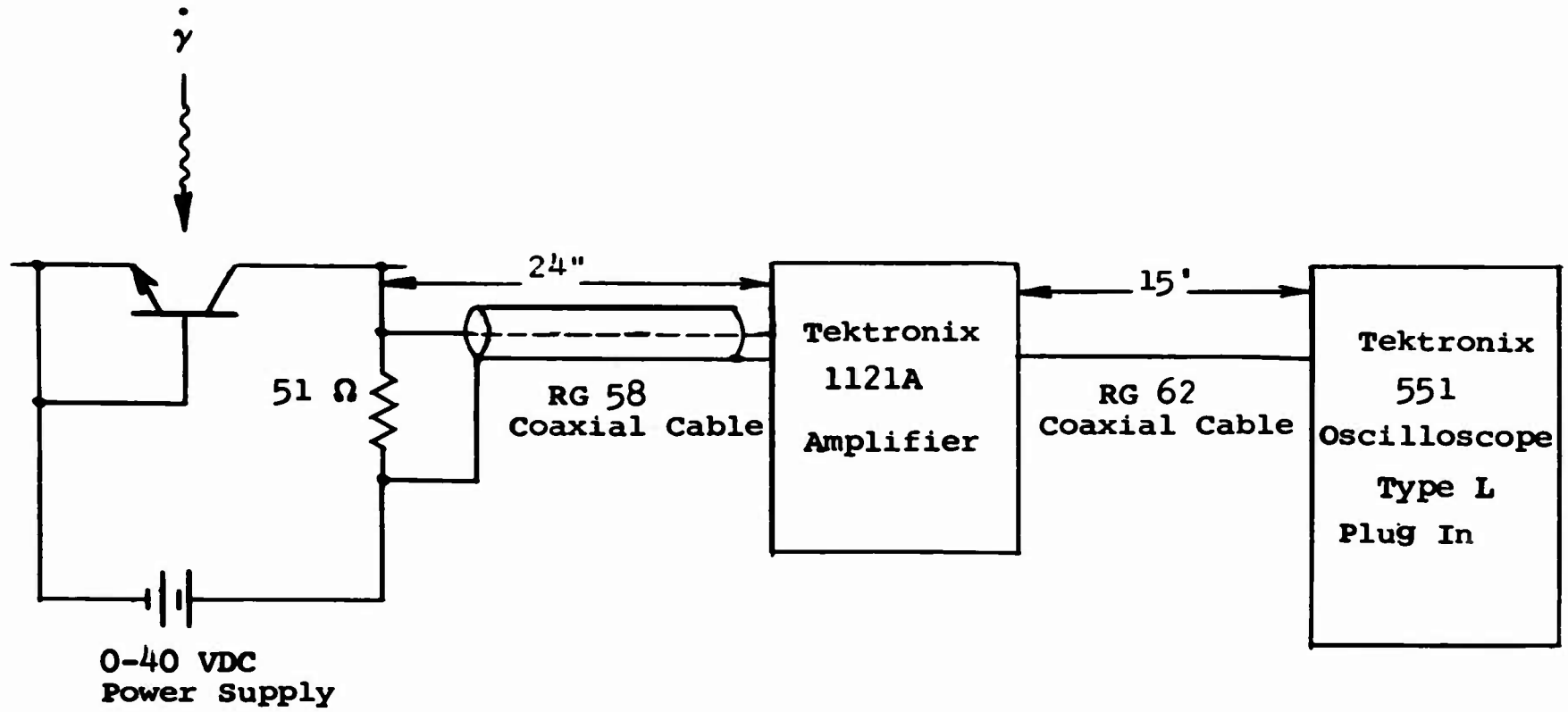

Figure 6. Schematic Diagram of Transistor Test Circuit

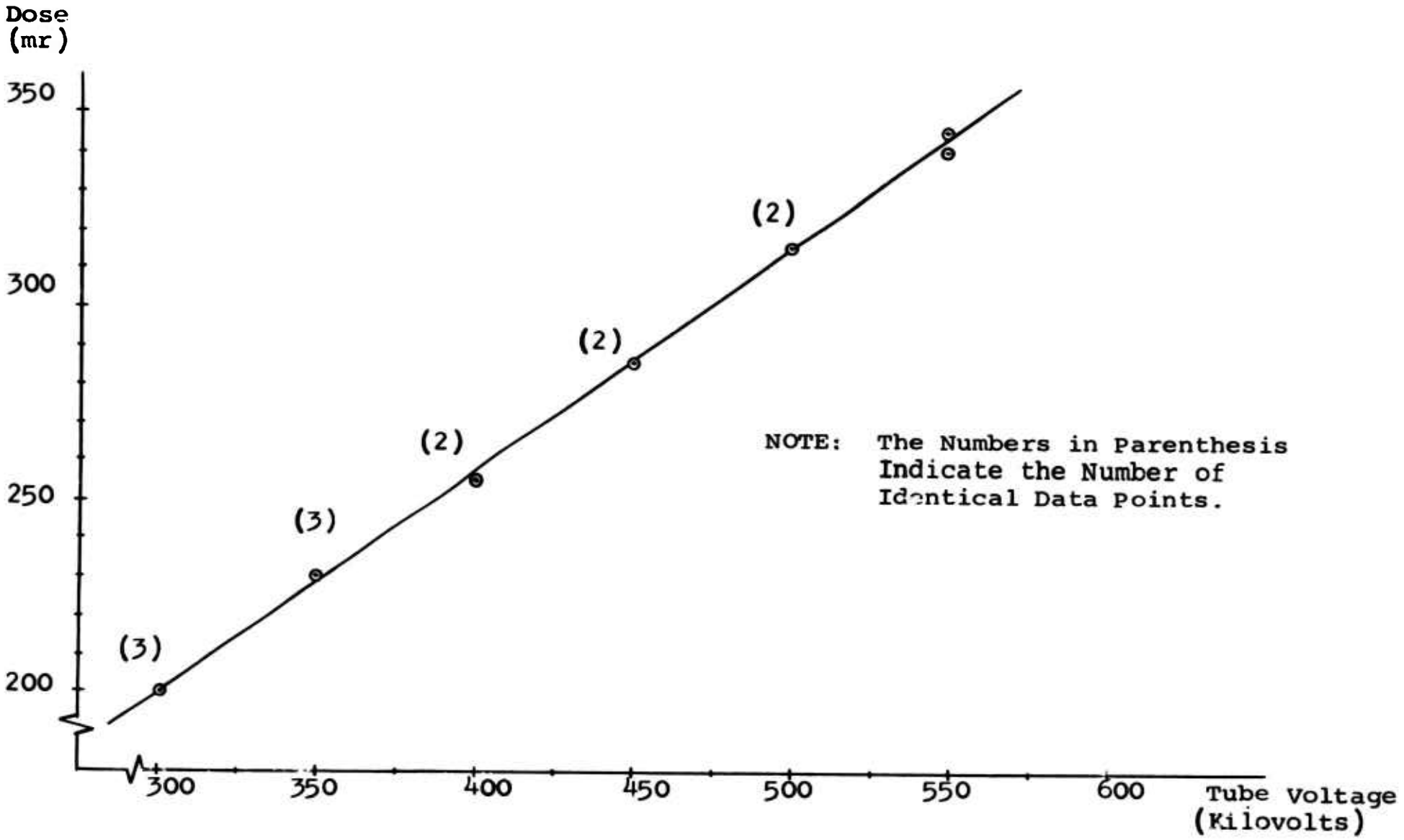

Figure 7. Dose as a Function of X-ray Tube Voltage
4 Inches from the Front of the Anode

X-ray source and the circuit. A 1-inch hole was drilled in the block to allow the X rays to impinge upon the target transistor.

c. Noise Level

The ambient noise level is due primarily to the noise generated in the amplifier. The amplifier noise level is specified as less than 50 microvolts peak to peak.

The transient noise level is caused by the operation of the flash X-ray system. A second screen room would probably reduce the transient noise level sufficiently that it would be masked by the ambient noise from other sources.

Noise level is particularly important when irradiating devices with small active volumes and fast response times. Small active volumes will give low amplitude response, and fast response times will force small viewing resistors to keep the time constant down. The combination of these two factors forces use of maximum gain of the amplifier and oscilloscope preamplifiers. The use of maximum gain of the amplifier is the worst condition from a noise standpoint. During recent tests, the response of a 2N917 transistor was masked by noise so that only crude order-of-magnitude results could be obtained.

4. Experimental Results

a. Dose Dependence

Tests were run using the circuit shown in figure 6 to determine peak collector current as a function of dose in milliroentgens. The variation in dose was obtained by varying the anode voltage on the flash X-ray tube.

A plot of dose vs. X-ray tube voltage is shown in figure 7. The resultant curve was linear with a constant slope in the region of interest. The curve can be approximated by equation 4.

$$mr = 0.572V + 29 \qquad (4)$$

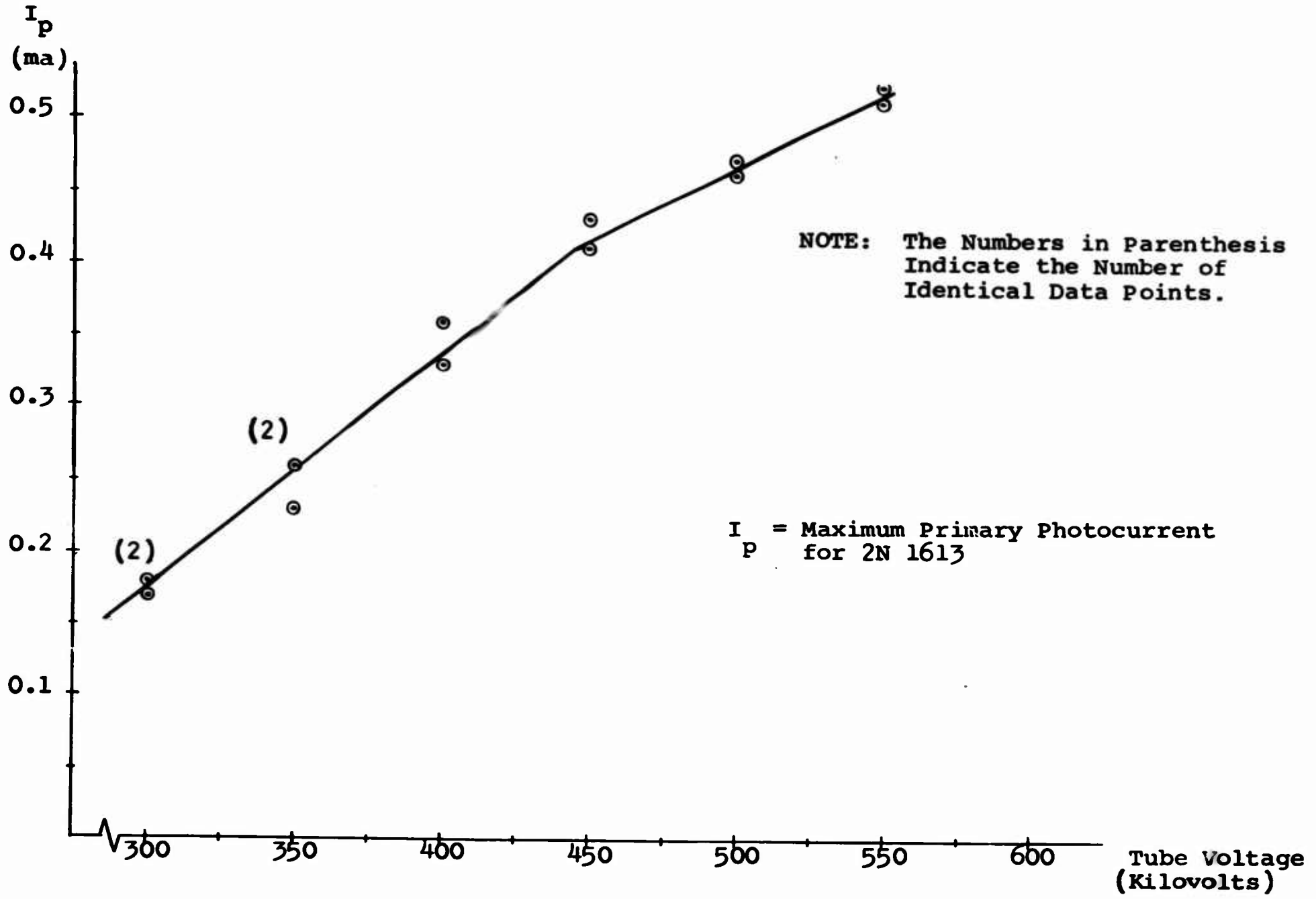

Figure 8. I_p as a Function of X-ray Tube Voltage

where

mr = dose in milliroentgens

V = X-ray tube voltage in kilovolts

As a result of this experiment all further tests were run using anode voltage as an approximate measure of dose.

A plot of peak primary photocurrent vs. anode voltage for a 2N1613 transistor is shown in figure 8. The slight flattening of the curve above 450 KV can be attributed to two factors: (1) The transistor response is to some extent sensitive to dose rate. As the anode voltage is increased the shape of the X-ray pulse is distorted. This distortion is much more pronounced at high anode voltages and causes a change in dose rate which is less than the expected linear change with anode voltage. (2) The transistor may be approaching a hole-electron pair production rate saturation.

As a result of this experiment, testing for variation with other parameters was done in the linear portion of the response curve; 400 KV anode voltage was selected to give maximum dose and still remain in the desired portion of the curve.

b. Active Volume

The active volume depends upon junction area, diffusion length, and depletion width. All of these are constant except depletion width, which is a function of applied voltage. An experiment was set up to determine the effect of bias voltage upon the peak collector current.

Using the circuit shown in figure 6, the voltage was varied in steps from 0 to 40 V DC. A plot of log I_p vs. log bias voltage resulted in a straight line, where I_p is the peak transient current due to an X-ray pulse. From the slope of the line the relationship between I_p and bias voltage is given by

$$I_p = KV^{1/18} + I_o \qquad (5)$$

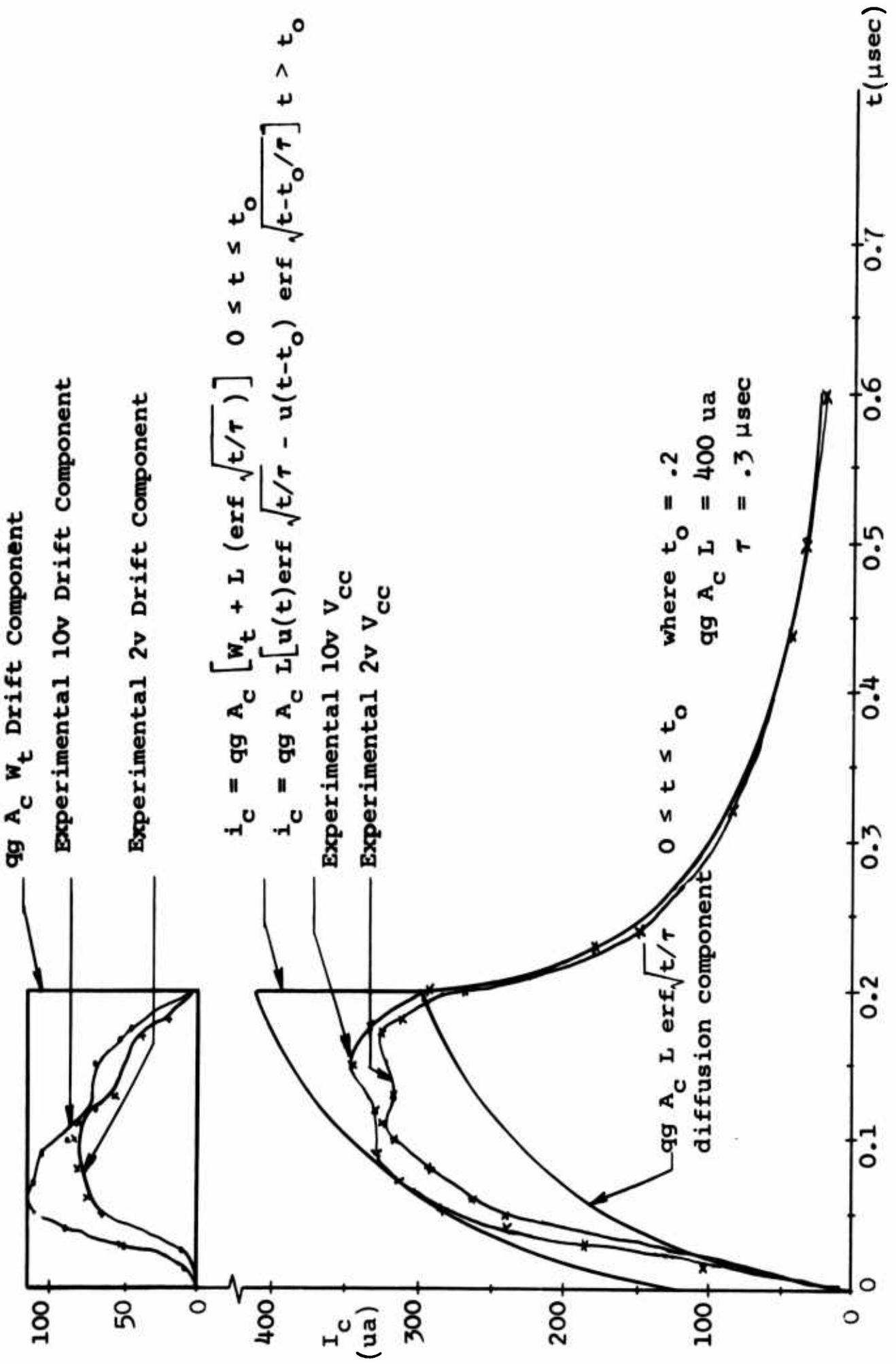

Figure 9. Collector Primary Photocurrent vs Time for a 2N 1613

where

I_p = peak collector current in ma
V = bias voltage in volts
K = constant
I_o = zero bias current

This result shows an apparent conflict with the theoretical results derived in appendix II. The conflict can be resolved by considering the relative times and magnitudes of the two components of the primary photocurrent.

The drift component of the primary photocurrent is developed in the depletion region. The diffusion component comes from the region up to one diffusion length beyond the depletion region. In a semiconductor with a moderately long minority carrier lifetime, a diffusion length is much longer than the depletion region width. Therefore, the contribution from the diffusion current is much larger than that from the drift current.

The diffusion current is of the form $K_1\sqrt{D\tau}$ erf $\sqrt{t/\tau}$. The time to peak current is a function of τ, the minority carrier lifetime. The drift current is of the form $K_2 g(t)$ where $g(t)$ is the generation rate. The drift current will follow the radiation pulse with no delay.

Figure 9 shows theoretical and experimental curves of photocurrent plotted against time. When the theoretical curve for diffusion current is subtracted from the experimental curve, the result is the drift component of the photocurrent. The drift component has followed the radiation pulse as can be seen by a comparison with figure 10 which shows the shape of the radiation pulse as determined by a scintillator.

The peak of the drift component does not coincide with the peak of the diffusion component of the photocurrent. The peak of the sum lies somewhere in between. Measurement of the peak photocurrent is, therefore, not an accurate measurement of the change in amplitude of the drift component of the photocurrent.

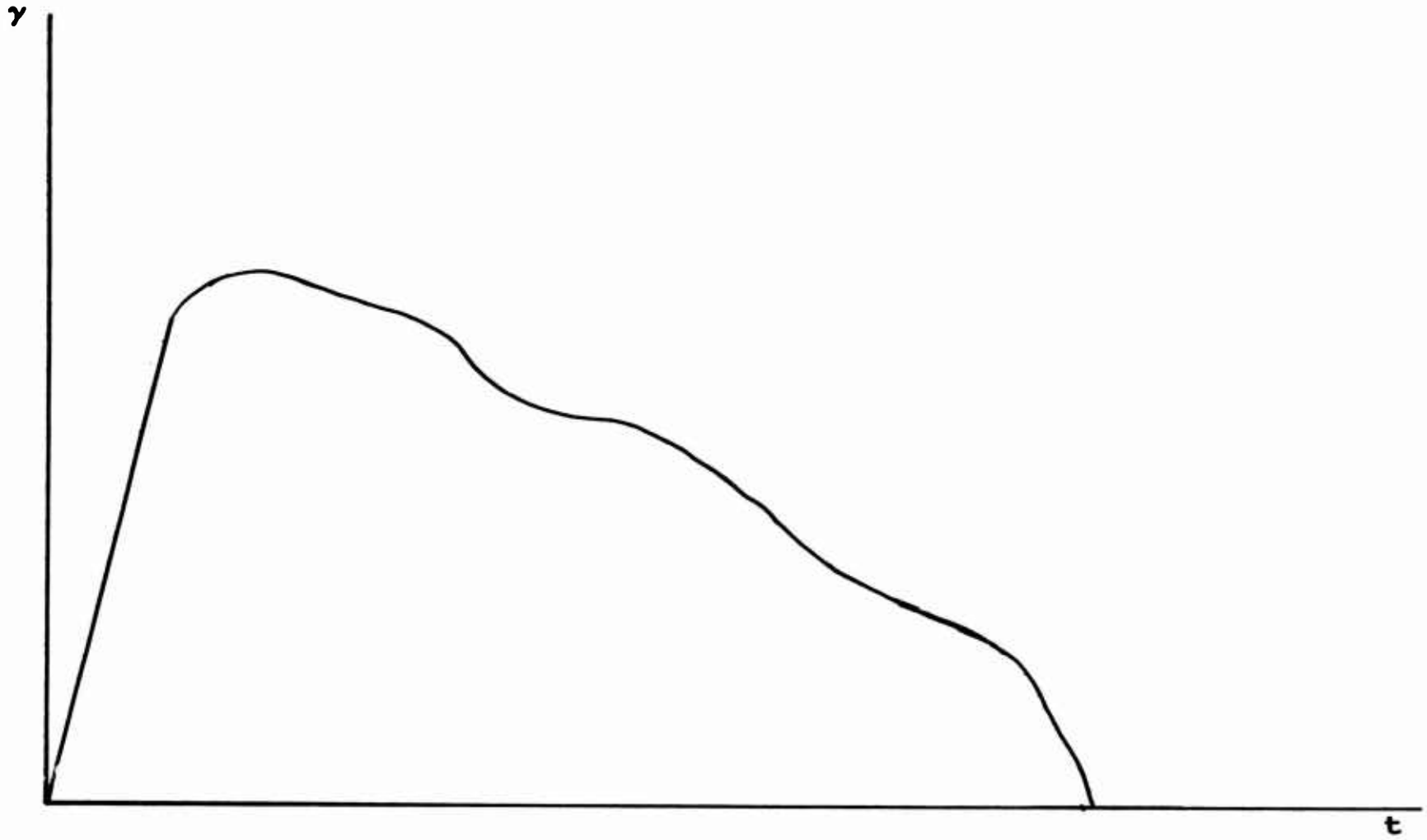

Figure 10. Radiation Pulse Shape as Determined by Scintillator

The drift components of the photocurrent for two different bias levels were separated from the total photocurrent. Their average values were determined to be approximately 70 μa for a bias of 10 volts and 45 μa for a bias of 2 volts. When the points were plotted on log log graph paper, the slope of the line was found to be 0.275. This result may be stated as

$$I_d \alpha V^{1/3.64} \tag{6}$$

where I_d is the drift component of the photocurrent which compares favorably with the result from appendix II, equation (162)

$$I_d = K V^{1/3} \tag{7}$$

c. Transistor Response

Two transistor types were experimentally investigated. They were the 2N1613 and 2N917. The transistors were operated with a 10-volt collector bias voltage. Data were obtained for a base emitter short circuit configuration as shown in figure 6 and for a base open circuit configuration.

The intent was to obtain comparative results for the two transistor types. This intent was not realized because of the noise problems discussed earlier.

(1) Base Emitter Short

Equation (1a) will give an approximate theoretical expression for the primary photocurrent if the base component is neglected, as

$$I_{pp} = qA_c\, g\left[W_t + L_p \operatorname{erf} \sqrt{t/\tau_p}\right] \quad 0 \le t \le t_o \tag{8}$$

The prompt current, $i_p(t)$, can be separated from the diffusion component, $i_d(t)$; they are given from above as

$$i_p(t) = q\ A_c\ g\ W_t \qquad 0 \leq t \leq t_o \tag{9}$$

$$i_d(t) = q\ A_c\ g\ L_p\ \text{erf}\ \sqrt{t/\tau_p} \qquad 0 \leq t \leq t_o \tag{10}$$

In figure 9 the experimental depletion component (prompt or drift component) was separated from the diffusion component (delayed component). The diffusion component data can be fitted with an expression given by

$$i_d(t) = q\ A_c\ g\ L_p\ \text{erf}\ \sqrt{t/\tau_p} = (400\ \mu a)\ \text{erf}\ \sqrt{t/.3\ \mu sec}$$

$$0 \leq t \leq t_o \tag{11}$$

for a type 2N1613 transistor collector-base junction.

Since $L = \sqrt{D\tau}$, one can calculate out the value of L_p by choosing a typical value for the diffusion constant ($D_p = 13.3\ cm^2/sec$)

$$L_p = \sqrt{D_p \tau_p} = \sqrt{13.3\ \frac{cm^2}{sec}\ (.3 \times 10^{-6}\ sec)} \tag{12}$$

$$L_p \approx 2 \times 10^{-3}\ cm \tag{13}$$

From equation (10) and figure 9 it is seen that

$$q\ A_c\ g\ L_p = 400\ \mu a \tag{14}$$

Or, solving for $q\ A_c\ g$, one may obtain

$$q\ A_c\ g = \frac{400\ \mu a}{L_p} \tag{15}$$

Using the value calculated for L_p in equation (13) equation (14) becomes

$$q\ A_c\ g = \frac{400\ \mu a}{2 \times 10^{-3}\ cm} = 200\ \frac{ma}{cm} \tag{16}$$

The shape of the experimental depletion current followed the shape of the X-ray pulse. This pointed to the fact that the radiation pulse was not constant for the 0.2 μsec. The variation in the radiation rate can be compensated for by taking the average value of the depletion component as an approximation. Using an average value of about 70 μa for an applied reverse bias of 10 v across the diode composed of the collector-base junction of the 2N1613, one can solve for an average value of the depletion width W_t. Solving for W_t out of equation (9) one obtains

$$W_t = \frac{i_p(t)}{q\ A_c\ g} \tag{17}$$

Using the results of equation (16) and an average value for $i_p(t)$, the average value for W_t becomes

$$W_t = \frac{70\ \mu a}{200\ ma/cm} = 3.5 \times 10^{-4}\ cm \tag{18}$$

This value of the depletion width is about the same value one would theoretically calculate.

If an average energy of 3.6 ev is required to create an electron-hole pair in silicon, a dose rate of 1.4×10^6 r/sec will produce a generation rate of about 7×10^{19} electron-hole pairs/cm^3-sec. Equation (16) gave

$$q\ A_c\ g = 200\ \frac{ma}{cm} = .2\ \frac{amp}{cm} \tag{19}$$

If $q = 1.6 \times 10^{-19}$ coulombs and $g = 7 \times 10^{19}$, one can solve for A_c.

$$A_c = \frac{0.2}{qg} = \frac{0.2}{(1.6 \times 10^{-19})(7 \times 10^{19})} \tag{20}$$

$$A_c = 0.01785 = 17.85 \times 10^{-3} \text{ cm}^2 \tag{21}$$

In table I, the values which were able to be predicted from radiation measurements and the measured transistor values are tabulated.

Table I

Physical Parameters for Transistors

	Measured 2N1613	Radiation Predicted 2N1613	Measured 2N917
Collector Impurity Concentration	5×10^{15} cm^{-3}		2×10^{16} cm^{-3}
Base Impurity Concentration	10^{17} cm^{-3}		5×10^{17} cm^{-3}
Emitter Impurity Concentration	10^{20}		10^{20}
Collector Base Junction Area	5×10^{-3} cm^2	17.85×10^{-3} cm^2	5×10^{-5} cm^2
Emitter Base Junction Area	3×10^{-4} cm^2		6×10^{-6} cm^2
Collector Lifetime	0.3 μsec	0.3 μsec	
Base Width	2 microns		0.5 micron
Chip Thickness	[illegible] microns		80 microns
Collector-Base Depletion Width at -10 volts	~2.5 microns	3.5 microns	

The discrepancy between the radiation predicted and the measured values reflects the uncertainties in measuring the absorbed dose, measuring the physical parameters of the transistor, experimental errors and the approximations used in the analysis, such as the [illegible] geometry of the junction.

By looking at table I again, it can be seen that the collector-base junction area of a 2N1613 is a hundred times larger than the 2N917. If all the other parameters remained the same, a reduction of a hundred would be theoretically predicted from equation (1) in the peak transient current of the 2N917 over the peak transient current of the 2N1613. Experimental results showed a reduction of approximately forty.

(2) Base Open

Figure 11 shows the collector current wave form of a 2N1613 transistor that was irradiated in the base open configuration. The current consists of primary and secondary photocurrent. The amplitude of the primary photocurrent is approximately the same as the amplitude of the photocurrent obtained in the base shorted configuration.

In a transistor whose drift component is small compared to the diffusion component of the primary photocurrent, the magnitude of the secondary photocurrent can be approximated by

$$I_{sp} \cong h_{fe}\ i_{pp} \tag{22}$$

where

I_{sp} = peak secondary photocurrent
h_{fe} = small signal current gain measured at I_{sp}
i_{pp} = peak primary photocurrent.

This approximation is good for open base configuration only and does not contain any time information.

The secondary photocurrent is attributed to a positive charge build-up in the base. It remains until the charge in the base is dissipated. An experiment was run to determine what impedance between base and emitter is necessary to eliminate the secondary photocurrent. Starting with the base emitter impedance of zero, the impedance was increased to 100 kilohms without observing any secondary photocurrent for doses up to 250 mr. One hundred kilohms is much larger than any resistors

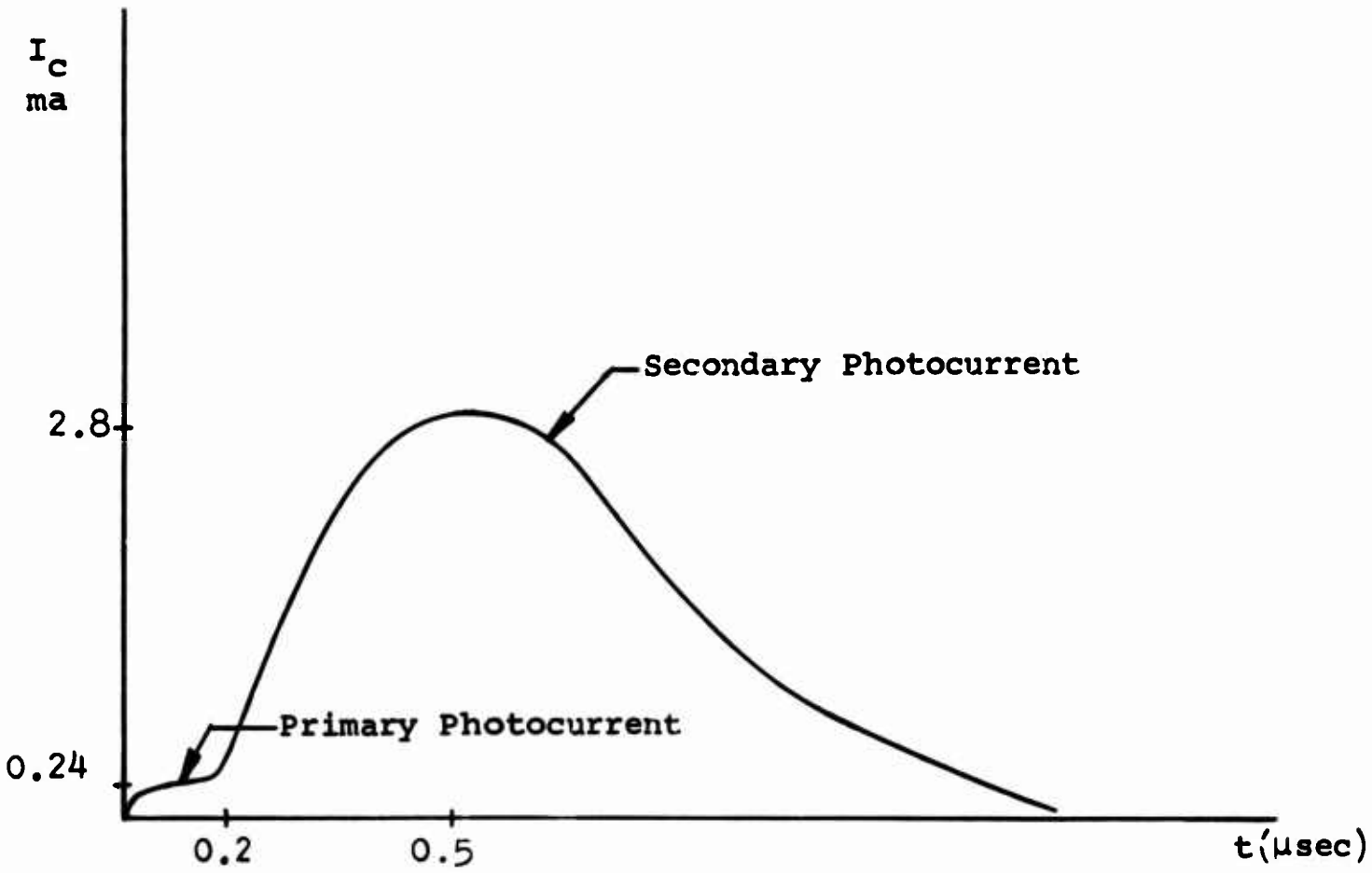

Figure 11. Collector Photocurrent for a 2N1613, Base Open Configuration

used in molecular integrated circuits. This would imply that most transistors used in integrated circuits may be treated as if their base emitters were shorted.

5. Conclusions

The following conclusions can be made from the theoretical and experimental studies that were carried out: (1) The active region should be kept as small as possible. This implies minimization of emitter-base junction and collector junction areas, minority carrier lifetimes, and depletion widths. The base collector junction area can be minimized by using epitaxial techniques and selecting the smallest possible device consistent with the required power or current levels. Minority carrier lifetime can be reduced by gold doping and using high-frequency devices. The depletion width can be minimized by using a minimum collector bias voltage. (2) The circuit should use the lowest impedances consistent with design criteria. The current source behavior of the radiation effect indicates the desirability of using low impedances. The secondary photocurrent which is a result of a high base emitter impedance is another factor in the desire for low impedances. (3) The experimental data with the theory developed here offer a method of obtaining minority carrier lifetimes, depletion layer width, junction area, diffusion length, and active volume when the absorbed dose and the ionization efficiency are known. Conversely, given the above parameters, it is possible to determine the primary photocurrent from the junction. Thus, it is possible using these techniques to make some general recommendations for design and fabrication of integrated circuits for use in a transient radiation environment.

In current molecular integrated circuit design, many of these features that are desired for radiation hardening are being incorporated for other reasons. Minimizing transistor size will increase manufacturing yield. Minimizing lifetime leads to higher frequency devices. Gold doping tends to reduce

inverse α and therefore leakage current in some transistor configurations. Small valued resistors take up less space and thus tend to increase manufacturing yield.

SECTION II

TRANSIENT RADIATION TESTING OF ELECTRONIC COMPONENTS AND INTEGRATED CIRCUITS

1. Introduction

Concurrent with the theoretical and experimental studies described in the previous section, radiation tests on numerous components and integrated circuits were conducted at the Air Force Weapons Laboratory flash X-ray facility and on the WSMR LINAC. The purposes of these tests were (1) to attempt to isolate factors in the design and fabrication of integrated circuits which have the greatest effect on the circuit response during a pulse of ionizing radiation; and (2) to evaluate several special thin-film devices which appeared to be less affected by the radiation than integrated circuit active devices. The results of these tests are presented in this section.

2. Motorola MC-201 and XC-201 Integrated Circuits

a. Background Information

The Motorola MC-201 and XC-201 are monolithic silicon, epitaxial, passivated, integrated circuits. They are used as four input "nand" or "nor" gate circuits for high-speed, low-power computer systems. Their attractive features include high stray noise immunity, fast switching speeds, and low-power dissipation. The XC-201 and the MC-201 are quite similar in operation except that the XC-201 has a much faster switching time response. The MC-201's have switching time turn-on delays and turn-off delays of 60 and 50 nsec, while the XC-201's are respectively 8 and 17 nsec. The MC-201 and XC-201 average propagation delays are respectively 30 and 17 nsec. The increased speed of the XC-201 is achieved by the use of the EPIC process. In the usual monolithic semiconductor circuits, isolation between various elements on the same substrate is

accomplished by means of a diffusion which yields back-to-back p-n junctions between different elements. With the application of bias voltage, these junctions represent reverse biased diodes with a very high back resistance which provides adequate DC isolation. Unfortunately, as each p-n junction is also a capacitance, there remains capacitive coupling between components and the substrate at high frequencies. The EPIC process completely isolates all components from each other without the use of back-biased isolation junction diodes. Isolation, both electrical and physical, is achieved by a layer of nonconductive material which completely surrounds and separates the components from each other and from the common substrate. This insulating layer can be made thick enough that its associated capacitance is negligible.

From the transient radiation sensitivity standpoint the EPIC process offers promise of increased hardening because of the elimination of the highly radiation-sensitive back-biased diodes for isolation. The main purpose of the MC-201 and XC-201 transient radiation tests was to determine what gains (if any) in radiation hardening have been achieved over the MC-201 by the use of the EPIC process in the XC-201.

In figure 12 are shown the logic and approximate circuit diagrams for the MC-201 and XC-201.

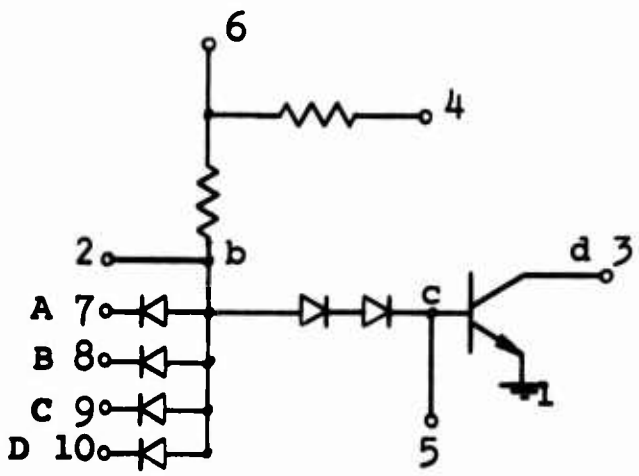

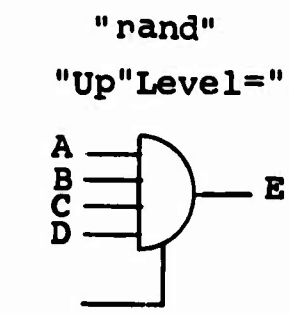

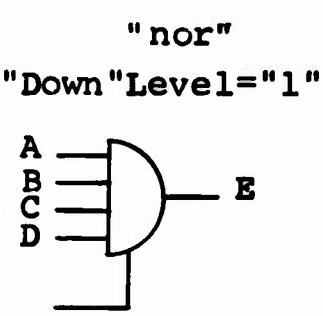

$V_{3,4,6}$ = + 8 volts

V_5 = - 8 volts

Figure 12. MC-201 and XC-201 Circuit Diagram

The operation of the circuit as a "nand" gate, for example, is as follows: When any of the inputs are at ground potential, the voltage at point "b" is also at ground potential, except for the small positive diode forward voltage drop. The voltage at point "c" is two diode voltage drops below point "b" or negative. This reverse biases the transistor's emitter-base junction, and thus the gate is turned off. When all of the inputs have positive applied voltages, the gate is turned on and the potentials at points "b" and "c" increase to provide base current to the transistor. This drives the transistor into saturation and thus reduces the voltage at "d" to a small value.

b. FXR Tests of MC-201 and XC-201

The MC-201 and XC-201 were tested at the AFWL flash X-ray system at Kirtland AFB, New Mexico. The tests were performed at the 400-KV level with a 0.2-μsec pulse width. This yields an approximate dose rate of 2×10^6 roentgens/sec.

In figure 12, the external test circuit and conditions were as follows:

a) a 510-Ω resistor was connected from terminals 6 to 3

b) $V_6 = +4$ volts

c) $V_5 = -3$ volts

d) Inputs 7, 9, and 10 open

e) $V_8 = 0$ or +4 volts

The XC-201 was tested during irradiation with V_8 both zero and plus four volts. No transient radiation response was detectable above the noise level when using an oscilloscope gain of 0.005 volt/cm with a peak-to-peak noise voltage present of approximately 0.0015 volt. It is concluded that the XC-201 is highly radiation resistant to gamma doses up to at least 2×10^6 roentgens/sec.

The testing of the MC-201 (under identical test conditions as for the XC-201) did yield a transient radiation response output (V_3). These transient outputs were of approximately the same duration as that of the gamma radiation pulse, and the peak values were:

a) V_3(peak) ≙ -0.0035 volt when V_8 = 0 volts,

and

b) V_3(peak) ≙ +0.0025 volt when V_8 = +4 volts.

The difference in polarity for the two states is most likely attributable to the radiation trying to push the transistor into conduction for V_8 = 0 (i.e., V_3 decreases), and the radiation causing an injection of negative current from the diodes into the base of the transistor for V_8 = 4 (resulting in an increase of V_3).

The overall conclusion from the gamma testing at this level is that the XC-201 is less sensitive to radiation than the MC-201.

c. LINAC Test Results

The XC-201 and MC-201 were also tested on the LINAC test facility at the White Sands Missile Range, White Sands, New Mexico. Both of the units irradiated were subjected to electron radiation at the 22-mev electron energy level. The dose measurements for the LINAC were provided by WSMR personnel using thermal luminescence dosimetry. There was considerable variation in the indicated dose per shot. Average figures for total dose per shot were about 130 rads (H_2O). The dose rate may be calculated approximately by dividing the total dose by the radiation pulse width. For the electrons on the LINAC the result is 130 rads divided by 0.5 μs or approximately 2.6×10^8 rad/sec.

In figure 12, the external test circuit and conditions were as follows:

a) a 510-Ω resistor was connected from terminals 6 to 3

b) V_6 = +8 volts

c) V_5 = -2.5 volts

d) Inputs 7, 9, and 10 open

e) V_8 variable

f) The effect of output loading is shown by the test for R_L equal infinity (i.e., open) and R_L equal 1.6 K.

The data were recorded by a Tektronix type 555 oscilloscope. In all cases, effectively, the microcircuits only were irradiated. The electron beam was sufficiently narrow to allow the positioning of only the microcircuits within the radiation.

In table II the LINAC results are summarized.

Table II

LINAC 22 Mev Electron Results on the MC-201 and XC-201

R_L Output Loading Resistance	V_8 Input Voltage	MC-201 Maximum Peak-to-Peak Transient Voltage Output (V_3)	XC-201 Maximum Peak-to-Peak Transient Voltage Output (V_3)
Open Circuit	0	0.37 volt	0.48 volt
"	1 volt	no shot	0.20
"	1.5	0.29	no shot
"	2	no shot	0.16
"	3	"	0.10
"	0	0.34	0.32
R_L = 1.6 K	1	no shot	0.24
"	2	1.0	0.14

For the XC-201 the transient response was a fast-rising negative-going pulse which decayed back to zero with a time constant of approximately 3×10^{-6} sec. The peak-to-peak (i.e., here the same as the peak) maximum transient voltage output (V_3) is shown in the fourth column of the table. Note that the output response rather conclusively decreases as the input V_8 increases. This is as to be expected as the output transistor is cut off for $V_8 = 0$, but is going toward saturation for V_8 increasing.

For the MC-201 the test results are inconclusive. Its transient response was a fast-rising positive-going pulse lasting for the duration of the radiation pulse. Then the output abruptly switched to a negative pulse which also decayed with a time constant of approximately 3×10^{-6} sec. Apparently two simultaneous phenomena are occurring, one pushing the output positive, the other pushing it negative. This results in a cancellation effect which for low values of input voltage makes the peak-to-peak response of the MC-201 and the XC-201 approximately the same. Further analysis of the MC-201 will require additional shots on the LINAC.

d. Summary of MC-201 and XC-201 Tests

In general the XC-201 is less sensitive than the MC-201 to transient radiation effects. For gamma radiation up to 2×10^6 roentgens/sec these results are conclusive. For electron radiation at the 22-mev level the difference is less pronounced.

3. Fairchild μL-903 Micrologic Element and Mock-up

a. Background Information

The Fairchild micrologic elements are a set of compatible, integrated logic building blocks. The elements are manufactured using the planar epitaxial process by which all the necessary transistors and resistors are diffused into a single silicon wafer. The individual RTL gates within the logic elements are

interconnected by metal over oxide. These units are characterized by low propagation delays for use in high-speed systems. Typical propagation delay for the basic RTL circuit is 12 nsec, and pulse widths of 50 nsec produce reliable triggers for the storage elements.

The micrologic gate element, μL-903, is a three-input resistor-transistor-logic (RTL) circuit. In Figure 13 are shown the circuit and logic diagrams for the device. For a positive input on 1, 2, or 3 the associated transistor goes into saturation which reduces the potential at the output (6) to a low value (i.e., the "down" state). For no positive inputs on 1, 2, or 3 the gate is off (i.e., the "up" state).

Gate Element

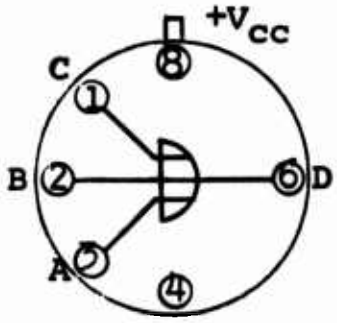

Gnd.
(Top View)

Positive Logic: $D = \overline{A+B+C} = \overline{A}\,\overline{B}\,\overline{C}$

Negative Logic $D = \overline{ABC} = \overline{A}+\overline{B}+\overline{C}$

Schematic

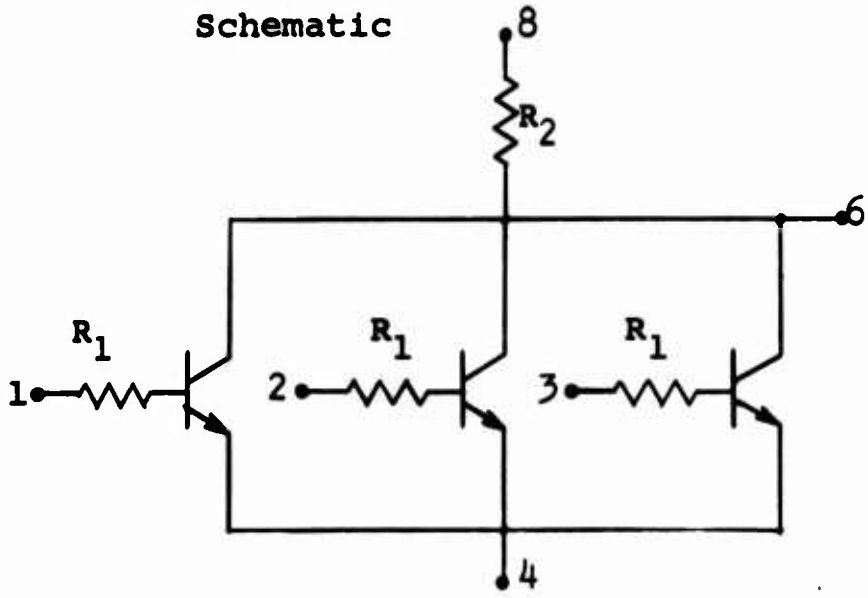

$R_1 \triangleq 450\Omega$
$R_2 \triangleq 640\Omega$

Figure 13. μL-903 Logic and Circuit Diagrams

b. FXR Tests of μL-903 and Mock-up

The Kirtland Air Force Base flash X-ray unit was used to irradiate the μL-903. The tests were made while operating the X-ray tube at a potential of 400 kev. The incident doses were from 200 to 500 milliroentgens with a pulse duration of 2×10^{-7} sec. The dose rates were of the order of 10^6 to 2.5×10^6 roentgens/sec. In addition to irradiating the μL-903 per se, a mock-up of the device was constructed from discrete diffused components as shown in figure 14. The components of the mock-up are similar to those in the microcircuit, each diffused on a p-type substrate. The mock-up circuit was irradiated in whole and in part, thereby giving some insight into those components which showed maximum sensitivity to the X-ray pulse.

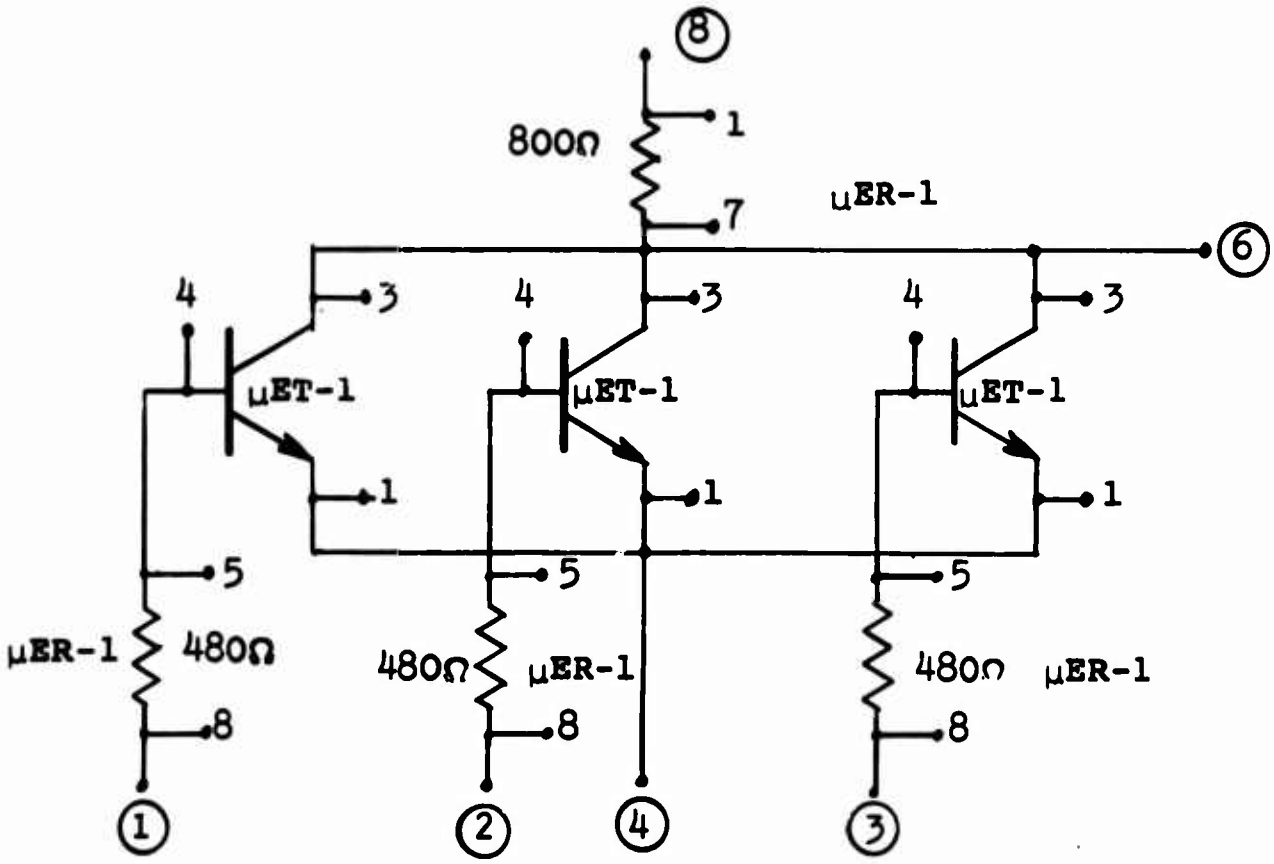

Figure 14. Mock-up of Fairchild μL-903

c. FXR Test Results

Figure 15 shows the transient radiation response of the Fairchild μL-903 circuit and its mock-up when the substrates (p-type) of the circuits were grounded. When the whole circuits are irradiated, the time responses of both circuits are almost identical. The sensitivity of the mock-up circuit to the X ray is about four times that of the μL-903. The explanation for this lies in the fact that the active volumes of the transistors in the mock-up circuit are probably greater.

When the substrate of the μL-903 mock-up is tied to the source of the collector bias voltage (see figure 15 h), the diffusion tail shown in figure 15(a) disappears. The collector-substrate junction is in a forward biased state in this case. Results of a test are shown in figure 15(h). The μET-1 transistor was in the cut-off state during this test to prevent transistor burn-out, because this arrangement essentially puts V_{cc} on the collector of the transistor. It is pointed out that one does not normally operate a circuit with the substrate tied to V_{cc}. This was only a diagnostic procedure.

When the substrate of the μL-903 mock-up is tied to the collector, the collector and substrate are at the same potential. Under operating conditions of this kind, the diffusion tail is about 1/3 of its value when tied to ground. The μET-1 was operated in the cut-off state in this test. The test results are shown in figure 15(g).

d. Comments on FXR Test Results

There exists a negative bias at the substrate-collector junction when the μL-903 is operating under normal conditions. When this condition holds, there is a diffusion tail across the barrier with a time constant of the order of 2.5 μsec. This diffusion tail disappears under zero bias operation. If, then, zero bias operation does not affect circuit performance, it would be preferable, from a point of view of radiation resistance, to operate "nand" elements in that condition. This

μL 903

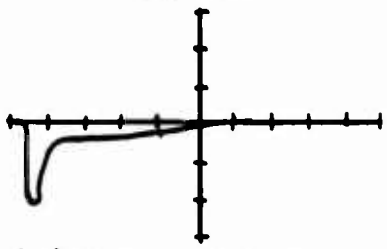

(a) Dose ≈ 500 mr
.002 V/div
.5 μsec/div
Inputs Grounded

μL-903 Mock-up

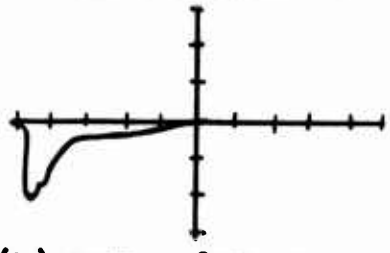

(b) Dose ≈ 200 mr
0.1 V/div
0.5 μsec/div
Inputs Grounded

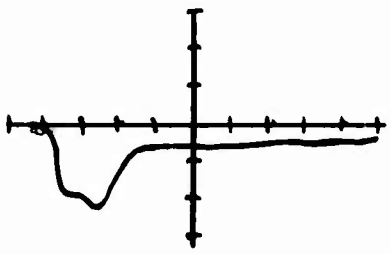

(c) Dose ≈ 500 mr
.002 V/div
0.1 μsec/div
Inputs Grounded

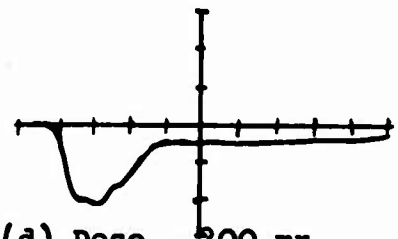

(d) Dose ≈ 200 mr
0.1 V/div
0.1 μsec/cm
Inputs Grounded

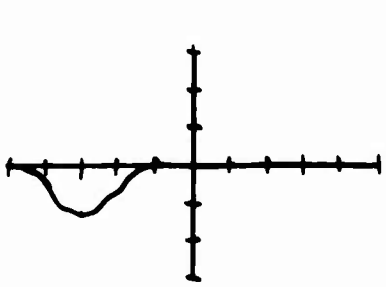

(e) Dose ≈ 500 mr
.002 V/div
0.1 μsec/div
Inputs + 1.5 Volts

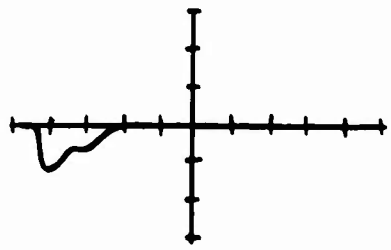

(f) Dose ≈ 200 mr
.005 V/div
0.1 μsec/div
Inputs + 1.5 Volts

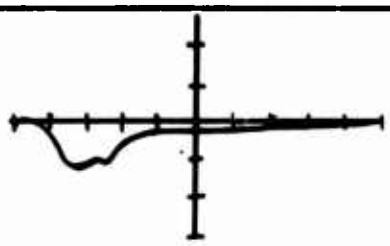

(g) Dose rate ≈ 200 mr
.005 V/cm
0.1 μsec/cm
Inputs Grounded
Substrate Tied to Collector

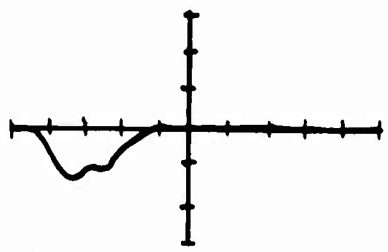

(h) Dose rate ≈ 200 mr
.005 V/div
0.1 μsec/div
Inputs Grounded
Substrate Tied to V_{cc}

Figure 15. Transient Response of the μL-903 "nand" Gate and Its Mock-up

again points out the importance of isolating individual components on the microcircuit chip.

The identical shape of the responses of the two circuits indicates that this mock-up method is better than that of using conventional components. It also appears to be a method of studying more complicated microcircuits in a radiation environment.

e. LINAC μL-903 and Mock-up Tests

The μL-903 and its mock-up (see figure 14) were irradiated at the WSMR LINAC facility. The μL-903 was irradiated by electrons and the mock-up was irradiated by both electrons and gamma rays. All of the tests were performed at the 22-mev electron energy level. Average figures for total dose are about 10 rads (H_2O) for gamma and about 130 rads (H_2O) for electrons.

In table III the results of the μL-903 test are summarized. In most cases, data were taken with no load ($R_L = \infty$), fan-out of one ($R_L = 500\ \Omega$) and maximum fan-out of five ($R_L = 100\ \Omega$). A 1N645 diode was additionally inserted in series with the resistor loads to better simulate the μL-903 input loading. Tests during the irradiation testing at the flash X ray indicated that these resistor-diode combinations adequately represented the μL-903 inputs as loads.

Table III. μL-903 Electron Radiation-Induced Response

	Output response	
Load (R_L)	For $V_3 = 0$:	For $V_3 = 1.5$:
$R_L = \infty$	1.2 volts	1.2 volts
$R_L = 500\ \Omega$	0.4	0.52
$R_L = 100$	0.3	0.28

In this test the input (V_3) was either 0 volt or 1.5 volts. The response was a negative-going pulse lasting only slightly longer than the radiation pulse. As expected, the transient pulse response decreases for increased loading.

The μL-903 mock-up was also irradiated. The results are summarized in table IV. Note in the test results that the collector resistor seems to be the most sensitive element. Two gamma ray exposures were also made. The output peaks were respectively 0.05 volt and 0.04 volt for $R_L = \infty$ and $R_L = 500\ \Omega$. For these two exposures the whole mock-up circuit was irradiated.

Table IV. LINAC Electron Test of μL-903 Mock-up

Load Resistance	$V_3 = 0$	$V_3 = 1.5$
$R_L = \infty$	0.4 volt (collector resistor only irradiated)	0.15 volt (input 2 resistor only)
	0.36 volt (center transistor only irradiated)	
	0.2 volt (input 2 resistor only irradiated)	
$R_L = 500\ \Omega$	0.2 volt center transistor only irradiated)	
		No data
	0.06 volt (input 2 resistor only irradiated)	

4. TI - Series 51 Microcircuits

a. Introduction

Some of the Texas Instruments "Series 51" microcircuits were irradiated with the AFWL 600-KV flash X-ray machine. Tests on the different "Series 51" circuits yielded similar results. Therefore, only the SN 513 "nand" or "nor" gate was studied in detail. A circuit similar to the SN 513 was

was built up using conventional components. The transient radiation effect of the mock-up circuit compared favorably with the SN 513 when the parasitic transistors were taken into account.

b. Test Details

The Texas Instrument SN 512 and SN 513 are six-input "nor" or "nand" logic networks made from diffused silicon. The schematic of the SN 512 and SN 513 is shown in figure 16. Transistors Q_1 thru Q_6 are input transistors; Q_7 is an emitter-follower output transistor. D_1 is part of the emitter-follower output and supplies the biasing for the output transistor. This emitter-follower output circuit is useful in switching applications where a low collector leakage current is required and a negative supply voltage is not available for reverse biasing the base of the transistor. A six-volt bias was used as the operating voltage. Normally the circuit has a rise time of about 150 nsec and a fall time of 1.4 μsec. The circuit operates in the current mode, which means it is always in the active region of operation. It appears that in the current mode of operation the failure mechanisms caused by radiation may be different for the "on" state and "off" state.

When the circuit is operated with the emitter-follower output (SN-513), it has a maximum fan-out capability which will drive 25 other inputs.

This circuit was irradiated in the flash X-ray beam with each exposure delivering about 300 mr at 400 KV. The circuit was operated in the "off" mode by connecting all inputs to ground, and in the "on" mode by applying a positive 1.5 volts to the input of the base circuit for each transistor. Both outputs (8) and (9) of figure 16 were monitored by using a six-foot length of RG-58 cable terminated in a series combination of a 51-Ω resistor and a 47-μμf capacitor at the monitoring oscilloscope. The capacitor was put in so as not to interfere with the DC bias level of the circuit. The results are shown in the first column of figure 17. The maximum

*Dotted portion of circuit pertains to SN 513 only.

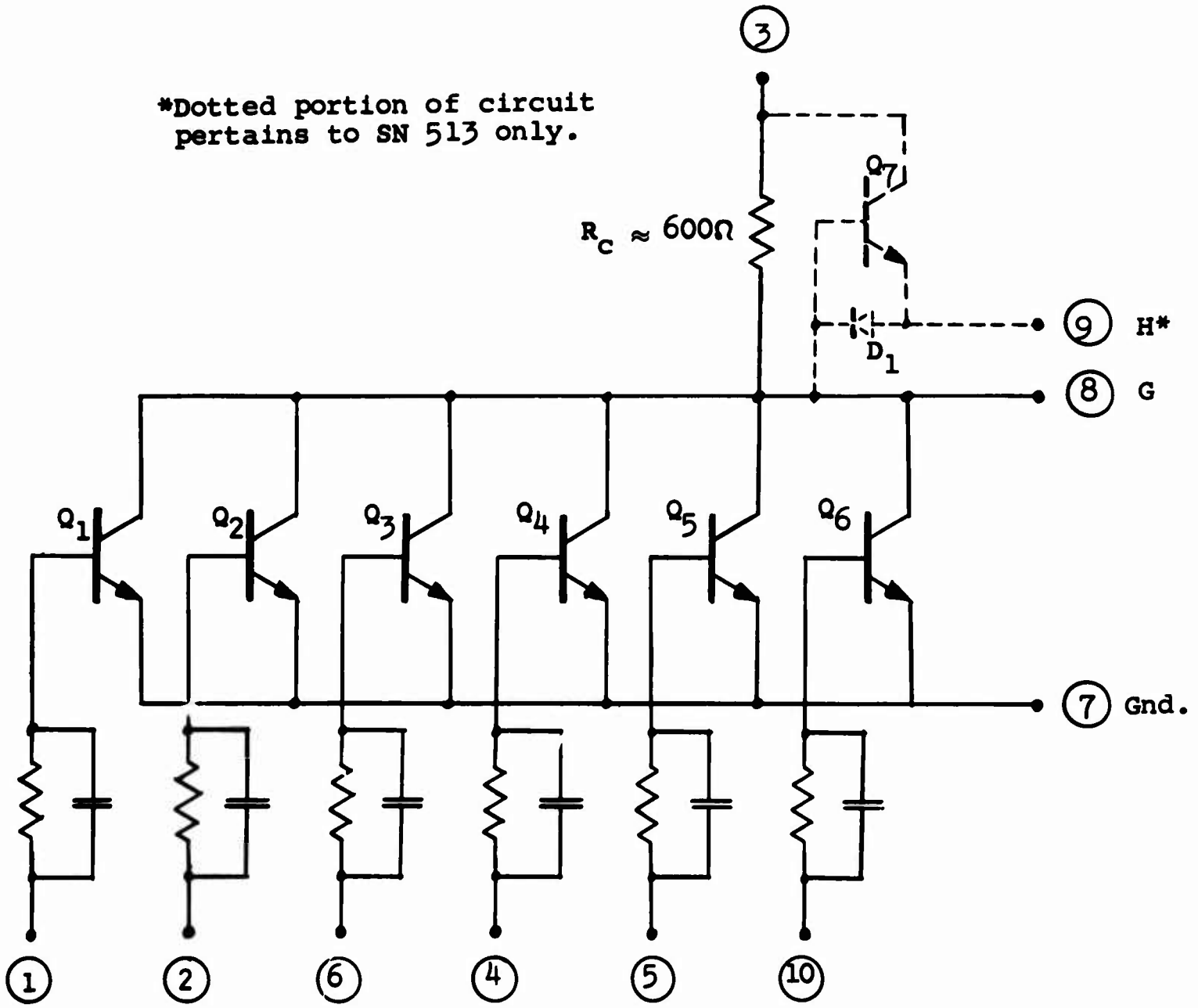

Figure 16. Circuit Diagram of SN 512 and SN 513 Micrologic Circuit

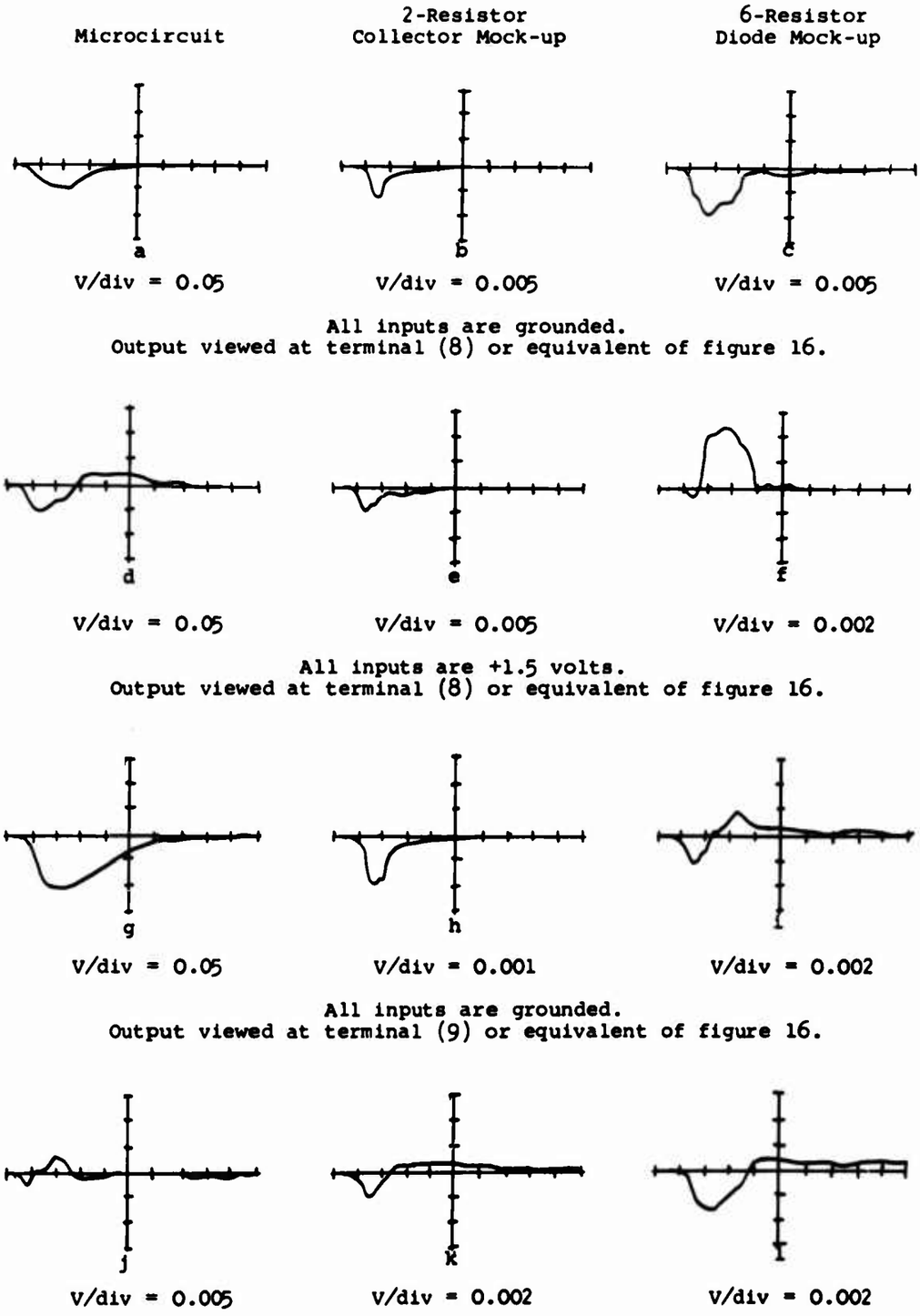

Figure 17. The Response of SN 513 Microcircuit and Mock-up to Flash X-Ray Pulses. All Time Scales are 0.1 μsec/div. The Dose was 300 mr. V_{CC} = 6 Volts. The 50 Ω Cable was Terminated With a 51 Ω Resistor in Series With a 47 μμf Capacitor

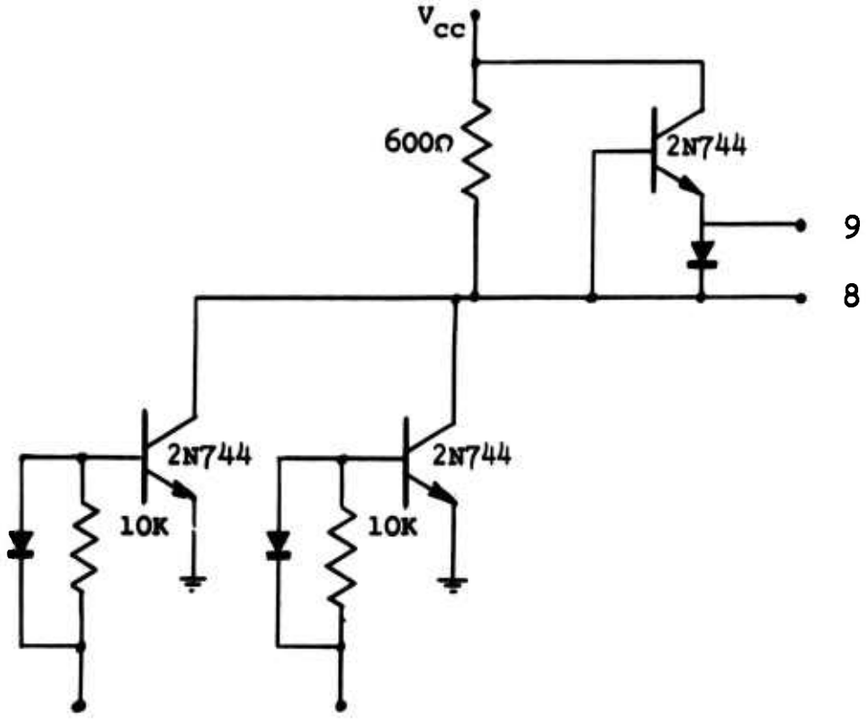

Figure 18. Circuit Representing TI SN 513 Made of Conventional Components

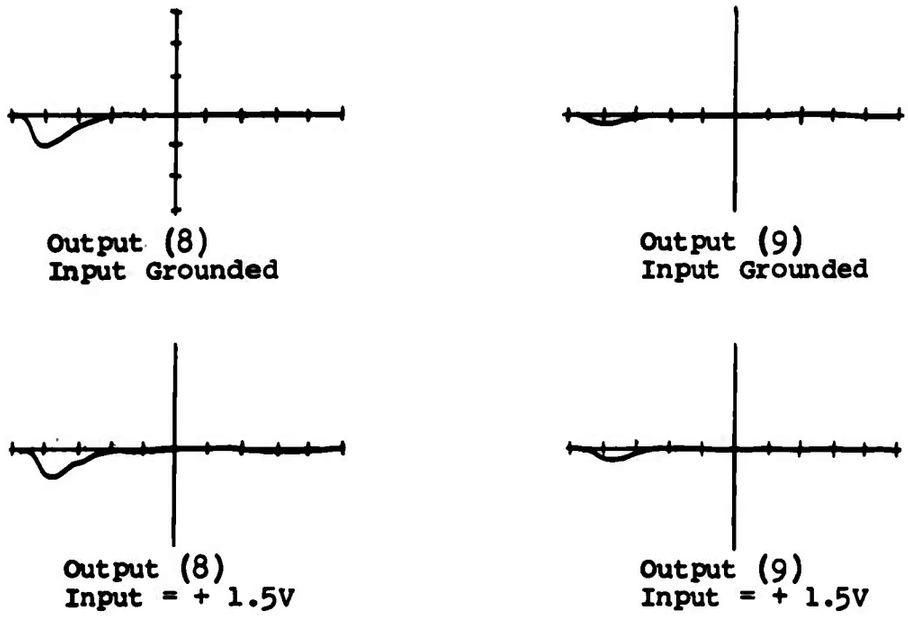

All sensitivities = .005 V/div.

All time scales = 0.1 $\frac{\mu sec}{div}$

Figure 19. Radiation Pulses of SN 513 Mock-up Made of Conventional Components

fan-out at the emitter-follower output (terminal 9) is 25, and at the collector output (terminal 8) it is 5. Since the input resistance of similar circuits is about 1000 Ω, the range of driving point impedance ranges from about 40 Ω to 1000 Ω.

From figure 17 it can be seen that when the gate transistors are in the "on" state the transient pulse has a positive component which is not present when the gate transistors are in the cut-off state.

An SN 513 circuit was built using conventional transistors of the same general type, carbon resistors, and back biased diodes for capacitors. This circuit is shown in figure 18. The results of irradiating the circuit are shown in figure 19. The radiation effect when the inputs are grounded is to try to turn the transistors on. There was a 5-millivolt peak pulse at output (8). The emitter-follower output under the same radiation conditions (300-mr dose) was about 2 millivolts. When the inputs were biased 1.5 volts positive, a similar effect was noticed, indicating that the transistor tended to be driven harder into saturation.

At this point it was obvious that there was something present in the microcircuits that was not in the mock-up circuit because the positive peaks did not occur when the gate transistors were in the "on" state. The next step was to consider the parasitic effects in the microcircuits and, if possible, to introduce them into the mock-up circuit.

c. Parasitic Effects in SN 512 and SN 513

In figure 20 one has a simple transistor circuit which is constructed in microcircuit form as shown in figure 21. Careful examination of figure 21 shows that for both the transistor and the resistor elements there exists a p-n-p sequence of junctions starting from the substrate and ending at the base of the n-p-n transistor.

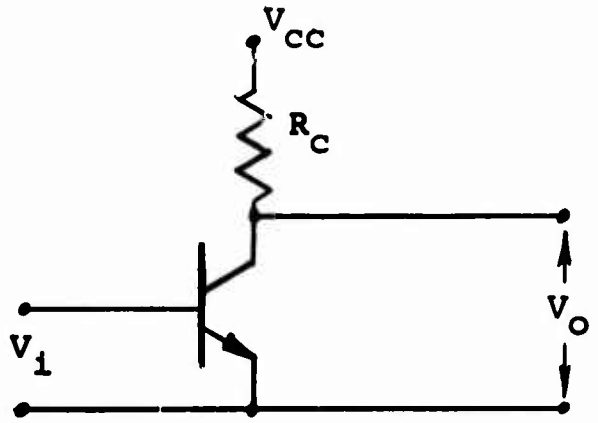

Figure 20. Transistor Circuit Schematic

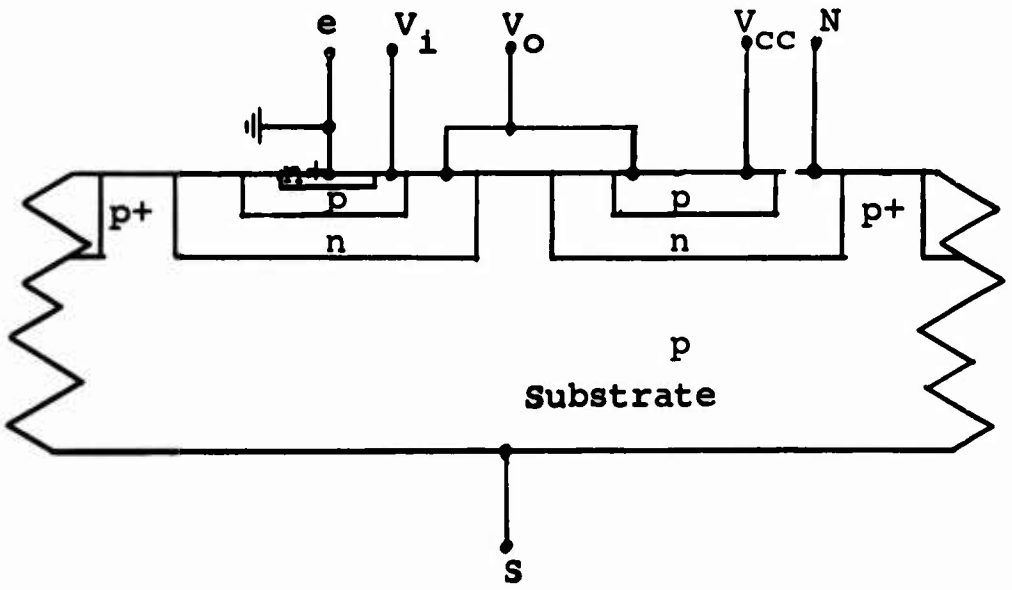

Figure 21. Cross Section of Microcircuits

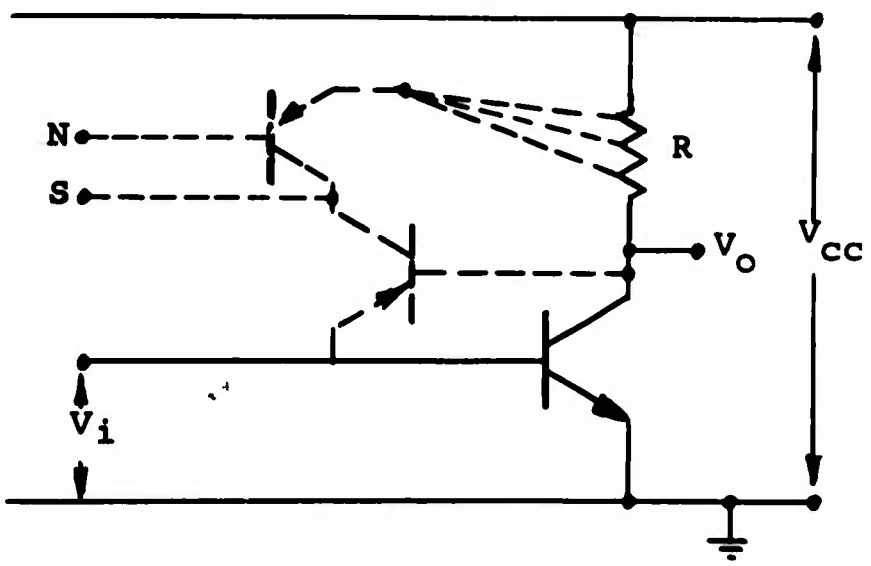

Figure 22. Equivalent Circuit Showing Parasitic Transistors

The terminals marked N and S correspond to the isolation region for the resistor and the substrate. N is usually tied to the V_{cc} terminal of the device, and S is tied to ground. In this case the parasitic transistor associated with the resistor will always be cut off, since its base emitter potential is either zero or reverse biased. The parasitic p-n-p transistor associated with the n-p-n transistor is also cut off, provided the n-p-n transistor is not saturated. The equivalent circuit is shown in figure 22.

Since a current mode switch does not normally saturate, it is not necessary to resort to gold doping in order to avoid parasitic transistor action. Actually, an active p-n-p transistor action will exhibit a beneficial effect here, in that it will prevent the circuit from going into hard saturation if the operation of the circuit is such that it is overdriven.

d. Complete Mock-up of the SN 513

To simulate the parasitic transistors in the SN 513, some 2N995 p-n-p transistors were put in the circuit as shown in figure 23. The collector resistor was divided into two 300-ohm resistors with the parasitic transistor emitter connected between the two. A comparison of the radiation effects between the actual microcircuit and the more complete mock-up is shown in figure 17. Also included for comparison is the six-part collector resistor, back biased diode model. This circuit is shown in figure 24. The simple two collector resistor model produced similar radiation effects except for part "e", figure 17. This positive part of the pulse in the microcircuit is probably due to the capacitance associated with the diffused collector resistor. The six-resistor, back biased diode model had too much capacitance in the back biased junctions to accurately simulate the microcircuit with the diffused collector resistor. A model somewhere between these two would be a fair approximation.

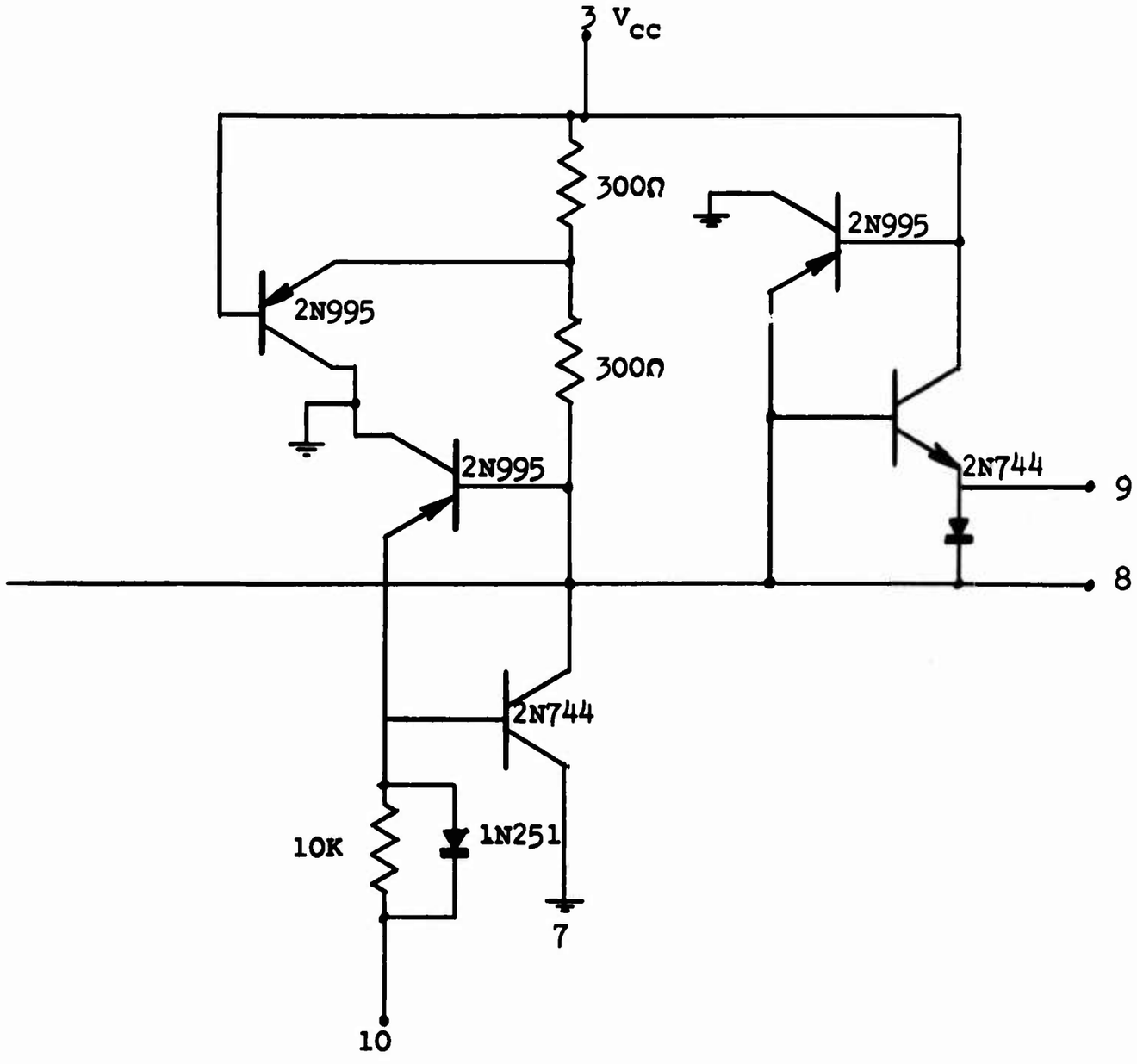

Figure 23. Mock-up Circuit of SN 513 Using Conventional Components and p-n-p Transistors to Represent Parasitic Transistors. The Collector Resistor is Divided Into Two 300 Ω Resistors

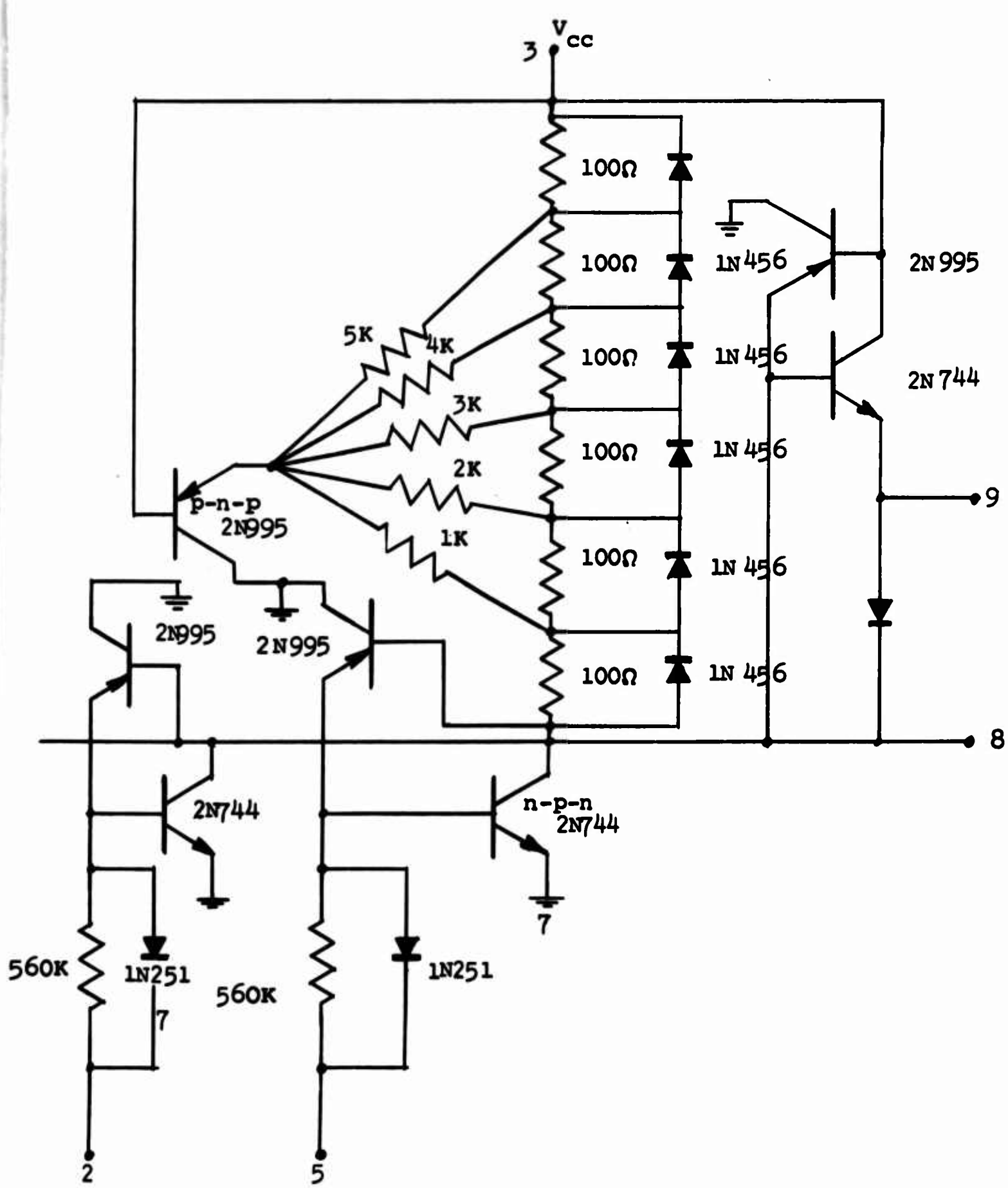

Figure 24. A Six-Resistor and Diode Conventional Component Mock-up Circuit of TI Microcircuit SN 512 (Only Two Inputs Shown)

e. LINAC Test of TI SN 511 and SN 511A

The Texas Instruments SN 511 and SN 511A are diffused silicon microelectronic bistable reset-set flip-flop counter networks. They find applications in digital computer systems, data handling systems, and control systems. The only difference between the SN 511 and SN 511A is in the packaging.

In figure 25 is shown the circuit diagram of the SN 511 and SN 511A. These circuits were irradiated on the LINAC at White Sands Missile Range. The supply voltage used was V_{cc} = 6 volts.

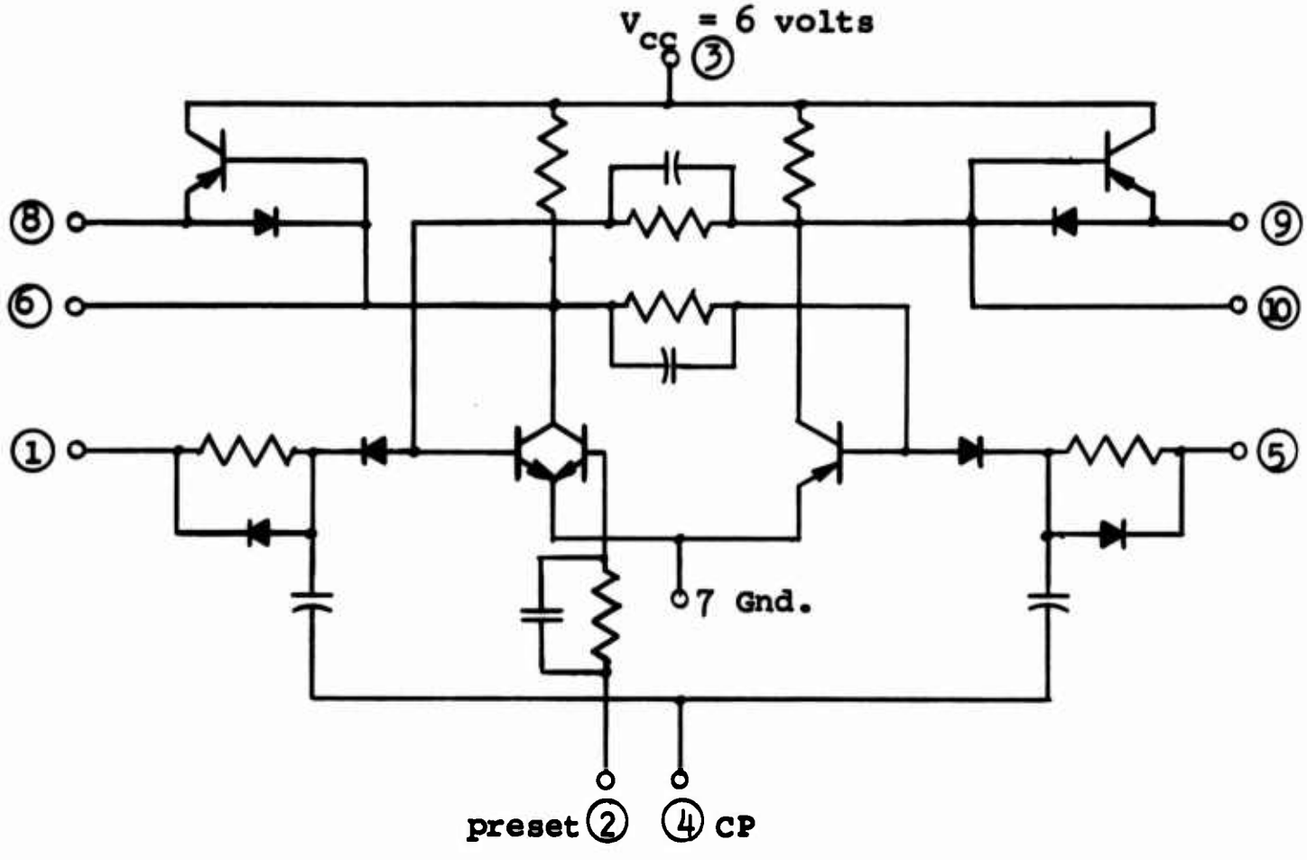

Figure 25. TI SN 511 and SN 511A Schematic

The tests were performed with the output 10 in the down state and output 6 in the up state. The results for both gamma ray irradiation and electron irradiation were essentially the same. Output 10 was a positive output pulse of approximately

7.5-μsec duration. After 7.5 μsec the output 10 returned to its original down state. Output 6 was a negative output pulse with an exponential decay (TC = 15 μsec) back up to its original up state level. The irradiation tended to try to switch the flip-flop but it restored itself to its original state.

The tests were made with no loading on the circuits other than the oscilloscopes. In table V the peak values of the output pulses are shown.

Table V

SN 511 and SN 511A Radiation-Induced Outputs

Device	Radiation	Output - 10 Peak	Output - 6 Peak
SN 511	Gamma	+3.0 volts	-2.7 volts
SN 511	Electrons	+2.0	-2.7
SN 511A	Electrons	+2.6	≈ -4

5. Signetics SU-315K

a. General Information

The SU-315K is an integrated "nor" circuit fabricated within a monolithic silicon substrate by the planar technique. The circuit is designed for use in high-speed logic applications and is designed for a maximum of flexibility. Its input and output characteristics are compatible with those of other Signetic SU-300 series circuits. Its electrical features include high noise immunity, high speed with capacitive loading, and high fan-out.

The SU-315K is a dual 3-input "nor" gate. Average propagation time delays run from 20 to 40 nsec depending upon the loading. This gate has a maximum fan-out capability of 12 source loads plus 5 sink loads.

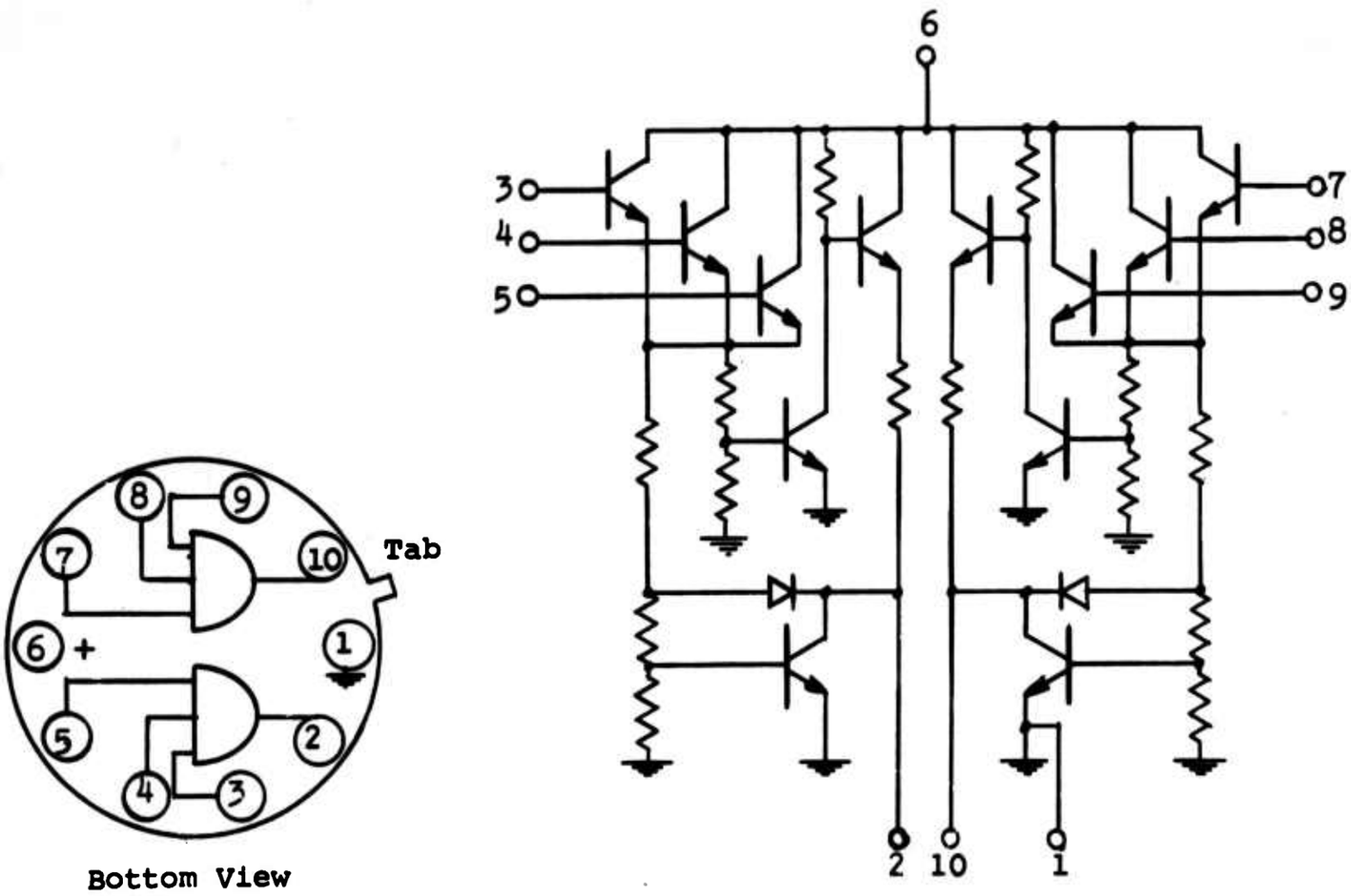

Figure 26. SU-315K Dual "Nor" Gate Schematic

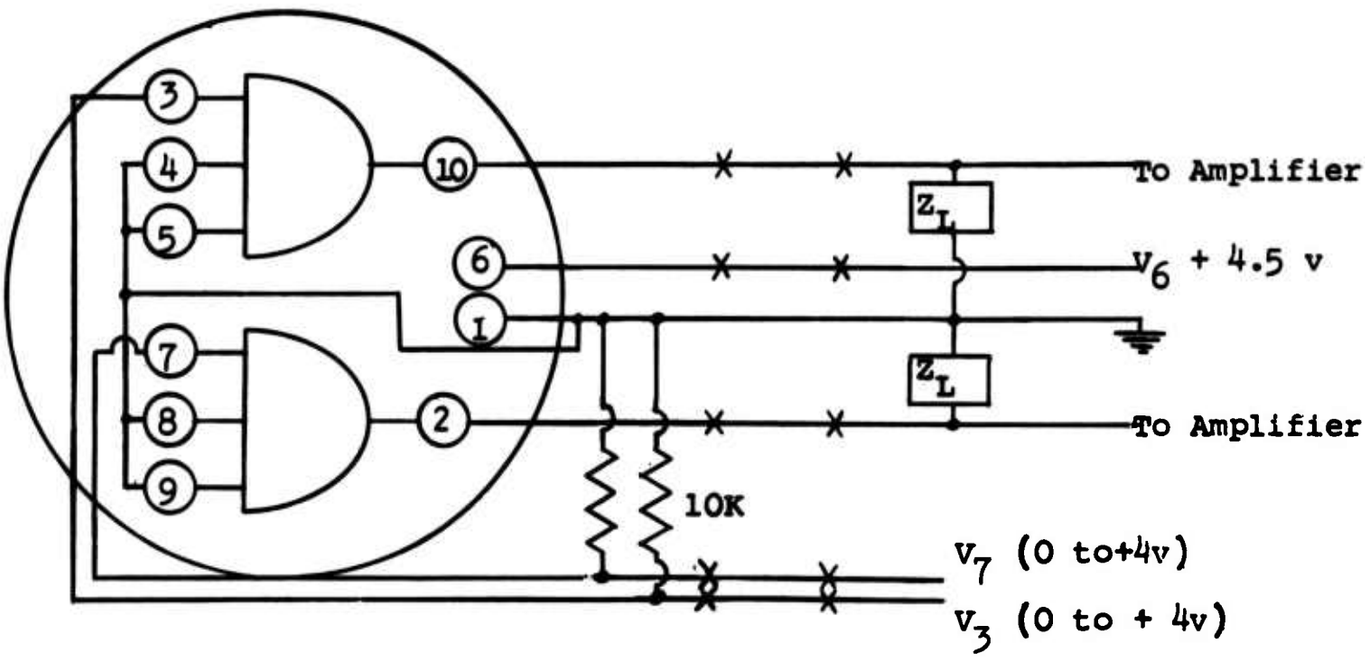

Figure 27. SU-315K Tesc Circuit

b. Test Circuit

Figure 26 shows the schematic of the SU-315K dual "nor" gate. There are two identical circuits within the same substrate. The half of the circuit associated with inputs 3, 4, and 5, as well as output 10, was actually tested. Inputs 3, 4, and 5 control the logic output state of output 10. V_6 is the supply voltage for the transistor collectors. The absolute maximum voltage rating for all the inputs is 5.5 volts.

Figure 27 shows the actual test circuit. Inputs 4 and 5 were grounded, and the logic state of output 10 was controlled by input 3. The logic "1" output voltage is greater than 3.3 volts for $V_3 \geq 1.4$ volts. The logic "0" output voltage is a maximum of 0.6 volt for $V_3 = 0$. Loading impedances, Z_L, were placed on the output to simulate varying fan-out conditions.

c. FXR Test Results

The SU-315K was tested on the AFWL flash X-ray system. The tests were performed at the 400-KV level with a 0.2-μsec pulse width. This yields an approximate dose rate of 2×10^6 roentgens/sec.

Table VI summarizes the SU-315K FXR test results. As shown in the table, shots were taken for varying values of V_6, V_3, and Z_L.

Shots 695, 690, and 694, in order, correspond to increasing values of Z_L. As expected, increasing values of Z_L result in an increase in the negative peak value of the transient output V_{10} and an increase in the time constant of the decay. Shots 691, 697, and 698 indicate that in the logic "1" state this circuit is highly radiation resistant to gamma dose rates up to 2×10^6 roentgens/sec. For shot 692 the SU-315K was set to just below the switching level (from "0" to "1") by experimentally adjusting V_3 to 1.3 volts. Irradiation at this level produced maximum transient output for a fixed load. Shots 690, 692, and 691 indicate that the transient output increases as V_3 is increased up to the point of switching. Increasing

V_3 beyond that point results in the transient output being reduced to a negligible value. Shots 690 and 696 indicate that the transient output decreases (within certain limits) as the supply voltage (V_6) is increased. Shot 705 was made with the device behind a lead brick. As this shot resulted in only a small output, it can be concluded that the stray voltage pick-up contribution to the output pulses is correspondingly small.

Table VI

SU-315K FXR Test Results

Shot No.	V_6	V_3	Z_L	Transient Peak of Output V_{10}
690	4	0	1.6 K ‖ 75 pf.	0.02 volt
691	4	4	1.6 K ‖ 75 pf.	Negligible
692	4	1.3	1.6 K ‖ 75 pf.	0.03 (V_3 set just below switching level)
694	4	0	1 meg.	0.025 long decay
695	4	0	500 Ω	0.01
696	6	0	1.6 K ‖ 75 pf.	0.015
697	6	4	1.6 K ‖ 75 pf.	Negligible
698	0	4	1.6 K ‖ 75 pf.	Negligible
705	0	0	1.6 K ‖ 75 pf.	0.001 (device behind lead brick)

d. LINAC Test Results

The SU-315K was also tested on the WSMR LINAC test facility. The unit was subjected to gamma radiation with the LINAC at the 22-mev electron energy level. Average figures for total dose per shot were about 10 rads (H_2O) for the gamma ray mode. The dose rate may be calculated approximately by dividing the total dose by the radiation pulse width. For the gamma LINAC this result is 10 rads divided by 0.5 μsec or approximately 2×10^7 rads/sec.

Table VII gives the results of the gamma LINAC testing. The results indicate that at this high radiation level the transient output response is independent of the logic state and input voltage (V_3). Further confirmation of this conclusion would be interesting if additional tests are scheduled on the LINAC.

Table VII

SU-315K LINAC Test Results

Shot No.	V_6	V_3	Z_L	Transient Peak of Output V_{10}
269	4.5 volt	0 volt	Open	0.05 volt
270	4.5	2	Open	0.05
271	4.5	3.5	Open	0.05

e. Summary of SU-315K Testing

The SU-315K is insensitive to gamma radiation while in the logic "1" state up to at least 2 x 10^6 roentgens/sec. It is sensitive to radiation at this level while in the logic "0" state.

At high radiation levels the SU-315K becomes sensitive to gamma radiation irrespective of its logic state.

6. FXR Test of Crystalonics 2N3084 FET

The 2N3084 is a silicon epitaxial junction N-channel field effect transistor which is specifically designed for use in high-impedance amplifiers that require ultra-low gate leakage currents. The absolute maximum gate leakage is 0.1 nA. It is manufactured by the epitaxial junction process which combines the advantages of alloy, epitaxial, and planar techniques. The device is bed mounted, oxide passivated, and utilizes a gold bonding process which eliminates the "purple plague."

The 2N3084 was tested at the AFWL flash X-ray facility. Both the gate current and the drain current radiation-induced transient responses were recorded. The test circuit is shown in figure 28.

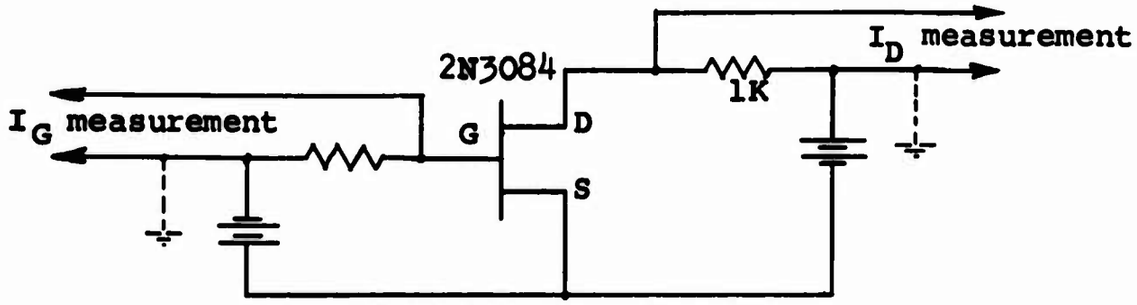

Figure 28. 2N3084 Test Circuit

In table VIII the test results for the gate current, I_G, are presented. The transient response was a negative pulse lasting slightly longer than the radiation pulse. The test results indicate that the transient peak of I_G increases as V_{GS} decreases and that the peak of I_G increases as V_{DS} decreases.

Table VIII

Peak Value of Gate Current from 2N3084

V_{DS}	V_{GS}	Radiation	I_G Peak
10 volt	1 volt	yes	0.013 ma
10 volt	2	yes	0.011
10 volt	3	yes	0.010
10 volt	4	yes	0.010
2	4	no	0.002
2	2	yes	0.013

In table IX the test results for the drain current, I_D, are presented. The transient response was a negative pulse lasting slightly longer than the radiation pulse. The test

results indicate that the transient peak of I_D increases with increasing V_{DS} at the V_{GS} = 4 volt level, and I_D decreases with increasing V_{DS} at V_{GS} = 0 volt level.

Table IX

Peak Value of Drain Current (I_D)

V_{GS}	V_{DS}	Radiation	I_D Peak
	10 volt	no	0.0015 ma
0 volt	10	yes	0.0055
	15	yes	0.0035
	20	yes	0.0025
4	10	yes	0.002
	20	yes	0.004

7. FXR Test of Diffused Resistor

A silicon, phosphorous, diffused resistor was obtained from the microcircuit laboratory at Rome Air Development Center, Griffis AFB, New York. The impurity concentration was $10^{20}/cm^3$, and about 1.5 to 2 microns deep. The resistance was 4 ohms per square cm. There was a 100-ohm resistance between points 1 or 2 and 3, and no connection to the substrate. See figure 29.

When irradiating this resistor with a dose rate of 5×10^6 r/sec, or a total dose of about 1 r in air, a peak transient current of 16 microamperes was obtained. The current pulse followed the X-ray pulse except for a tail. This tail was initially 2 microamperes and decayed out in about 3 μsec. The same pulse was observed when the resistor was irradiated in oil to eliminate any possible air effects. The oscilloscope trace is shown in figure 30. The diffused resistors appear to have a large transient current similar to that observed in microcircuits; the current pulse is probably caused by the isolation junction.

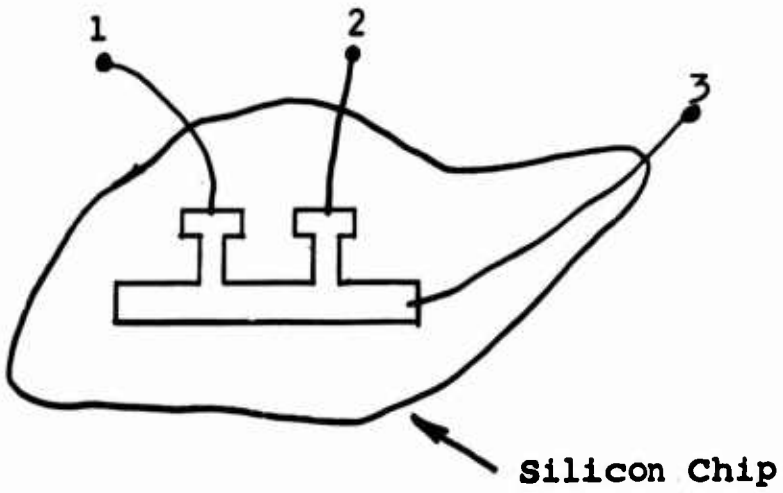

Figure 29. Silicon Diffused Resistor

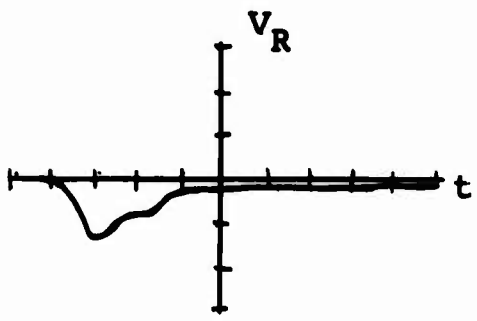

Sensitivity = .01 V/div

Time = 0.1 $\frac{\mu sec.}{div.}$

Figure 30. Transient Radiation Response of a Diffused Silicon Resistor

8. Thin-Film Nichrome Resistors

Several thin-film nichrome resistors ranging in resistance value from 16 ohms to 11.4 K were irradiated in the 600-KV flash X ray. No effect was observed on the smaller resistance values in a radiation field up to 5×10^6 r/sec. The 11.4-K resistor has a radiation response in air that is similar to a carbon resistor. The response is due to air ionization effects. When the 11.4-K nichrome resistor was irradiated in oil, most of the effect observed in air disappeared. There was a small pulsed response of about 2.5 microamp peak and 1 microsecond in duration. This is (most likely) secondary emission of electrons and the resulting replacement current.

9. The WSMR Gamma LINAC Experimental Results on Hall Devices

a. General Results

The theory of the operation of Hall devices in a radiation environment was developed and reported in AFWL Report No. TDR-64-38. However, the experimental data was not complete until the present WSMR gamma LINAC was made available.

The theory predicted that there should be no radiation effects for the constant voltage mode of operation and that the Hall voltage should vary as a function 1/n for the constant current bias condition, where n is the number of free carriers per unit volume of the Hall material.

The thin-film Hall devices were found to be highly radiation resistant as was predicted in the theory. There were no radiation effects observed for dose rates up to 10^{10} r/sec when the devices were operated in the constant voltage mode. This is the operating mode that should be used for any Hall device where gamma radiation environments or extreme temperature changes might be encountered.

When operating Hall devices in the constant current mode, the observed effects followed closely those predicted in the above report. The percentage change in Hall voltage for the

constant current case is given in table X. The results from the LINAC experiments are shown in figures 31 and 32 for the HS-51 and figures 26, 27, and 33 for the Beckman device.

Table X

Hall Voltage Change (Constant Current) During Irradiation

Dose Rate $\dot{\gamma}$ Roentgen/Sec	ΔV_h %					
	Device HS-51		Device 335		Device 331	
	exp.	theory	exp.	theory	exp.	theory
10^8	0	9.1×10^{-8}	0	-	0	-
10^9	0	.01	0	-	0	-
10^{10}	5.9 to 9	9	0.75	0.8	0	0.187
10^{11}	-	50	-	7.5	-	3.44
10^{12}	-	90	-	44.8	-	15.76
10^{13}	-	99	-	89	-	65.28

The Hall voltage change in a pulsed radiation environment for the constant current mode of operation is given in figure 31a. The percentage change in Hall voltage was 5.5 percent at a dose rate of 8.2×10^9 r/sec. When the magnetic field was removed, no change was observed as can be seen in figure 31b. And when the magnetic field is reversed, tne ΔV_h (change in magnitude of Hall voltage) is in the opposite direction as predicted. In figure 31c the percentage change was 9 percent, for a dose rate of 9.2×10^9. If the bias current is reversed, the direction of the Hall voltage is also reversed and a similar result was obtained (figure 32a). The theory predicted no change in Hall voltage for a constant voltage operating mode and this is what was observed as can be seen in figure 32b. Referring to the constant bias current case, theory demands that a change of input impedance equal the change in Hall voltage. This was observed and the results are shown in figure 32c. The radiation

a.

B = 4 kilogauss N-S

I_B = 300 ma (+ -)

$\dot{\gamma}$ = 8.2 x 10^9 r/sec

t = 2 μsec/cm

%δV_h = 5.5%

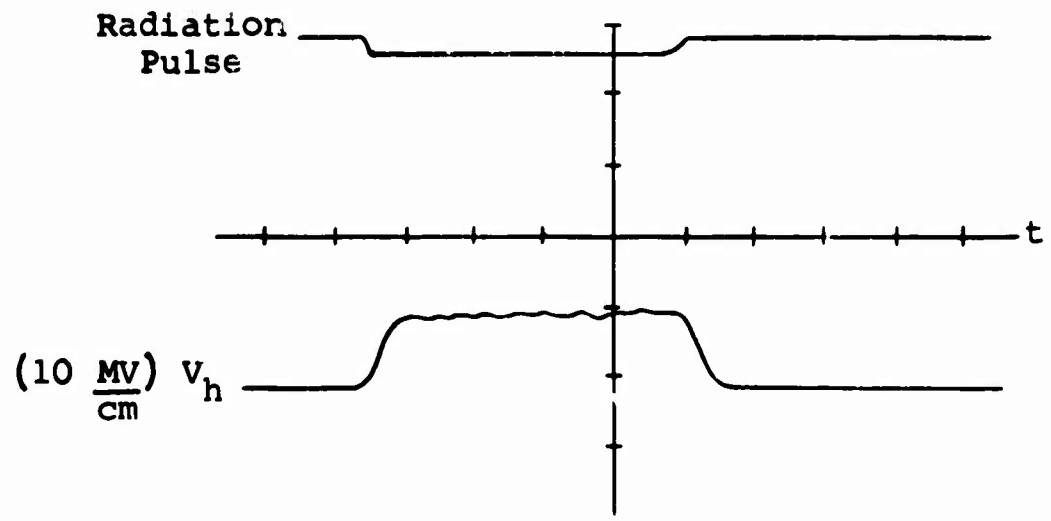

b.

B = 0

I_B = 300 ma

$\dot{\gamma}$ = 8.1 x 10^9 r/sec

t = 2 μsec/cm

δV_h = 0

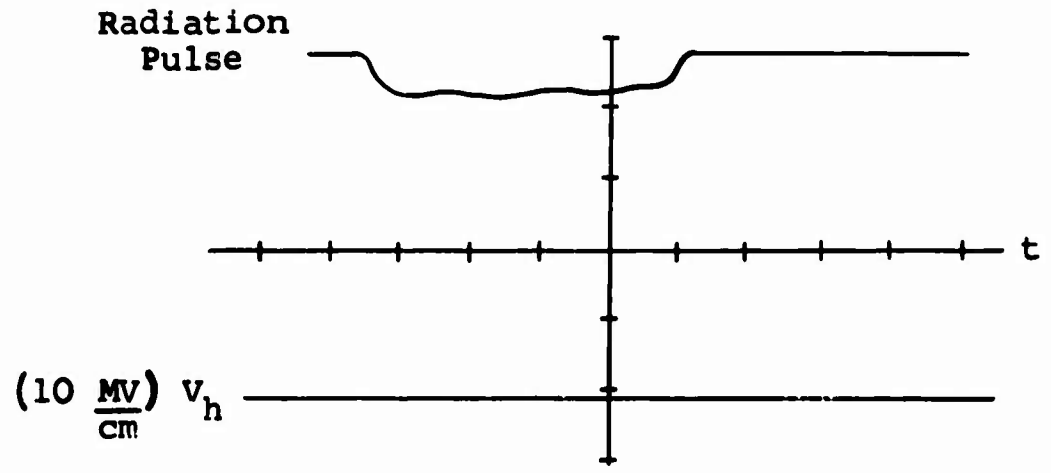

c.

B = 4 kilogauss

I_B = 300 ma

$\dot{\gamma}$ = 9.2 x 10^9 r/sec

t = 2 μsec/cm

%δV_h = 9%

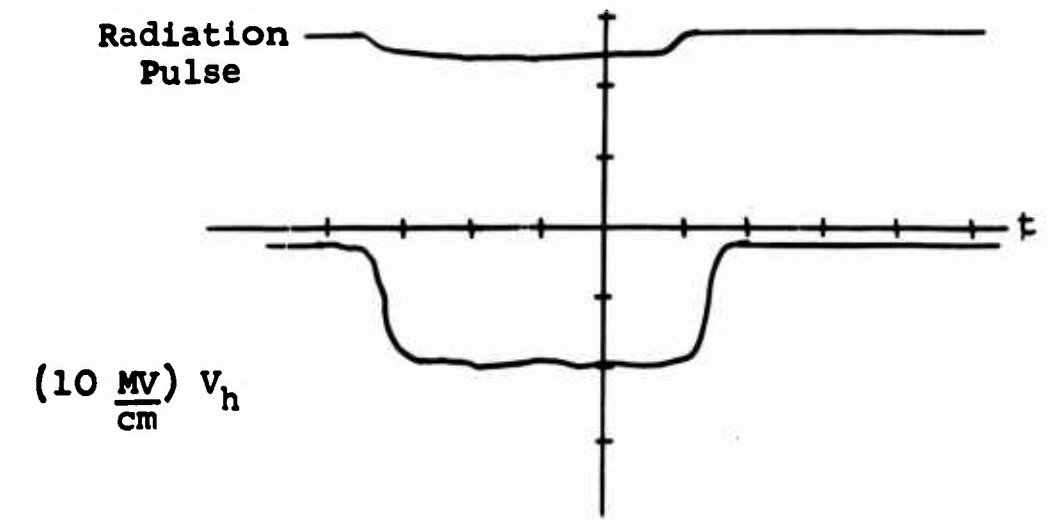

Figure 31. Radiation Effect on the Ohio Semiconductor HS-51 Hall Device

a.

B = 4 kilogauss S-N

I_B = 300 ma (- +)

$\dot{\gamma}$ = 9 x 10^9 r/sec

t = 2 μsec/cm

$\%\delta V_h$ = 9%

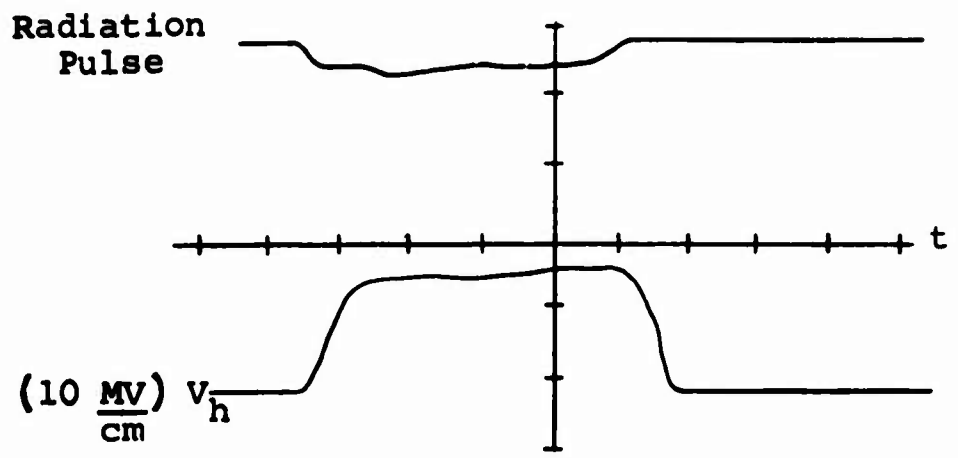

b.

B = 4 kilogauss S-N

V_B = 0.3 Volts

$\dot{\gamma}$ = 9 x 10^9 r/sec

t = 2 μsec/cm

δV_h = 0

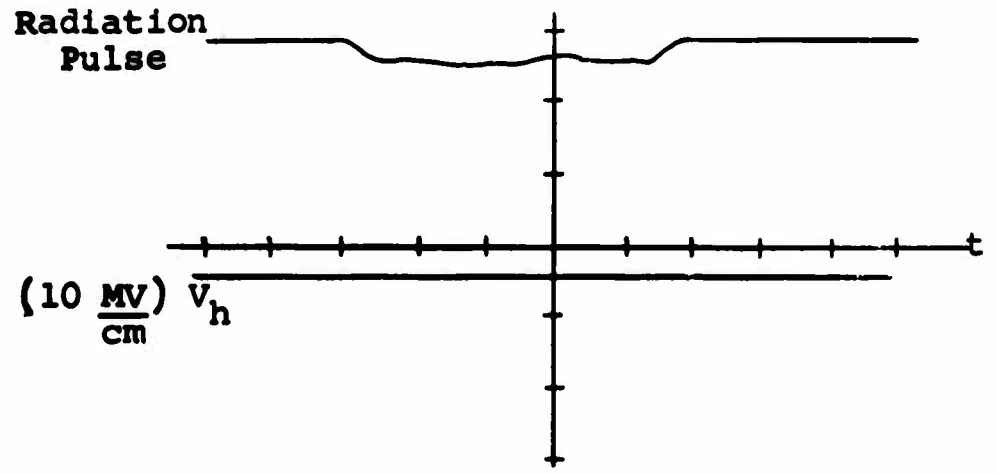

c.

B = 4 kilogauss S-N

$\dot{\gamma}$ = 9 x 10^9 r/sec

δZ_{in} = 10%

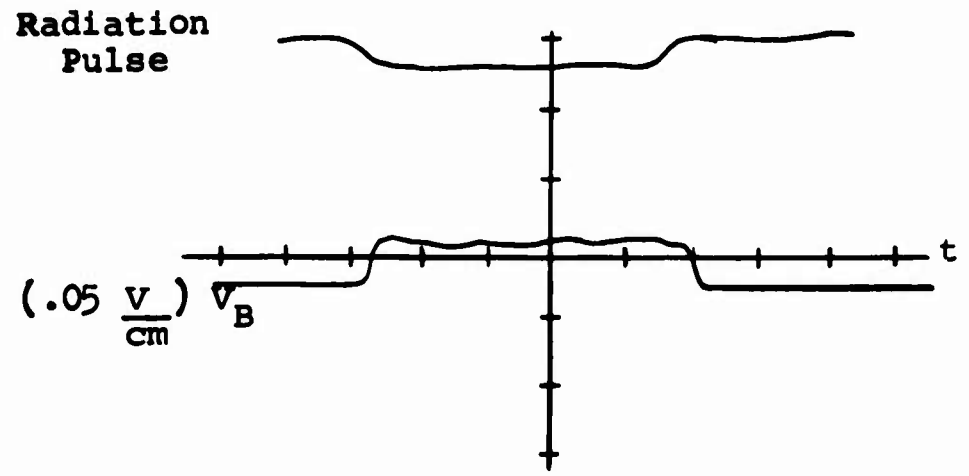

Figure 32. Radiation Effects on the Ohio Semiconductor HS-51 Hall Device

a.

B = 4 kilogauss

I_B = 20 ma

Air Gap = 0.7 cm

$\%\delta V_h$ = 1.37%

$\dot{\gamma} = 10^{10}$ r/sec

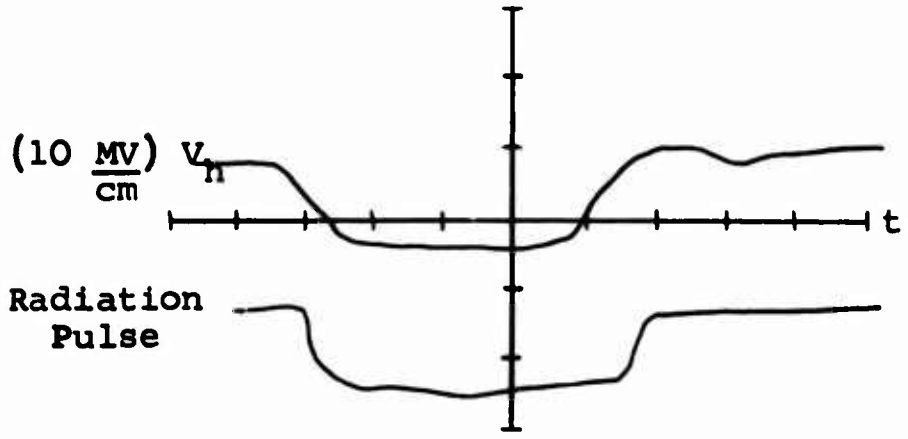

b. Constant Voltage Bias

$\delta V_h = 0$

$\dot{\gamma} = 10^{10}$ r/sec

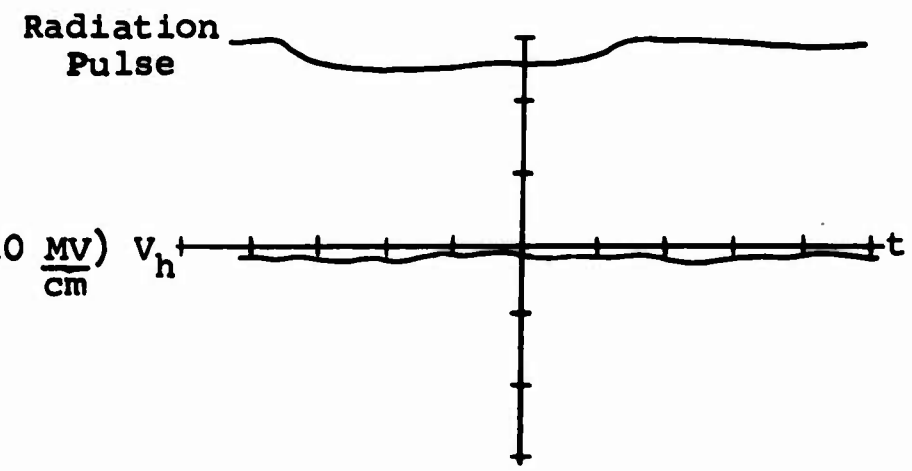

c. Input Current

δI_B = 150 μa

or

0.75%

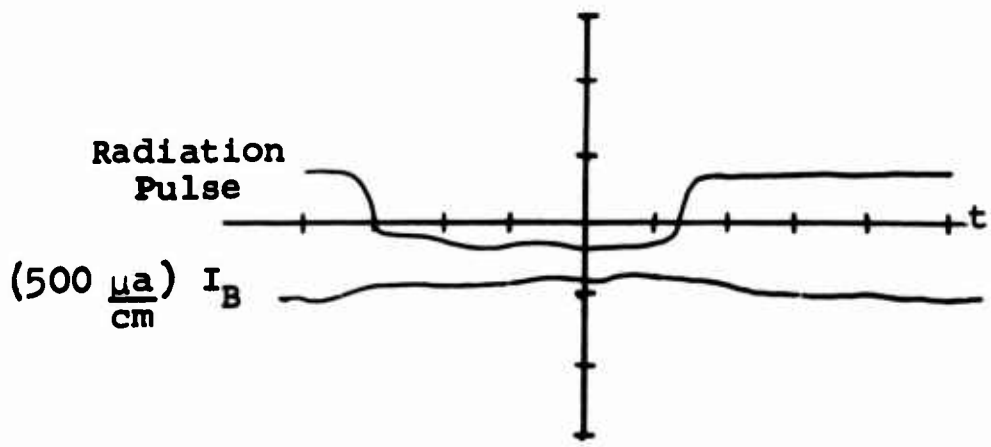

Figure 33. Radiation Effect on Beckman 335 Device

pulse as monitored by a photodiode and plastic scintillator is also shown on each picture.

It was found when irradiating the thin-film devices that a much larger effect is observed when a small air gap is used. This indicates that secondary electrons knocked out of the magnet have an effect on the Hall device. If the oscillographs for the Beckman 335 device are observed, a 28-MV change is recorded at the Hall terminals. In this case, the device was fitted closely in the air gap of the magnet. When the device was mounted in the center of a three-centimeter air gap, the ΔV_h decreased to 1.5-MV change or 0.75-percent change, which agreed with the values predicted from theory (Table X). The thin-film devices also have a larger input impedance and the current did not remain constant during the pulse. The impedance of the current source was not quite large enough to hold the current constant. As can be seen from figure 33c, there was a change in input current of about 150 microamperes during the radiation pulse. Figure 33a shows the transient effect when an air gap of 0.7 centimeter was used. The change in Hall voltage is 1.37 percent in this case and is higher than the predicted value of 0.8 percent indicating that secondary electrons are present, but not as much as in the smaller air gap. Figure 33b indicates no change in Hall voltage for the constant voltage operating mode which is the same as observed for the HS-51.

Similar results were obtained using the Beckman 331 device. This is a device which is five microns thick, and the predicted ΔV_h at 10^{10} r/sec is less than 0.19 percent. There was no change observed for this device.

b. Conclusions

A theory was developed that predicts the transient radiation effects on Hall devices. These effects depend on the type of biasing used. Experimental results agree with the theory for both constant voltage and constant current modes of operation. The theory for the constant voltage case predicted no change in Hall voltage and none was observed. The highest dose

rate available was 10^{10} r/sec. Therefore, whenever high-intensity gamma radiation is a factor in the environment, the constant voltage mode of operation should be used. This would also be true for any other factor in the environment which would cause a change in carrier density, such as large temperature variations.

The Hall voltage was found to vary as 1/n for the constant current mode of operation. At a dose rate of 10^{10} r/sec a maximum change in Hall voltage of 9 percent was predicted for the Ohio semiconductor HS-51 device. A change of 5.5 percent to 9 percent was observed.

The high-impedance thin-film devices are better suited for constant voltage drive than the bulk-type devices. They are also more radiation resistant. At a dose rate of 10^{10} r/sec they had a percentage change in Hall voltage of at least one order of magnitude less than the bulk-type devices in the constant current mode of operation.

10. Summary of Conclusions

Several conclusions may be drawn from this research:

(1) In general, the EPIC process XC-201 is less sensitive than the MC-201 to transient radiation effects. For gamma radiation up to 2×10^6 roentgens/sec these results are conclusive. For electron radiation at the 22-mev level the difference is less pronounced.

(2) Testing of the μL-903 indicated that the substrate-collector junction introduced a diffusion tail in the transient radiation response which can be reduced by elimination of the isolation junction. The successful mocking up of the μL-903 showed this technique to be a useful one for research.

(3) Mock-up circuits for the SN 513 required the inclusion of the parasitic elements for accurate simulation.

(4) The SN 511 and SN 511A flip-flops were irradiated. The irradiation tended to try to switch the flip-flop, but it restored itself to its original state.

(5) The SU-315K is insensitive to gamma radiation while in the logic "1" state--at least up to 2×10^6 roentgens/sec. It is sensitive to radiation at this level while in the logic "0" state. At high radiation levels the SU-315K becomes sensitive to gamma radiation irrespective of its logic state.

(6) The Crystalonics 2N3084 field effect transistor was tested on the 600-KV flash X ray. The test results indicate that the transient peak of I_G increases as V_{GS} decreases and that the peak of I_G increases as V_{DS} decreases. The test results also indicate that the transient peak of I_D decreases with increasing V_{DS} around the $V_{GS} = 0$ volt level, and that I_D increases with increasing V_{DS} at the $V_{GS} = 4$ volt level.

(7) Diffused resistors have a large transient current similar to that observed in many microcircuits. The current pulse is probably caused by the isolation junction.

(8) The transient radiation response of thin-film nichrome resistors is primarily due to air ionization effects.

(9) Thin-film Hall devices were found to be highly radiation resistant as was predicted by the theory. There were no radiation effects observed for dose rates up to 10^{10} r/sec when the devices were operated in the constant voltage mode. This is the operating mode that should be used for any Hall devices where gamma radiation environments or extreme temperature changes might be encountered.

SECTION III

PRELIMINARY DISCUSSION OF ENGINEERING MODELS FOR THIN-LAYERED DEVICES

1. Introduction to Fundamentals of Diffusion Theory

The purpose of this discussion is to establish very generally the basis of the diffusion theory used in semiconductor device analysis. Diffusion theory is obtained from the more rigorous transport theory by making simplifying approximations to the Boltzmann transport equation. This procedure leads to the diffusion, or continuity, equation for holes and electrons in semiconductors. The assumptions made in the development of the theory are then shown to be false in their application to thin-layered devices.

2. The Distribution Function

The various electronic transport properties of a conductor, or semiconductor, can be found if the behavior of the electronic distribution function can be determined under the influence of externally applied fields. The electronic distribution function, $f(\vec{r}, \vec{k}, t)$, gives the probability at time t of the occupation of the energy state corresponding to the wave vector $\vec{k}$ at a point in the crystal given by the position vector $\vec{r}$. More rigorously, since f is a continuous probability density function, one should say that the quantity

$$f(\vec{r}, \vec{k}, t)d\vec{r}\ d\vec{k} \tag{23}$$

is the probability at time t of particles occupying the volume element $d\vec{r}$ which is located by the position vector $\vec{r}$ and in the element of wave vector space $d\vec{k}$ about the wave vector $\vec{k}$. Using either definition, it should be clear that the function f gives one the information necessary to determine the manner in which particles change energy and position within the crystal.

3. The Boltzmann Transport Equation

The basic problem in the study of conductors and semiconductors is the determination of the function f under the influence of externally applied fields (electric, magnetic, and thermal). This problem is usually attacked through the Boltzmann transport equation which described the manner in which the particles behave in the material.* Fundamentally, the transport equation postulates that the total time rate of change of $f(\vec{r}, \vec{k}, t)$ is caused by particle collisions with the fixed atoms of the lattice. Mathematically this is stated as

$$\frac{df}{dt} = \left.\frac{\partial f}{\partial t}\right|_{coll.} \tag{24}$$

Before considering the collision terms, one should look at the total derivative of f given by

$$\frac{df}{dt} = \frac{\partial f}{\partial x}\frac{dx}{dt} + \frac{\partial f}{\partial y}\frac{dy}{dt} + \frac{\partial f}{\partial z}\frac{dz}{dt} + \frac{\partial f}{\partial k_x}\frac{dk_x}{dt} + \frac{\partial f}{\partial k_y}\frac{dk_y}{dt} +$$

$$\frac{\partial f}{\partial k_z}\frac{dk_z}{dt} + \frac{\partial f}{\partial t} \tag{25}$$

where $\vec{r}$ and $\vec{k}$ have been replaced by their components in rectangular coordinates. Interpreting dx/dt, dy/dt, and dz/dt as components v_x, v_y, and v_z, respectively, of the particle velocity $\vec{v}$, and dk_x/dt, dk_y/dt, and dk_z/dt as components of a vector $d\vec{k}/dt$ one can write equation (25) as

$$\frac{df}{dt} = \vec{v} \cdot \nabla_{\vec{r}} f + \frac{d\vec{k}}{dt} \cdot \nabla_{\vec{k}} f + \frac{\partial f}{\partial t} \tag{26}$$

*For more detail see the books by Wilson (reference 20), Sietz (reference 21), and Smith (reference 22), and the article by Blatt (reference 23).

where

$$\nabla_{\vec{r}} f = \frac{\partial f}{\partial x}\,\vec{a}_x + \frac{\partial f}{\partial y}\,\vec{a}_y + \frac{\partial f}{\partial z}\,\vec{a}_z$$

$$\nabla_{\vec{k}} f = \frac{\partial f}{\partial k_x}\,\vec{a}_x + \frac{\partial f}{\partial k_y}\,\vec{a}_y + \frac{\partial f}{\partial k_z}\,\vec{a}_z$$

with $\vec{a}_x$, $\vec{a}_y$, and $\vec{a}_z$ unit vectors in the respective directions. Since electrons in a crystal behave as free particles with energy

$$E = \frac{p^2}{2m} \tag{27}$$

where $\vec{p}$ is the momentum of the particle and m the effective mass, one can transform (26). The momentum is given by $\vec{p} = m\vec{v}$; thus $d\vec{p}/dt = d/dt\ (m\vec{v})$ and if m is a constant in time,

$$\frac{d\vec{p}}{dt} = m\,\frac{d\vec{v}}{dt} = m\vec{a} = \vec{F} \tag{28}$$

where $\vec{F}$ is the force on the particle and $\vec{a}$ is its acceleration. Bragg's relation relates the momentum to the wave vector as $\vec{p} = \hbar\,\vec{k}$, where $\hbar$ = Planck's constant/2π. Thus,

$$\frac{d\vec{p}}{dt} = \hbar\,\frac{d\vec{k}}{dt} = \vec{F} \text{ implying that } \frac{d\vec{k}}{dt} = \frac{\vec{F}}{\hbar} \tag{29}$$

and using (20) in (26) one finally arrives at

$$\frac{df}{dt} = \vec{v} \cdot \nabla_{\vec{r}} f + \frac{1}{\hbar}\,\vec{F} \cdot \nabla_{\vec{k}} f + \frac{\partial f}{\partial t} \tag{30}$$

The collision terms to which (30) must be equal should now be considered. The collision term is described by a scattering process which takes an electron from a given state $\vec{k}$ to a state

$\vec{k}'$ and vice versa. Let $W(\vec{k}, \vec{k}', \vec{r}, t)$* be the probability that a particle in $\nabla_{\vec{r}}$ about $\vec{r}$ at time t will change its wave vector from $\vec{k}$ to $\vec{k}'$ due to some type of collision. Then to include the exclusion principle one may multiply $W(\vec{k}, \vec{k}')$ by the probability that the initial state $\vec{k}$ is occupied, $f(\vec{k})$, and the probability that the final state is empty $(1 - f(\vec{k}'))$. Then the probability of a transition from state $\vec{k}$ to state $\vec{k}'$ becomes

$$W(\vec{k}, \vec{k}')f(\vec{k})(1 - f(\vec{k}')). \tag{31}$$

Equation (31) represents a loss, by collision, of particles from an original state. The gain, from collisions, to the original state is given similarly by

$$W(\vec{k}', \vec{k})f(\vec{k}')(1 - f(\vec{k})). \tag{32}$$

The total change in f, due to collisions, at $\vec{r}$ and $\vec{k}$ is given by integrating the difference of (31) and (32) over all $\vec{k}'$ The collision term then becomes

$$\left(\frac{\partial f}{\partial t}\right)_{coll} = \int[-W(\vec{k}, \vec{k}')f(\vec{k})(1 - f(\vec{k}')) + W(\vec{k}, \vec{k}')f(\vec{k}')(1 - f(\vec{k}))]d\vec{k}'. \tag{33}$$

Equating (30) to (33) gives the fundamental equation for determining the properties of conductors and semiconductors:

$$\frac{\partial f}{\partial t} + \vec{v} \cdot \nabla_{\vec{r}} f + \frac{1}{\hbar} \vec{F} \cdot \nabla_{\vec{k}} f = \int[-W(\vec{k}, \vec{k}')f(\vec{k})(1 - f(\vec{k}')) + W(\vec{k}, \vec{k}')f(\vec{k}')(1 - f(\vec{k}))]d\vec{k}'. \tag{34}$$

*The symbol $W(\vec{k}, \vec{k}', \vec{r}, t)$ will be labeled $W(\vec{k}', \vec{k})$ in the interests of brevity.

Some discussion of equation (34) is in order. It is the type of classical integro-differential equation first developed in the study of gas dynamics. Solutions obtained to date for this equation are at best approximate and usually done only in the steady state, i.e., when $\partial f/\partial t = 0$. It should be realized that (34) itself is only an approximate relation for the phenomena that occur within the crystal. It is the best known and probably the most widely used relation in the study of metals and semiconductors. It is not the purpose here to develop this equation but merely to recognize it as the starting point for the study of various phenomena in metals and semiconductors. The first term on the left is the time variation of the density function f. The second term introduces the effects of particle density and thermal gradients in the material. The third term on the left brings in the effects of applied electrical and magnetic fields through the force $\vec{F}$, which in the case of charged particles is given by

$$\vec{F} = q(\vec{E} + \vec{v} \times \vec{B}) \text{ (MKS)} \qquad (35)$$

where

q = particle charge

$\vec{E}$ = applied magnetic field

$\vec{v}$ = particle velocity

and

$\vec{B}$ = applied magnetic field.

Thus the left-hand side introduces the effects of the externally applied fields and of particle density gradients. The right-hand side of equation (34) is at best a guess at what goes on inside the material on a microscopic scale, integrated to give the macroscopic effect.

The solution to equation (34), when undertaken, is done by approximate means. The assumption that the density function for the disturbed system, $f(\vec{k}, \vec{r}, t)$, is different from some equilibrium distribution $f_o(\vec{r}, \vec{k}, t)$ by only a small amount is

usually made. Such an assumption allows one to expand f in a power series about f_o and keep only the first-order expansion term. Surprisingly enough, this has been a fairly satisfactory approach in providing agreement with experiments. The results of this approach will not be studied, but a simplifying assumption will be made which shall be discussed in detail, that of the existence of a characteristic relaxation time for the material.

a. Relaxation Time and the Collision Integral

By far the most often made simplifying assumption in discussing equation (34) is to represent the collision integral by a process of relaxation given by

$$\left(\frac{\partial f}{\partial t}\right)_{coll} = - \frac{f(\vec{k}, \vec{r}, t) - f_o(\vec{k}, \vec{r}, t)}{\tau} . \qquad (36)$$

Equation (36) implies that for any suddenly applied or removed fields, the density function f relaxes to an equilibrium density function f_o with a characteristic time τ. The existence of a relaxation time immensely simplifies the transport problems. The validity and consequences of the assumption of a relaxation time shall now be discussed at some length.

Whether or not a relaxation time can be defined for the collision integral depends basically on two things, the first being the assumed nature of the collision, and the second being the temperature at which the process takes place. There are generally two scattering processes encountered by the particles, one being due to lattice motion, and the other being due to impurities and lattice defects. The lattice scattering can be further divided into particle interactions with acoustical or optical modes of the lattice vibration. In the interaction with the acoustic mode of lattice vibration, the energy change of the charged carrier is small compared to its average energy. This is essentially due to the low-frequency nature of the acoustic phonon. In this case the phonon energy $\hbar\omega \ll kT$ for

any temperature greater than the Debye temperature of the material.* Consequently, during a phonon-particle collision, the particle can only gain small amounts of energy. Therefore, the density function f will not differ appreciably from the equilibrium function f_o, and the collision then can be approximated by the relaxation time assumption.

The optical mode scattering of particles, because of the higher frequency of the optical phonons, allows the relaxation time approximation only at higher temperatures. At very low temperatures one can have $kT < h\omega$ and a phonon-particle collision would result in a large particle energy change. At temperatures where $h\omega << kT$, the same condition holds as for acoustic phonons, and a relaxation time can be defined. It has also been shown that for nonpolar solids, a relaxation time always exists (reference 24). Therefore, one concludes that for scattering by lattice vibrations the relaxation time can be defined for temperatures in excess of the Debye temperature.

In considering scattering by impurities and lattice defects, one assumes the collisions to be perfectly elastic. In such cases $f(\vec{k}') = f(\vec{k})$ and a relaxation time can always be defined.

It is concluded that one can, in general, define relaxation times for the scattering processes if the energy of the particles is changed only a small amount by the interactions. The first τ_V due to lattice vibration is temperature dependent; the second τ_L due to impurities and defects is independent of temperature. These are combined to define a total relaxation time τ by

$$\frac{1}{\tau} = \frac{1}{\tau_V} + \frac{1}{\tau_L} \quad . \tag{37}$$

Now one may consider equation (33) and see under what conditions a relaxation time can be a valid representation for the

*k here is the Boltzmann constant and should not be confused with the wave vector $\vec{k}$.

l. According to the principle of microscopic reversabil-
he intrinsic transition rate must be the same in either
cion so that

$$W(\vec{k}, \vec{k}') = W(\vec{k}', \vec{k}) \quad . \tag{38}$$

s allows one to write the integral as

$$\left(\frac{\partial f}{\partial t}\right)_{coll} = \int [-f(\vec{k})(1 - f(\vec{k}')) + f(\vec{k}')(1 - f(\vec{k}))] \, W(\vec{k}, \vec{k}') d\vec{k}' \quad . \tag{39}$$

For elastic scattering processes the equilibrium distribution
function for state $\vec{k}$ will be identical with that for state $\vec{k}'$,
since f depends only on energy. Consequently,

$$f_o(\vec{k}') = f_o(\vec{k}) \tag{40}$$

and one can write (39) in the form

$$\left(\frac{\partial f}{\partial t}\right)_{coll} = \int [(f(\vec{k}') - f_o(\vec{k}')) - (f(\vec{k}) - f_o(\vec{k}'))] \, W(\vec{k}, \vec{k}') d\vec{k}' \quad . \tag{41}$$

A further simplifying assumption is that f is so little differ-
ent from f_o that in the left-hand side of equation (34) one can
replace f with f_o. This results in what is called the linearized
form of the Boltzmann equation (reference 25).

$$\frac{\partial f}{\partial t} + \vec{v} \cdot \nabla_{\vec{r}} f_o(\vec{k}) + \frac{1}{\hbar} \vec{F} \cdot \nabla_{\vec{k}} f_o(\vec{k}) = \int [(f(\vec{k}') - f_o(\vec{k}')) - (f(\vec{k}) - f_o(\vec{k}'))] W(\vec{k}, \vec{k}') d\vec{k}' \quad . \tag{42}$$

The relaxation time comes from the solution of this linear inhomogeneous integral equation in terms of $f(\vec{k}) - f_o(\vec{k})$ with $\partial f/\partial t = 0$. The relaxation times which can be obtained depend on the form of the left-hand side of equation (42).

b. Relaxation Times from the General Solution of Boltzmann's Equation

The Boltzmann equation (42) has an exact analytic solution under certain simplifying circumstances. The first of these is that the energy surfaces in k-space are spherical so that $\vec{v}$ and $\vec{k}$ point in the same direction. This allows one to write the left-hand side of (42) as a scalar product of $\vec{v}$ (with a vector which is constant on a spherical surface in k-space and is therefore proportional to cos ψ, where ψ is the angle between $\vec{k}$ and the constant vector). The second condition is that the scattering probability depends only on the angle between $\vec{k}$ and $\vec{k}'$ and not on their absolute orientations in the crystal. Then one can define a differential transition probability $\omega(\vec{k}, \theta)d\Omega$, which is the probability that a particle of momentum $\hbar k$ is scattered through the angle θ into the solid angle $d\Omega$.

Under these assumptions it can be shown that equation (42) has the exact solution given by

$$f(\vec{k}) - f_o(\vec{k}) = \frac{-\vec{v}_{\vec{k}} \cdot \nabla_{\vec{r}} f_o(\vec{k}) - \frac{1}{\hbar}\vec{F} \cdot \nabla_{\vec{k}} f_o(\vec{k})}{\int (1 - \cos\theta)\omega(\vec{k}, \theta)d\Omega} . \qquad (43)$$

Now the integral in the denominator of (43) is, dimensionally, a reciprocal transition rate for electrons of momentum $\hbar k$. Recognizing this, one writes

$$\frac{1}{\tau(\vec{k})} = \int (1 - \cos\theta)\omega(\vec{k}, \theta)d\Omega \qquad (44)$$

From (44), for experimentally determined $\omega(\vec{k}, \theta)$, a valid relaxation time can be determined which provides one with a distribution function $f(\vec{k})$ from which one can determine the various

electronic transport properties of the material. On the other hand, from measurements of thermal and electrical transport characteristics a relaxation time can be determined.

Examples of such relaxation times determined from measurements of electrical and thermal conductivities are:

$$\tau_e = \frac{m\sigma}{ne^2} \qquad \text{electrical} \qquad (45)$$

$$\tau_t = \frac{3mK}{n\pi^2 k^2 T} \qquad \text{thermal} \qquad (46)$$

In these last relations the notation is:

m = effective mass
n = density of electrons
e = electronic charge
k = Boltzmann constant
σ = electrical conductivity
K = thermal conductivity
T = absolute temperature

In general τ_e and τ_t are not equal except in cases where the Wiedemann-Franz Law holds. Thus the fact that the Lorenz number L, defined by

$$L = \frac{k}{\sigma T} = \frac{\pi^2}{3}\left(\frac{k}{e}\right)^2 \qquad (47)$$

is a constant independent of the properties of the material is a consequencesof the existence of a unique time of relaxation. The fact that at temperatures below the Debye temperature L is no longer a constant is due to the relatively large energy exchanged in electron-phonon interactions.*

*For a more detailed discussion see (reference 23, pp. 222-224) or (reference 20, pp. 201-202).

It is clear from (44) that the type of scattering process will determine the relaxation time. Equation (43) need only be satisfied on each constant energy surface. In the case of metals, the only value of $\tau(k)$ of importance is that determined on the Fermi surface.

c. The Diffusion Equation for Electrons and Holes

The assumed form of Boltzmann's equation leads directly to the fundamental diffusion equation for charged particles in a semiconductor, which is the basis for all the analysis to date of semiconductor devices. If the definition (44) is used in (42), one finds the diffusion equation in the form

$$\frac{\partial f}{\partial t} = - \frac{f - f_o}{\tau} - \vec{v} \cdot \nabla_{\vec{r}} f - \frac{\vec{F}}{\hbar} \cdot \nabla_{\vec{k}} f \qquad (48)$$

from which one obtains the continuity equation for charged carriers in the material. To obtain the continuity equation for electrons in the conduction band, one multiplies by the density of states for energy levels in the conduction band and integrates over all energy states. After proper manipulation of the terms, one finds

$$\frac{\partial n}{\partial t} = - \frac{n - n_o}{\tau_n} + \frac{1}{q} \nabla \cdot I_d + \frac{1}{q} \nabla \cdot I_e \qquad (49)$$

where I_d is a diffusion current density resulting from a density gradient of electrons and I_e is a conduction current density caused by an electric field.

The current density I_d is obtained from the middle term of the right-hand side of (48) and can be shown to have the form given by reference 26

$$I_d = +q D \nabla n \qquad (50)$$

where

q = the charge on the particle

D = an appropriately defined diffusion constant

Equation (50) is the well-known Fick's Law approximation to the current, resulting from a density gradient of particles. Derivations of Fick's Law exist in many books and will not be presented here. Fick's Law is an approximation which depends, as does the relaxation time assumption, on the particles not being limited in their time and space movements. Such an assumption will not be strictly applicable to physical sizes that are of the order of a diffusion length.

The current density I_e is obtained from the last term on the right-hand side of (48) as is shown in reference 27 and reduces to the form

$$I_e = nq \mu_n E \tag{51}$$

where

μ_n = electron mobility

E = electric field intensity

The sum of equations (50) and (51) is the total electron current density I_n. Thus equation (49) can be put into the form

$$\frac{\partial n}{\partial t} = - \frac{n - n_o}{\tau_n} + \frac{1}{q} \nabla \cdot I_n \tag{52}$$

where the last two terms in (49) have been combined into I_n. A similar expression can be derived for the holes in the valence band. Equation (52) for electrons and the similar one for holes form the starting point for most semiconductor device analyses.

d. Limitations of Diffusion Theory

In the above analysis there have been two fundamental assumptions that limit the applicability of this approach to the transport problem. The first is that the definition of a relaxation process has been possible only because of the limitation to elastic or "almost elastic" scattering processes. The second is that all the above analyses have been based on bulk properties of the material. Surface and size effects of the sample were completely ignored. This latter fact may not have been stated explicitly, but it is implicit in the idea that one may define transport coefficients which are characteristic properties of the material, and are independent of the shape and size of the specimens.

The latter restriction will not be considered. Implicit in the development of equations (30), (33), and the definition of a valid relaxation time is the assumption that the particles will have the time and space in which the relaxation process may proceed uninhibited. Thus, the resulting diffusion equation (48) is a long-time, large-scale approximation to the solution of the small-scale problem of random motion in the material. In order that the approximation should be valid, it is necessary that one be concerned with distances covering many mean free paths and with intervals containing many relaxation times.

4. Remarks

In this discussion the fundamental Boltzmann equation (34), describing the transport process in semiconductors and metals has been discussed. This equation is valid for many analyses but also, in general, it is impossible to solve without some simplifying assumptions. The definition of a relaxation time allows one to solve the Boltzmann equation and to calculate steady-state transport parameters. The calculation of a relaxation time requires that the scattering of particles be elastic and that the scattering process be independent of the physical size of the specimen. These two conditions are satisfied for

most practical cases. The procedure for obtaining the charge continuity equation from the Boltzmann equation was indicated. This is one of the fundamental equations used in semiconductor analysis. Mention was also made of the approximation made in the use of Fick's Law for diffusion current. The net purpose of this discussion is to lay the foundation to the diffusion theory approach to transport phenomena and to point out the fact that diffusion is a bulk phenomenon and is not applicable to small regions. Thus, if physical dimensions of specimens in the direction of transport are not greater than a few diffusion lengths, diffusion theory will not, without modification, describe the transport process.

5. Introduction to Diffusion Theory and Semiconductor Analysis

Diffusion theory has been the basis of semiconductor device analysis since the advent of such devices. Such analysis, as was pointed out in the preceding discussion, is based on the fact that physical dimensions of the device are such as to have no effect on the scattering process. In this subsection the results of applying diffusion theory to the study of semiconductor devices will be discussed. The fundamental equations for semiconductor material analysis are written down. A brief discussion of a digital computer code developed at General Atomics, used to obtain the operating characteristics of a semiconductor diode in a radiation environment, is given. Finally, a discussion of general transistor models and, in particular, a comparison of the three most popular models after the fashion of Hamilton, et al.,concludes the subsection.

6. The Fundamental Semiconductor Equations

Almost all device analyses have been carried out in one spatial dimension; i.e., the assumed direction of current flow in the device. The fundamental equations used in the analysis are:

Charge continuity equations

$$\frac{\partial n}{\partial t} = - \frac{n - n_o}{\tau_n} + \frac{1}{q} \frac{\partial I_n}{\partial x} \qquad \text{(electrons)} \qquad (53)$$

$$\frac{\partial p}{\partial t} = - \frac{p - p_o}{\tau_p} - \frac{1}{q} \frac{\partial I_p}{\partial x} \qquad \text{(holes)} \qquad (54)$$

Total current equations

$$I_n = qn \mu_n E_x + qD_n \frac{\partial n}{\partial x} \qquad \text{(electrons)} \qquad (55)$$

$$I_p = qp \mu_p E_x - qD_p \frac{\partial p}{\partial x} \qquad \text{(holes)} \qquad (56)$$

Poisson's equation

$$\frac{\partial^2 \psi}{\partial x^2} = - \frac{\rho}{\epsilon} \text{ with } E_x = - \frac{\partial \psi}{\partial x} \qquad (57)$$

Charge neutrality equation

$$p + N_d = N_a + n \qquad (58)$$

The notation in equations (54) to (58) is:

- n = electron density
- n_o = equilibrium electron density
- p = hole density
- p_o = equilibrium hole density
- τ_n = relaxation time for electrons
- τ_p = relaxation time for holes
- D_n = diffusion constant for electrons
- D_p = diffusion constant for holes
- μ_n = electron mobility

μ_p = hole mobility
E_x = electric field in x-direction
I_n = electron current in x-direction
I_p = hole current in x-direction
q = electronic charge
ψ_x = electrostatic potential at x
ρ = charge density
ϵ = dielectric constant
N_d = density of ionized donor atoms
N_a = density of ionized acceptor atoms

Equations (54) to (58) with the appropriate boundary conditions, derived from basic semiconductor physics, form the starting point for all device analyses.

The diffusion equations can be solved explicitly for semiconductor devices under assumed boundary conditions, but for any device consisting of more than one p-n junction the solution becomes highly unwieldy. Therefore, there have been various attempts to develop useful device models that are accurate and yet less cumbersome. Before discussing some of the better known models, an attempt to investigate the decay of excess charges in a junction diode numerically will be reviewed.

a. Digital Computer Analysis of the Continuity Equation

The investigation was made under an Air Force Contract AF 29(601)6374 and reported in a technical report AFWL TR-65-44 (reference 28). The excess charge in this study was generated by an ionizing pulse of radiation. The diffusion equations are written in the form

$$\frac{\partial}{\partial t} = -R_j + \mu_n \frac{\partial}{\partial x}(nE) + D_n \frac{\partial^2 n}{\partial x^2} \quad \left(j = \text{region designations}\right) \qquad (59)$$

and

$$\frac{\partial p}{\partial t} = -R_j - \mu_p \frac{\partial}{\partial x}(pE) + D_p \frac{\partial^2 p}{\partial x^2} \quad (j = p \text{ or } n) \tag{60}$$

and Poisson's equation

$$\frac{\partial E}{\partial x} = \frac{4\pi q}{K}\left[p(x, t) - n(x, t) + \Delta N_j\right] \tag{61}$$

for each side of a p-n junction. The recombination term R_j has the form

$$R_n = \frac{pn - p_{on}n_{on}}{\tau_n n_{on}} \quad (n \text{ region}),$$

$$R_p = \frac{pn - p_{op}n_{op}}{\tau_p p_{op}} \quad (p \text{ region}) \tag{62}$$

where

K = the dielectric constant
ΔN_j = excess of donors to acceptors in the j region
p_o = equilibrium hole concentration
n_o = equilibrium electron concentration

The source term was taken to be proportional to the total radiation received. The differential equations were approximated by finite difference equations for which, after some difficulty, solutions were obtained. Some of the difficulties encountered were due to the large range of variables, errors introduced when using electric field and carrier density evaluated at the same point, and sensitivity of solutions to minor changes in boundary conditions. Most of the difficulties were overcome to a point where the time-dependent diffusion equations were solved for carrier densities and the electric field in the semiconductor diodes.

Specific calculations were made for the response of the above variables to a short (≈ .1 μsec) pulse of ionizing radiations. These results were then compared to experimental data on two particular diodes. Fairly close agreement was found for low values of excess carrier densities with the deviations greater at higher densities. It is interesting that, after an initial adjustment, computer time steps greater than the relaxation time for the material gave results agreeing with experimental data.

Although the computer calculations reported in reference 28 were carried out only for diodes, the authors propose to extend the solutions to multiregion devices in the future and to incorporate provisions for time-dependent recombination rates, electric field dependent mobilities, and other phenomena. This procedure has produced acceptable results for transient analysis of semiconductor devices. There are numerous studies reported of the transient response of semiconductor devices to ionizing radiation (see reference 29 and its references). These are not considered here.

7. General Transistor Models

It is to be noted that the set of equations (54) to (58) subject to the boundary conditions at a p-n junction can be solved explicitly for the currents in a diode or transistor. The diffusion theory approach to transistor analysis is presented in Chapter 7 of Middlebrook (reference 31) or Chapter 4 of Gartner (reference 30). These procedures develop the "law of the junction" which relates the minority carrier densities on both sides of the junction to the equilibrium carrier densities and the applied potential. The result is that

$$p = p_n \exp \frac{qV}{kT} \qquad \text{(n-material)} \qquad (63)$$

and

$$n = n_p \exp \frac{qV}{kT} \qquad \text{(p-material)} \qquad (64)$$

where

p_n = equilibrium density of holes

n_p = equilibrium density of electrons

V = applied voltage plus contact potential (contact potential is often small enough to neglect)

q = electronic charge magnitude

k = Boltzmann constant

T = absolute temperature

This "law of the junction" provides the necessary boundary conditions for the solution of the diffusion equation in the base region. By assuming only diffusion of minority carriers in a space-charge-neutral base region, the fundamental equations reduce to

$$i_p = -q\, D_p \frac{\partial p}{\partial x} \qquad (65)$$

$$\frac{\partial \rho}{\partial t} = 0 \rightarrow \frac{\partial p}{\partial t} = \frac{\partial n}{\partial t} \qquad (66)$$

$$\frac{\partial p}{\partial t} = D_p \frac{\partial^2 p}{\partial x^2} - \frac{p}{\tau_p} \qquad (67)$$

$$\frac{\partial n}{\partial t} = D_n \frac{\partial^2 n}{\partial x^2} - \frac{n}{\tau_n} \qquad (68)$$

for the n-material base of a p-n-p transistor. Solutions for equations (65) - (68) subject to the law of the junction at the collector and emitter edges of the base region are given in Middlebrook for the steady-state and time-varying cases for small signals. These solutions provide the emitter and collector currents under specified operating conditions. For the

exact form the reader is referred to reference 31.* For this discussion, it is sufficient to note that the collector and emitter currents can be put in the form

$$I_e(s) = A_{11}(s)\, P_e(s) + A_{12}(s)\, P_c(s) \qquad \text{(emitter)} \qquad (69)$$

$$I_c(s) = A_{21}(s)\, P_e(s) + A_{22}(s)\, P_c(s) \qquad \text{(collector)} \qquad (70)$$

where

P_e = hole density at emitter edge
P_c = hole density at collector edge

The A_{ij} are determined from the solution of the diffusion equation for holes subject to the boundary conditions given by

$$p = p_n \exp \frac{qV_c}{kT} \qquad \text{(at collector junction)} \qquad (71)$$

$$p = p_n \exp \frac{qV_e}{kT} \qquad \text{(at emitter junction)} \qquad (72)$$

where

p_n = equilibrium density of holes in base
V_c = collector to base voltage
V_e = emitter to base voltage

The forms for I_e and I_c lead one to treat the base region as a two-port network with parameters of emitter and collector currents and hole density at the emitter and collector boundaries. If the area and carrier lifetimes are uniform throughout the base, then the network will be symmetrical, with the results that $A_{11} = A_{22}$ and $A_{21} = A_{12}$. For such a case, the coefficients are given by

*See pages 138 and 140 for the steady-state and pages 142 and 143 for the time-varying case.

$$A_{11} = A_{22} = \frac{eAD_p}{L_p} (1 + s\tau_p)^{1/2} \coth \frac{W/L_p}{(1 + s\tau_p)^{1/2}} \qquad (73)$$

$$A_{12} = A_{21} = \frac{eAD_p}{L_p} (1 + s\tau_p)^{1/2} \operatorname{csch} \frac{W/L_p}{(1 + s\tau_p)^{1/2}} \qquad (74)$$

where

$L_p = \sqrt{D_p \tau_p}$

W = base region width

A = base area

It is apparent from (71) and (72) that if V_c is large and negative, then $p_c \cong 0$, and if V_e is large and negative $p_e \cong 0$. Thus, by making forward and inverse measurements under the above conditions, one can define forward and inverse short-circuit current ratios as

$$\alpha_n = - \left. \frac{I_c(s)}{I_e(s)} \right|_{p_c=0} \quad \text{and} \quad \alpha_i = - \left. \frac{I_e(s)}{I_c(s)} \right|_{p_e=0} \qquad (75)$$

In the symmetric case $\alpha_n = \alpha_i$, but in practice the base region is seldom symmetrical. Consequently, one will obtain, in general, different values for α_n and α_i. The measurements of α_n and α_i are made from direct current to very high frequencies, and ω_n and ω_i are then defined as the frequencies at which the values of α_n and α_i are three decibels below the low-frequency values.

From reference 30, one finds the result of applying diffusion theory to the problem of determining the time-dependent current in a transistor operated in the common base configuration. It is

$$i_e(t) = I_o \left\{ \sum_{n=1}^{\infty} n\left[\exp\left(\frac{nw}{L_p}\right)\right] \operatorname{erfc}\left[\frac{nw^2}{2D_p\sqrt{t}} + \frac{D_p\sqrt{t}}{L_p}\right] + \right.$$

$$\left. \left[\exp\left(-\frac{nw}{L_p}\right)\right] \operatorname{erfc}\left[\frac{nw^2}{2D_p\sqrt{t}} - \frac{D_p\sqrt{t}}{L_p}\right] \right\} \qquad (76)$$

where I_o is the final value of the collector current. Although this result can be used, it is cumbersome. Therefore, various attempts have been made to produce models that are easier to use and give results that are fairly accurate. Some of those models will now be discussed, following the review article by Hamilton, et al. (reference 32).

a. The Ebers-Moll Model

The α_i's and ω_i's determine transistor operating characteristics and are easily measured quantities; but they have somewhat less than a desirable analytical form: e.g., for the symmetric case

$$\alpha_n = \alpha_i = \operatorname{sech} \frac{W/L_p}{(1 + s\tau_p)^{1/2}} . \qquad (77)$$

The Ebers-Moll model assumes a more familiar form for current ratios in the forward and inverse regions. This model approximates the α's by a single-pole function of the complex frequency variable. In the forward active regions this is defined as

$$-\left.\frac{I_{cf}(s)}{I_{ef}(s)}\right|_{p_c=0} = \frac{\alpha_n}{1 + \frac{s}{\omega_n}} \qquad (78)$$

and in the inverse active regions as

$$- \left.\frac{I_{er}(s)}{I_{cf}(s)}\right|_{p_e=0} = \frac{\alpha_i}{1 + \frac{s}{\omega_i}} \tag{79}$$

This approximation allows each current in the transistor to be written as the sum of forward and reverse components. Then (78) and (79) yield equations for the transistor saturation currents in the form

$$I_e(s) = I_{ef}(s) - \alpha_i \, I_{cr}(s) \Big/ (1 + \frac{s}{\omega_i}) \tag{80}$$

and

$$I_c(s) = \frac{a\ \alpha_n I_{ef}(s)}{1 + \frac{s}{\omega_n}} + I_{cr}(s) \tag{81}$$

The characteristic equation for the transistor in saturation has the form

$$s^2 + (\omega_n + \omega_i)s + \omega_n\omega_i(1 - \alpha_n\alpha_i) = 0. \tag{82}$$

b. <u>The Charge Control Model</u>

The essence of the charge control model is the relationship it draws between terminal currents and total stored minority charge. The procedure is to remove the functional dependence on spatial corrdinates by integrating the continuity equations for the minority carrier charge density over the volume of the base regions. The validity of such an approach depends crucially on the steady-state ratios of currents to stored charge remaining the same for all time. Performing the integration leads to the equation

$$\frac{dq_{BF}}{dt} = -i_{BF} + q_{BF}\, w_{BF} \tag{83}$$

where, by definition, the charge control parameter is

$$w_{BF} = \frac{I_{BF}}{Q_{BF}}$$

and where I and Q are steady-state current and charge, and i and q are time-varying current and charge.

One can define charge control parameters between each current, collector, emitter and base, and the total charge for both normal and inverse operation. The operations of the transistor can then be described in terms of these parameters. Eventually the charge control parameter must be related to the α_I, α_n, w_n, and w_I since these are the measured quantities. If this relation is made (see formulas) then it is found that the model gives the same characteristic equation (82) as does the Ebers-Moll model. The charge control model has perhaps been used more than others in the study of radiation effects. Under radiation the total stored charge in the base includes the induced charge. Thus the effect of the radiation can more easily be determined since the induced charge is more directly related to the transistor operation.

c. The Linvill Model

The Linvill, or lumped model, is a circuit, or network analysis, approach to the problem of modelling semiconductor devices. The space dependence of the fundamental partial differential equations is removed by a group of finite difference equations written for a number of points throughout the base regions. Doing this gives the continuity equation at each point k in the form

$$\frac{dp_k}{dt} = D_p \frac{[p_{k+1} - 2p_k + p_{k-1}]}{h_k(h_{k+1} + h_k)/2} - \frac{(p_k - p_n)}{\tau_p} \tag{84}$$

To establish circuit-like elements to represent the diffusion, recombination, and storage process, Linvill defines diffusance as

$$H_{dk} = \frac{eAd_p}{h_k} , \tag{85}$$

the storance by

$$S_k = eA \frac{(h_{k+1} + h_k)}{2} \tag{86}$$

and combinance as

$$H_{ck} = (\frac{eA}{\tau_p}) \frac{(h_{k+1} + h_k)}{2} \tag{87}$$

Then equation (84) is reduced to

$$S_k(\frac{dp_k}{dt}) = H_{dk}(p_{k-1} - p_k) - H_{dk+1}(p_k - p_{k+1}) -$$

$$H_{ck}p_k + H_{ck}p_n \tag{88}$$

and gives the total base current as

$$i_B = \sum_{k+1}^{N} \left[H_{ck}p_n - H_{ck}p_k - S_h(\frac{dp_k}{dt}) \right] \tag{89}$$

where N = number of points in the base regions.

The above elements are given physical representation and network configurations, then are used to analyze the transistor actions. The most popular configuration is a single π section of the lumped elements. When a transistor is analyzed this way,

the result is the same characteristic equation (82) as predicted by the Ebers-Moll and charge control models when the lumped parameters are related to the ω_n, ω_e, α_i and α_n.

Thus each of the above models produces the same measure of approximations to the transistor analysis. In all models the result is the same: the space dependence has been removed from the fundamental equations leaving a set of ordinary differential equations. Also in each model, in one way or another, the steady-state characteristics are extrapolated to obtain the transient behavior.

Based on the diffusion theory approximation of the fundamental equations used in semiconductor analysis, the above models are at least as good as any others that have been proposed. Now the question to be raised is: Is there another basic approach to the problem of charge transport in semiconductors that will lead to equivalent results in devices where diffusion theory is applicable and also valid in devices where diffusion theory is not a good approximation? The approach should be correct in thin-film analysis where dimensions in the direction of charge transport are of the order of a diffusion length. Such an approach has been tried in the field of semiconductors by McKelvey in a specific application of the general method of invariant imbedding. This approach will be introduced in the next subsection.

8. Subsection Summary

In this subsection, the diffusion theory relations developed in the first subsection have been used to see how their application to semiconductor devices has led to the development of useful models for the analysis of such devices. First a specific computer attempt to solve the continuity equation under the effect of a short ionizing pulse of radiation was discussed. There was some difficulty in developing a working program, but finally calculations were made for specific diodes which agreed with experimental data. Next, models developed for the general

analysis of transistor operation (including the Ebers-Moll, charge control, and lumped models) were reviewed.

The most important point here is not that each of the models is just an approximation to the fundamental diffusion equations but that it is impossible to extend these models into thin-film semiconductor devices where diffusion theory on which they rest does not accurately describe the physical process. An attempt to do this through the general approach of invariant imbedding is the purpose of the rest of this section.

9. Introduction to the Application of Invariant Imbedding

Invariant imbedding essentially reverses the classical approach to solving transport problems. Historically, the solutions of a particular transport problem are obtained by considering special limiting cases of the general formulation when necessary restricting and simplifying approximations are made. This leads to a system of linear equations which one then solves. A good example of such a process is the diffusion theory application to semiconductor device operation. The invariant imbedding approach is to state the particular problem, then to phrase it in a more general manner and apply mathematical invariance principles in a systematic fashion to reduce the problem to the iteration of nonlinear transformations. This procedure then leads to new computational forms that seem well fitted to the capabilities of digital computers. It is not the desire of this study to formulate the general procedure but merely to apply it to a specific problem. In this vein of thinking the work of McKelvey will first be reviewed. He has applied invariant imbedding to semiconductor analysis. Next, the general time-dependent problem will be formulated and the general procedure for obtaining a solution will be indicated.

10. Time Independent Reflection and Transmission Coefficients

Invariant imbedding started as essentially a particle counting technique. This technique is used by McKelvey in his earlier

works (references 33, 34, and 35) to study recombination rates of injected carriers in semiconductors due to volume, and at dislocation edges in the material. In these papers the particle counting method was used to derive reflection and transmission coefficients for the surfaces, volumes, or dislocations considered. These coefficients were then used to determine appropriate boundary conditions for the solution of the diffusion equations in the material. In these earlier papers the reflection and transmission coefficients were related to previously defined physical properties and are not developed in the manner of invariant imbedding. Thus, these articles, although providing background for McKelvey's work, are not essential to an understanding of his application of invariant imbedding.

For purposes of introduction the formulation for the fundamental differential equations for the reflection and transmission coefficients as developed by McKelvey in reference 36 are given below. He considers the one-dimensional flow of particles through a given medium as presented in figure 34.

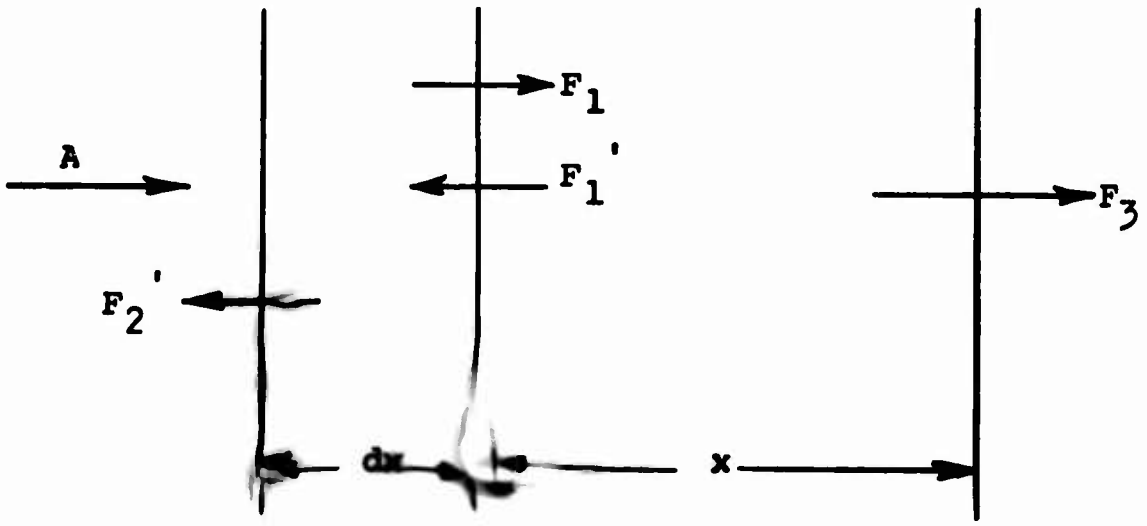

Figure 34. The Fluxes in a Stratified Medium

To develop the equations a material of length x + dx is considered; reflection and transmission coefficients R(x) and T(x) are defined as functions of the length x. Then the reflection and transmission for the thickness dx is proportional to dx and one writes

$$R(dx) = k\,dx \tag{90}$$

$$T(dx) = 1 - \alpha\,dx \tag{91}$$

The parameter α includes both scattering and absorption; therefore $\alpha \geq k$, the equality holding when there is no true absorption but only scattering. A is the source term of incident particle flux, and the F_i are fluxes across the boundaries in the direction indicated. One can obtain the equation by one of two equivalent methods: the first by considering multiple reflections and transmissions as was originally done in reference 37 or, second, by bulk considerations. The latter method will be used. From a consideration of figure 34 the following equation can be written

$$F_1 = A(1 - \alpha\,dx) + kF_1'\,dx \tag{92}$$

$$F_1' = R(x)F_1 \tag{93}$$

$$F_2' = Ak\,dx + (1 - \alpha\,dx)F_1' \tag{94}$$

$$F_3 = T(x)F_1 \tag{95}$$

From equation (93), by straightforward procedures one can obtain

$$F_1 = A\,\frac{1 - \alpha\,dx}{1 - R(x)\,k\,dx} \tag{96}$$

$$F_2' = A\left[k\,dx + \frac{R(x)(1 - \alpha\,dx)^2}{1 - R(x)\,k\,dx}\right] \tag{97}$$

$$F_1' = AR(x)\,\frac{1 - \alpha\,dx}{1 - R(x)\,k\,dx} \tag{98}$$

$$F_3 = AT(x)\,\frac{1 - \alpha\,dx}{1 - R(x)\,k\,dx} \tag{99}$$

Since F_2' is the reflected flux at $(x + dx)$, the reflection coefficient, $R(x + dx)$, is, from (97)

$$R(x + dx) = \frac{F_2'}{A} = k\,dx + \frac{R(x)(1 - \alpha\,dx)^2}{1 - R(x)\,k\,dx} \tag{100}$$

Then, neglecting second-order terms, one obtains for (100)

$$\frac{dR}{dx} = \frac{R(x + dx) - R(x)}{dx} = k - 2\alpha R(x) + kR(x)^2 \tag{101}$$

which provides a form for the reflection coefficient as

$$R(x) = \frac{\frac{k}{q}\sinh qx}{\cosh qx + \frac{\alpha}{q}\sinh qx} \tag{102}$$

where $q = (\alpha^2 - k^2)^{1/2}$

In a similar manner one can obtain the equation for T from

$$T(x + dx) = \frac{F_3}{A} = T(x)\,\frac{(1 - \alpha\,dx)}{1 - R(x)\,k\,dx} \tag{103}$$

leading to the differential equation

$$\frac{dT}{dx} = \frac{T(x + dx) - T(x)}{dx} = T(x)[R(x)k - \alpha] \tag{104}$$

Therefore, although the equation (101) for R involved only R itself, T cannot be found from (103) without knowing R. If R from (102) is used one can eventually show that T(x) is given by

$$T(x) = \frac{1}{\cosh\ (qx) + \frac{\alpha}{q} \sinh\ qx} \tag{105}$$

a. Analysis of a p-n Photodiode

McKelvey, after arriving at (102) and (105), relates k and α to the usual semiconductor parameters of mean free path, mean carrier lifetime, and mean thermal velocity. This will not be repeated here. McKelvey then goes on to use R(x) and T(x) as found to analyze the operation of a p-n photodiode on the flux basis. The expression for the differential flux dF across the junction due to a differential source term dA given by

$$dF(\gamma) = \Phi(x, \gamma)dA \tag{106}$$

where $\Phi(x, \gamma)$ takes on the identity of a Green's function for the problem and γ is a parameter of the material defined by

$$\frac{2}{3}\frac{\lambda}{L} = \gamma \equiv \frac{2}{3}\left(\frac{\text{scattering mean free path}}{\text{diffusion length of the particles}}\right) \tag{107}$$

For the diode a bulk generation rate of carriers g(x) is assumed. Thus dA = g(x) dx, and in order to find the total flux across the junction one integrates (106), giving

$$F(\gamma) = \int_0^d g(x)\Phi(x, \gamma)dx \tag{108}$$

where the surface is at x = 0, and the junction is at x = d.

The function Φ has the form

$$\Phi(x, \gamma) = \frac{\left[\frac{1}{T(x)} - R_o \frac{R(x)}{T(x)}\right]\left[\frac{1}{T(x)} + \frac{R(x)}{T(x)}\right] + R_o}{\frac{1}{T(a)}\left[\frac{1}{T(x)} - R_o \frac{R(x)}{T(x)}\right] - R_o \frac{R(a - x)}{T(a - x)}} \tag{109}$$

with R_o = surface reflection coefficient, and "a" the slab width. This equation can be put into other forms using (105) and (102) where γ is introduced through k and α.

The integral equation (108) is the fundamental equation involved in the analysis of the problem using the flux or invariant imbedding method. McKelvey analyzed the photodiode for the source term

$$g(x) = g_o \delta(x - x_o) \quad 0 \leq x \leq a \tag{110}$$

where $\delta(x)$ is the Dirac δ function, and showed that the results of such an analysis agree with diffusion theory results of the problem in the limit where the invariant imbedding method and diffusion theory are the same. This limit occurs when $\gamma << 1$, as can be seen from the definition

$$\gamma = \frac{2}{3} \frac{\lambda}{L} \tag{111}$$

If $\frac{2}{3} \frac{\lambda}{L} << 1$, then the mean free path is short compared to the diffusion length L. Or, if $L = \bar{c}\tau$ where $\bar{c}$ = average thermal velocity and τ = mean carrier lifetime, the condition implies a combination of short mean free path or long lifetime or high velocity that will make $\gamma << 1$. Then McKelvey established in this case that invariant imbedding and diffusion theory agree if diffusion theory is applicable. It was shown in the first subsection that diffusion theory was applicable if the physical size were large compared to a mean free path. Therefore, if, for example, the surface layer of the material were made very thin, the diffusion theory analysis would be invalid but invariant imbedding could still be used to analyze the operations of the junctions. In a following paper (reference 38) McKelvey continued the invariant imbedding analysis of a p-n junction. Alternative forms for T and R are defined which simplify the arithmetic somewhat. An expression for the total current across

a p-n junction is derived using invariant imbedding. The current is given by

$$I = q\left[n_p\left(\frac{D_n R_{\infty n}}{\tau_n}\right)^{1/2} + p_n\left(\frac{D_p R_{\infty p}}{\tau_p}\right)^{1/2}\right]\left(\exp\frac{qv}{kT} - 1\right) \qquad (112)$$

where

$R_{\infty n}$ = the reflection coefficient for n-material of infinite length

$R_{\infty p}$ = the reflection coefficient for p-materials of infinite length

and the other quantities are as defined in division 5. With the exception of $(R_{\infty n})^{1/2}$ and $(R_{\infty p})^{1/2}$ this equation is identical to the current found from diffusion theory given by

$$I = q\left[n_p \frac{D_n}{L_n} + p_n \frac{D_p}{L_p}\right]\left(\exp\frac{qv}{kT} - 1\right) \qquad (113)$$

where

$$L_p = \sqrt{\tau_p D_p}$$

and

$$L_n = \sqrt{\tau_n D_n}$$

The R_∞'s are given by the equation

$$R_\infty = 1 + 2\gamma^2 - 2\gamma(1 + \gamma^2)^{1/2} \qquad (114)$$

with $\gamma << 1$, the $R_\infty \cong 1$ and invariant imbedding agrees with diffusion theory as previously discussed. Where this condition fails, $R < 1$ and invariant imbedding predict a smaller saturation current than is given by diffusion theory. The article then continues with the invariant imbedding approach to the analysis of a p-n photovoltaic cell, but that will not be discussed here.

McKelvey's final article to date (reference 39) introduces the effect of an electric field into the above analysis. This considerably complicates the problem because it becomes necessary to consider reflection and transmission coefficients in the direction of the electric field and in opposition to it. More bookkeeping is required in this latter case but in no way alters the basic idea behind the applications of invariant imbedding.

McKelvey's work has been treated rather fully because it is a good example of the application of the invariant imbedding method to the study of semiconducting devices.

11. Remarks on Time Dependent Invariant Imbedding

McKelvey's series of papers do not permit the inclusion of time-varying fluxes. There exists, however, time dependent formulation of the invariant imbedding formalism, which has been applied to a study of neutron transport in a rod (references 40 and 41). The results of the treatment are expressions for two functions, $R(x, t)$ and $T(x, t)$, the reflection and transmission coefficients. The details leading to these expressions will not be repeated here for two reasons: the results are not strictly applicable to a study of semiconducting devices, and there is rather considerable algebraic detail. It is found, however, in the above-mentioned references, that the reflection and transmission coefficients satisfy equations of the form

$$\frac{\partial R}{\partial x} + \frac{2}{c}\frac{\partial R}{\partial t} = \sigma(x)B(x, t) + 2[F(x, t) - 1]\sigma(x)R(x, t) +$$

$$\sigma(x)B(x, t)\int_0^t \frac{\partial R(x, \tau)}{\partial \tau} R(x, t - \tau)d\tau \qquad (115)$$

and

$$\frac{\partial T}{\partial x} + \frac{2}{c}\frac{\partial T}{\partial t} = [F(x, t) - 1]\sigma(x)T(x, t) +$$

$$\sigma(x)B(x, t)\int_{o}^{t} \frac{\partial R(x, t)}{\partial \tau} T(x, t - \tau)d\tau \qquad (116)$$

In the above relations, $\sigma(x)\Delta x$ is the probability that an interaction will take place in the medium under discussion in the region $(x, x + \Delta x)$; $F(x, t)$ is the internal generated flux; the factor unity is the assumed external flux while $B(x, t)$ is proportional to the flux generated due to particle interactions.

If both R and T are independent of time and if $F \equiv 0$, one readily finds that the above relations reduce to

$$\frac{dR}{dx} = \sigma(x)B(x) - 2\sigma(x)R(x) + \sigma(x)B(x)R^2(x) \qquad (117)$$

and

$$\frac{dT}{dx} = T(x)[-\sigma(x) + \sigma(x)R(x)B(x)] \qquad (118)$$

These last two relations can obviously be compared term by term with McKelvey's fundamental equations. Indeed, to show that such a comparison is possible is the sole point of the remarks made in this paragraph to this point.

These studies have progressed to the point where a time dependent generalization of McKelvey's work will soon be available. The internal fluxes arising from the interaction of an external gamma pulse with the material have been specified. The terms in the equations which describe the absorption of the charge carriers due to the existence of trapping states in the material and electron-hole recombination need further work. When these equations are written down, the following results are expected. There will exist a diffusion type of equation in each of the (thin) layers of a (microelectronic) circuit which will contain

explicitly the effects of layer width on the total time-dependent current. When such equations are available, generalized models of thin-film devices will proceed in a straightforward way, after the fashion discussed in Hamilton et al.(reference 32).

SECTION IV

GENERAL CONCLUSIONS AND RECOMMENDATIONS

From the theoretical and experimental studies on this project, the following conclusions can be made:

(1) The most important contributing factors to transient radiation effects in microcircuits are the active junction regions of the transistor elements. Since the current pulse resulting from the radiation is directly proportional to the active volume, it would seem reasonable to keep these regions as small as possible. This implies the minimization of the emitter base junction and the collector junction areas, depletion regions, and minority carrier lifetimes. This further implies that the smallest possible transistor devices consisting of the required power and current levels should be used in microcircuits. Minority carrier lifetimes can be reduced by gold doping, which also implies the use of high-frequency devices. The depletion width can be minimized by using a low collector voltage.

(2) The microcircuit should be designed to use the lowest impedance consistent with other design criteria. This requirement is, of course, somewhat contradictory to the previous recommendation of reducing the active volume region for the transistor elements, so some compromise between these two factors must be made to minimize the radiation effect.

(3) Experimental data, with the theory developed here for use with the flash X ray, offer a method of obtaining minority carrier lifetimes, depletion layer width, junction area, diffusion length, and active volume when the absorbed dose and the ionization efficiency are known in the transistor elements of a microcircuit. Conversely, given the above parameters, it is possible to determine the primary photocurrent from the microcircuit junction under a variety of radiation conditions.

(4) It has been shown that the fundamental Boltzmann equation describing the charge transport in semiconductors can be said to modify the usual diffusion or continuity equation to obtain more accurate circuit models of transistor elements in microcircuits. This will result in changes in the Ebers-Moll model, charge control model, and the Linvill model. Further work will be required to complete the changes in these models, but adaptations to thin-layered microcircuit devices has been shown to be feasible.

(5) In general, the Motorola XC-201 is less sensitive than the Motorola MC-201 to transient radiation. The XC-201 and MC-201 are four-input integrated circuits "nand" or "nor" gates. The XC-201 has its components completely isolated from each other without the use of a back biased isolation junction diode.

(6) Testing of the Fairchild μL-903 RTL integrated circuit indicated that the substrate-collector junction introduced a diffusion tail in the transient radiation response which can be reduced by elimination of the diode isolation junction. The successful mocking up of the μL-903 showed this technique to be a useful research technique.

(7) Mock-up circuits for the TI SN-513 "nor" or "nand" integrated logic circuits required the inclusion of the parasitic elements for accurate simulation.

(8) The TI SN-511 and SN-511A integrated circuit flip-flops were irradiated. The irradiation tended to try to switch the flip-flop, but it restored itself to its original state.

(9) The Crystalonics 2N3084 field effect transistor was tested on the 600-KV flash X ray. The test results indicate that the transient peak of I_G increases as V_{GS} decreases. The test results also indicate that the transient peak of I_D decreases with increasing V_{DS} around the V_{GS} = 0 volt level, and that I_D increases with increasing V_{DS} at the V_{GS} = 4 volts level.

(10) Diffused resistors have a large transient current similar to that observed in many microcircuits. The current pulse is probably caused by the isolation junction.

(11) The transient radiation response of thin-film nichrome resistors is primarily due to air ionization effects.

(12) Thin-film Hall devices were found to be highly radiation resistant as was predicted by the theory. There were no radiation effects observed for dose rates up to 10^{10} roentgens/sec when the devices were operated in the constant voltage mode. This operating mode is therefore preferred for any Hall device where gamma radiation environments might be encountered. Transient radiation effects were observed for other modes of operation as predicted by the theory.

(13) The Signetics SU-315K integrated "nor" circuit is insensitive to gamma radiation while in the logic "1" state--at least up to 2×10^{6} roentgens/sec. It is sensitive to radiation at this level while in the logic "0" state. At high radiation levels the SU-315K becomes sensitive to gamma radiation irrespective of its logic state.

THIS PAGE INTENTIONALLY LEFT BLANK.

APPENDIX I

DERIVATION OF p-n JUNCTION TRANSIENT CURRENT

In order to evaluate an expression for the transient response of a p-n junction several assumptions have to be made. These assumptions are:

(1) The voltage applied across the p-n junction is assumed to occur only across the area in the immediate vicinity of the junction. The field available for drift within the main body of the p-region or n-region is therefore very weak.

(2) The diode has a one-dimensional carrier flow.

(3) The diode is uniformly doped.

(4) The ionizing radiation produces uniformly excess electron-hole pairs. These excess electron-hole pairs produced are assumed to be only in sufficient amount to significantly alter only the minority carriers in each region as shown in figure 2. When considering the transient response of a p-n junction, one runs into the problem of hole injection into an n-region, or electron injection into a p-region (reference 6). If holes injected into an n-region are considered, one can express in words the conservation of holes at a fixed point in space as

$$\begin{bmatrix}\text{time rate of}\\ \text{increase in}\\ \text{hole density}\end{bmatrix} = \begin{bmatrix}\text{thermal generation}\\ \text{rate of holes}\end{bmatrix} - \begin{bmatrix}\text{recombination}\\ \text{rate of holes}\end{bmatrix} - \begin{bmatrix}\text{outflow}\\ \text{of holes}\end{bmatrix} + \begin{bmatrix}\text{radiation}\\ \text{generation}\\ \text{rate of holes}\end{bmatrix} \tag{119}$$

The first term on the right-hand side of the above equation is equal to rn_i^2 and the second term is equal to rnp. If it is assumed that only the minority carrier density is altered

appreciably in excess of the equilibrium densities p_{no} and n_{no} due to hole injection, one can write

$$p_n = p_{no} + \delta p_n \tag{120}$$

$$n_n = n_{no} \tag{121}$$

Hence, if one neglects momentarily the radiation term, the first two terms on the right-hand side of equation (119) can be written

$$\frac{d(\delta p_n)}{dt} = rn_i^2 - rnp = rn_i^2 - r\, n_{no}(p_{no} + \delta p_n) \; . \tag{122}$$

Since rn_i^2 is equal to $rn_{no}p_{no}$, equation (122) becomes

$$\frac{d}{dt}(\delta p_n) = -rn_{no}\delta p_n \tag{123}$$

Solving for δp_n gives

$$\delta p_n = (\delta p)_o e^{-rn_{no}t} = (\delta p)_o e^{-t/\tau_p} \tag{124}$$

where one defines $rn_{no} = 1/\tau_p$, and $(\delta p)_o$ is the value of δp_n at $t = 0$. Solving for δp_n out of equation (120) and putting it into equation (123) obtains

$$\frac{d}{dt}(\delta p_n) = -r\, n_{no}(p_n - p_{no}) = \frac{p_{no} - p_n}{\tau_p} \tag{125}$$

The outflow of holes can be found by examining a cube of widths Δx, Δy, Δz. Net inflow into cube =

$$-\left[\frac{1}{q}\frac{\partial j_y}{\partial y}\Delta y + \frac{1}{q}\frac{\partial j_z}{\partial z}\Delta z + \frac{1}{q}\frac{\partial j_x}{\partial x}\Delta x\right] \tag{126}$$

On considering a unit cube, one can rewrite equation (126) as

$$\frac{1}{t}\left[\frac{\partial j_y}{\partial y} + \frac{\partial j_z}{\partial z} + \frac{\partial j_x}{\partial x}\right] = -\frac{1}{q}\nabla \cdot j_p \qquad (127)$$

where j_p is the current density.

The continuity equation for holes injected into an n-region becomes from the above derivation

$$\frac{\partial p_n(x, t)}{\partial t} = \frac{p_{no} - p_n(x, t)}{\tau_p} - \frac{1}{q}\nabla \cdot \vec{j}_p + g(t) \qquad (128)$$

where $g(t)$ is the carrier generation rate due to radiation. Similarly the continuity equation for electrons can be written

$$\frac{\partial n_p(x, t)}{\partial t} = \frac{n_{po} - n_p}{\tau_n} + \frac{1}{q}\nabla \cdot \vec{j}_n + g(t) \; . \qquad (129)$$

The change in signs arises due to the negative charge of electrons. Since the diffusion component is proportional to a carrier density gradient, the diffusion equations for electrons and holes are

$$j_p(x, t) = -qD_p \frac{\partial p_n(x, t)}{\partial x} \qquad (130)$$

$$j_n(x, t) = qD_n \frac{\partial n_p(x, t)}{\partial x} \qquad (131)$$

The transient response of a diode is made up of two components: One component is a prompt photocurrent, $i_p(t)$, which is produced by carriers generated in the junction transition region. Since this component is collected in a few nanoseconds, it can be treated as having no time delay with respect to the radiation pulse:

$$i_p(t) = qA\ W_t\ g(t) \tag{132}$$

The second component is a delayed component of photocurrent, $i_d(t)$, developing from the diffusion of carriers generated in the vicinity of the junction:

$$i_d(t) = qAD_p \left.\frac{\partial p_n}{\partial x}\right|_{x=0+} - qAD_n \left.\frac{\partial n_p}{\partial x}\right|_{x=0-} \tag{133}$$

If one uses the boundary conditions

$$p_n(0+, t) = p_{no}e^{qv/kT}, \quad n_p(0-, t) = n_{po}e^{qv/kT} \tag{134}$$

$$\lim|p_n(s, t)| < \infty, \quad \lim|n_p(x, t)| < \infty \tag{135}$$

equations (128) and (129) can be solved by use of Laplace transforms. By using equation (131) one can write equation (129) as

$$\frac{\partial n_p(x, t)}{\partial t} = D_n \frac{\partial^2 n_p}{\partial x^2}(x, t) + \frac{n_{po} - n_p(x, t)}{\tau_n} + g(t) \tag{136}$$

Taking the Laplace transform of this equation one obtains

$$sN_p(x, s) - n_{po}(x, 0) = D_n \frac{\partial^2}{\partial x^2} N_p(x, s) + \frac{n_{po}(x, 0)}{s\tau_n} -$$

$$\frac{N_p(x, s)}{\tau_n} + G(s) \tag{137}$$

or

$$0 = \frac{d^2 N_p(x, s)}{dx^2} - \frac{1}{D_n}(S + \frac{1}{\tau_n})N_p(x, s) +$$

$$\frac{1}{D_n}\left[\frac{n_{po}(x, o)}{s\tau_n} + G(s) + n_{po}(x, 0)\right] \qquad (138)$$

This equation is of the form

$$0 = \ddot{y} + Ay + B \qquad (139)$$

The solution to this equation is

$$y = N_p(x, s) = \frac{G(s)}{s + \frac{1}{\tau_n}}\left[1 - \exp x\sqrt{\frac{1}{D_n}(s + \frac{1}{\tau_n})}\right] + \frac{n_{po}(x, o)}{s} \qquad (140)$$

Similarly it can be shown

$$p_n(x, s) = \frac{G(s)}{s + \frac{1}{\tau_p}}\left[1 - \exp -x\sqrt{\frac{1}{D_p}(s + \frac{1}{\tau_p})}\right] + \frac{p_{no}(x, o)}{s} \qquad (141)$$

Upon substituting equations (140) and (141) into the Laplace transforms of equations (132) and (133) the equation for the transient current is found to be

$$I_{pp}(s) = qA\ G(S)\left[W_t + \frac{\sqrt{D_n\tau_n}}{\sqrt{1 + s\tau_n}} + \frac{\sqrt{D_p\tau_p}}{\sqrt{1 + s\tau_p}}\right] \qquad (142)$$

where $I_{pp}(s)$ is radiation-induced primary photocurrent Laplace transforms composed of depletion and diffusion components.

If G(s) is a pulse of magnitude g and duration t_o the inverse transform of $I_{pp}(s)$ becomes

$$i_{pp}(t) = qAg\left[W_t + \sqrt{D_n\tau_n}\ \text{erf}\ \sqrt{t/\tau_n} + \sqrt{D_p\tau_p}\ \text{erf}\ \sqrt{t/\tau_p}\right] \qquad 0 \le t \le t_o \qquad (143)$$

$$i_{pp}(t) = qAg\left[\sqrt{D_n\tau_n}\left(\text{erf}\ \sqrt{t/\tau_n} - \text{erf}\ \sqrt{\frac{t - t_o}{\tau_n}}\right) + \sqrt{D_p\tau_p}\left(\text{erf}\ \sqrt{t/\tau_p} - \text{erf}\ \sqrt{\frac{t - t_o}{\tau_p}}\right)\right] \qquad t > t_o \qquad (144)$$

The above results are similar to those obtained by previous investigators (references 2, 7, 8, 9, 10, 11, 13, and 17).

In planar and mesa transistors most of the primary photocurrent originates in the collector. By making this assumption for an n-p-n transistor the rest of the terms in the above equation may be neglected, which results in

$$i_{pp}(t) = qAg\left[\sqrt{D_p\tau_p}\left(u(t)\ \text{erf}\ \sqrt{t/\tau_p} - u(t - t_o)\ \text{erf}\ \sqrt{\frac{t - t_o}{\tau_p}}\right)\right] \qquad (145)$$

where

q = the electron charge = 1.6×10^{-19} coulombs
A = the base-to-collector junction area
g = electron-hole pair generation rate
W_t = width of the depletion region
D_p = the diffusion constant for holes in an n-type material
τ_p = the lifetime of holes in an n-type material

D_n = the diffusion constant for electrons in a p-type material

τ_n = the lifetime of electrons in a p-type material

$L_n = \sqrt{D_n \tau_n}$ = the diffusion for electrons in a p-type material

$L_p = \sqrt{D_p \tau_p}$ = the diffusion length for holes in an n-type material

$u(t)$ and $u(t - t_o)$ = unit step functions turned on at $t = 0$ and $t = t_o$, respectively.

Figure 35 shows a typical response one would expect for various approximations of W_t, L_p, and L_n.

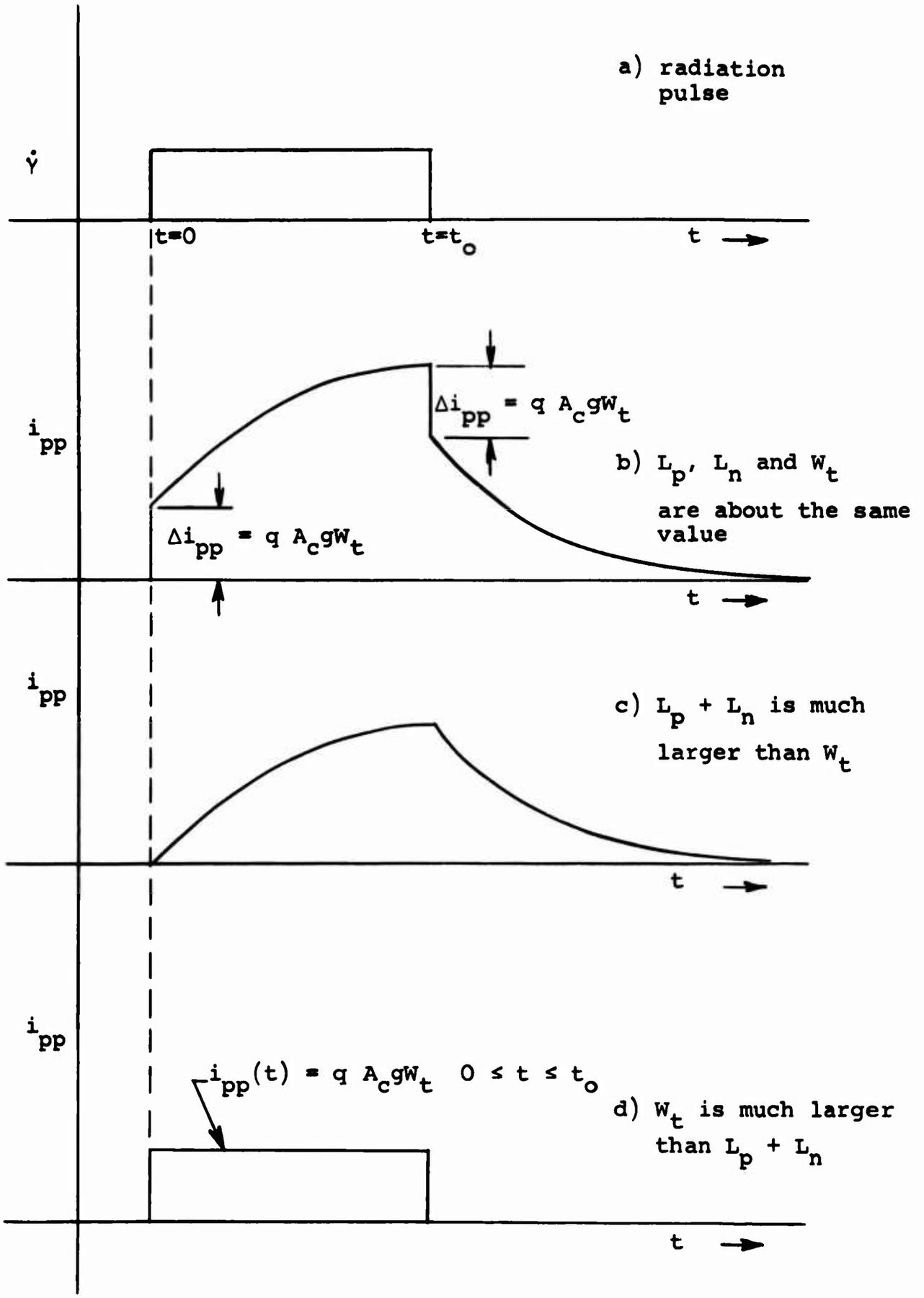

Figure 35. Typical Transient Radiation Response of a p-n Diode for Various Values of L_p, L_n, and W_t

APPENDIX II

DEPENDENCE OF DEPLETION REGION WIDTH UPON VOLTAGE

For a grown junction n-p-n transistor, the base conductivity is usually at least an order of magnitude larger than the collector. This means that the positively charged donor ion concentration in the collector N_d is smaller than the negatively charged acceptor ion concentration in the base N_a. The impurity concentration near the junction may then be approximated by a charge density which changes linearly from a predominantly p-doped region to a predominantly n-doped region as shown in figure 36a (references 6 and 12): that is,

$$N_d - N_a = ax \tag{146}$$

In figure 36, the origin has been arbitrarily chosen at the point of zero net impurity concentration. When the collector is biased negatively the mobile carriers near the junction are swept away, and the remaining immobile impurity ions result in a net charge density in the region of depletion of the mobile carriers. This net charge density ρ will give a change in electrostatic potential V as given by Poisson's equation

$$\nabla^2 V = \frac{-4\pi}{\epsilon} \rho \quad \text{(cgs units)} \tag{147}$$

where ϵ is the absolute dielectric constant of the material. In figure 36c, the net charge density has been linearly approximated, and it is given by the equation

$$\rho = +qax \qquad \frac{-W_t}{2} < x < \frac{+W_t}{2} \tag{148}$$

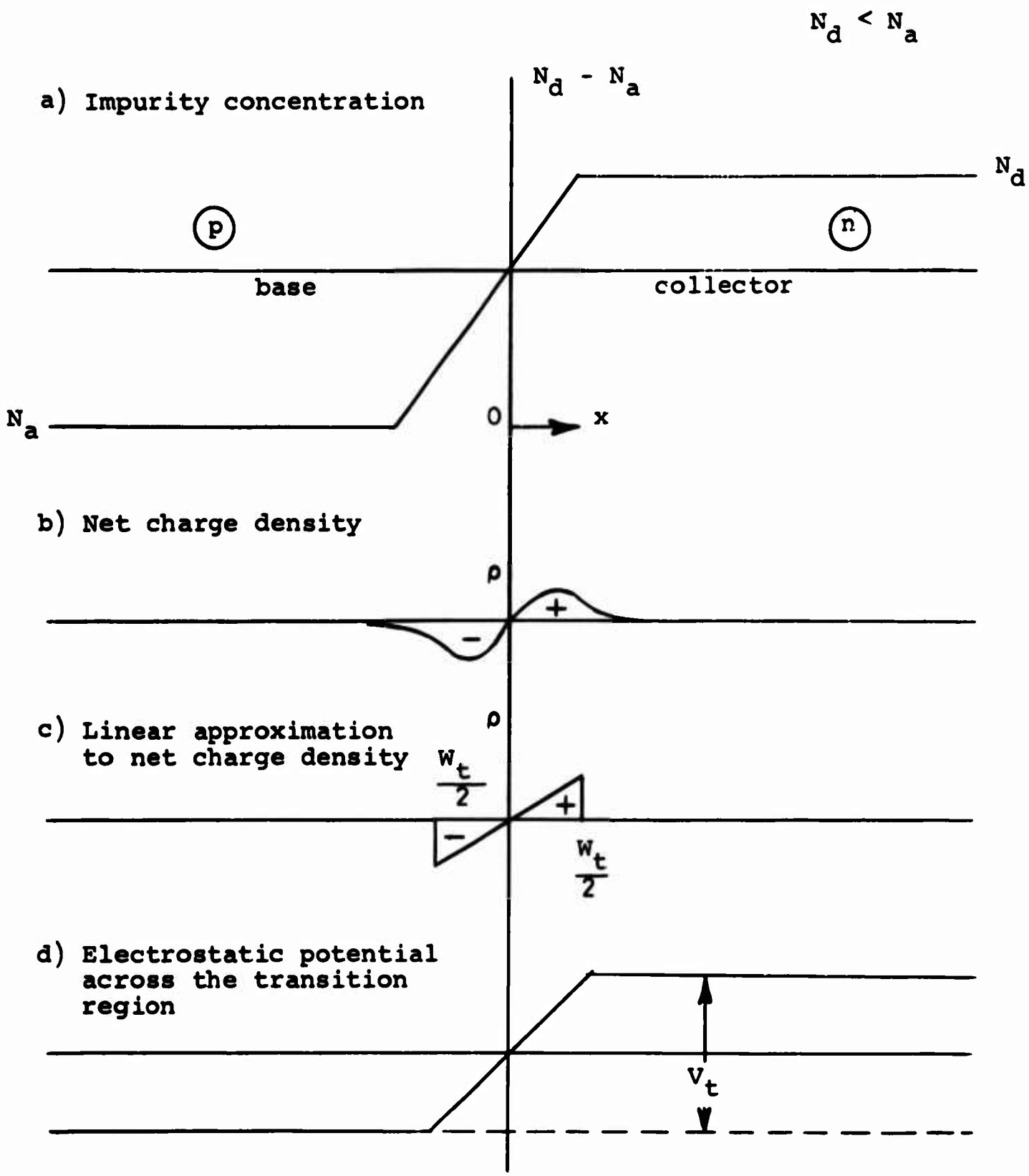

Figure 36. Characteristic Results of Charges Across the Transition Region at the Base Collector Junction of a Grown Junction Transistor

By using equation (148) and assuming one-dimensional analysis, equation (147) becomes

$$\frac{\partial^2 V}{\partial x^2} = \frac{-4\pi qa}{\epsilon} x \tag{149}$$

Integrating with respect to x gives

$$-E = \frac{\partial V}{\partial x} = \frac{-4\pi qa}{\epsilon} \frac{x^2}{2} + C_1 \tag{150}$$

where E is the electric field.

Using the boundary conditions that the electric field $(\partial V/\partial x)$ goes to zero at the edges of the depletion region $(\pm\frac{W}{2} t)$, the constant of integration (C_1) must be

$$C_1 = \frac{\pi qa}{2\epsilon} W_t^2 \tag{151}$$

and therefore

$$\frac{\partial V}{\partial x} = - \frac{2\pi qa}{\epsilon} (x^2 - \frac{W_t^2}{4}) \tag{152}$$

Integrating again with respect to x gives

$$V = \frac{-2\pi qa}{\epsilon} \left[\frac{x^3}{3} - \frac{W_t^2}{4} x\right] + C_2 \tag{153}$$

Using the boundary condition that the electrostatic potential is zero at the origin, the constant of integration (C_2) must be zero. This gives

$$V = \frac{-2\pi qa}{\epsilon} x \left[\frac{x^2}{3} - \frac{W_t^2}{4}\right] \tag{154}$$

But the total potential change V_t across the junction is given by

$$V_t = V\Big|_{x = \frac{W_t}{2}} - V\Big|_{x = \frac{-W_t}{2}} \tag{155}$$

which from equation (154) is found to be

$$V_t = \frac{\pi q a}{\epsilon 3} (W_t^3) \tag{156}$$

From the above equation it is seen that

$$W_t = \left(\frac{3\epsilon V_t}{\pi q a}\right)^{1/3} \tag{157}$$

The ionized charge in one side of the space charge volume is obtained by integrating equation (148) from x = 0 to $x = W_t/2$; this gives

$$Q = \int_0^{W_t/2} qa\, x\, dx = \frac{qa\, W_t^2}{8} \tag{158}$$

Using equation (157), equation (158) becomes

$$Q = \frac{qa}{8} \left(\frac{3\epsilon V_t}{\pi q a}\right)^{2/3} \tag{159}$$

The incremental capacitance per unit area ($\partial Q/\partial V_t$) is the value required for the small signal equivalent circuit, which from equation (159) is

$$C = \frac{\partial Q}{\partial V_t} = \frac{\epsilon}{4\pi} \left(\frac{\pi q a}{3\epsilon V_t}\right)^{1/3} \tag{160}$$

With the use of equation (157), the above equation may also be written as

$$C = \frac{3}{4\pi}\left(\frac{\pi q a}{3\epsilon V_t}\right)^{1/3} = \frac{\epsilon}{4\pi W_t} \tag{161}$$

The above capacitance is for a unit junction, and therefore the capacitance measured on a device must be divided by its junction area. In equation (160) it can be seen that capacitance varies proportionally $(1/V_t)^{1/3}$. Depending on the processes of transistor manufacturing, doping, etc., the capacitance can vary from $(1/V_t)^{1/6}$ to $(1/V_t)^{1/2}$. From equation (157) it can be seen that the depletion width W_t is proportional to $(V_t)^{1/3}$, and it also can vary from $(V_t)^{1/6}$ to $(V_t)^{1/2}$.

If L_p, L_n, and W_t are about the same value, one should be able to see the transient radiation effect of the depletion component as shown in figure 35. In equation (157) it is shown that the depletion width varies as $V^{1/3}$. Thus, as the reverse bias is increased the depletion width gets larger, which in turn increases the active volume of the device. This should increase the transient current due to the depletion component by a factor of $V^{1/3}$; that is,

$$i_p(t) = q A_c g W_t = I_o + KV^{1/3} \tag{162}$$

where I_o is the zero bias depletion component, K is a constant, and V is the magnitude of the applied voltage.

THIS PAGE INTENTIONALLY LEFT BLANK.

APPENDIX III

AFWL 600-KV FLASH X-RAY FACILITY

The AFWL flash X-ray system consists of a 600-KV Fexitron unit manufactured by Field Emission Corporation. The characteristics of the unit are summarized in table XI. A double-walled rf shield room houses the experimental measuring equipment. By this means the rf noise level is reduced by 120 db. The X-ray beam is fired through a special window in the shielded room. This window is shown in figure 37. The beam area and dose rates are shown in figure 38. The room layout is shown in figure 5, Section I. The energy spectrum of the system is shown in figure 39 for 400-KV X rays. A graph showing the conversion of gamma flux equivalent to 1 roentgen-hour as a function of gamma energy is shown in figure 40.

Table XI

Operating Characteristics of the 600-KV Fexitron Flash X-ray System

Output voltage (peak)	600 KV
Output current at peak output voltage	2000 amp
Pulse width (at half maximum amplitude)	0.2 μsec
Pulse rise time	50 nanosec
Dose rate maximum	$\approx 2 \times 10^7$ r/sec

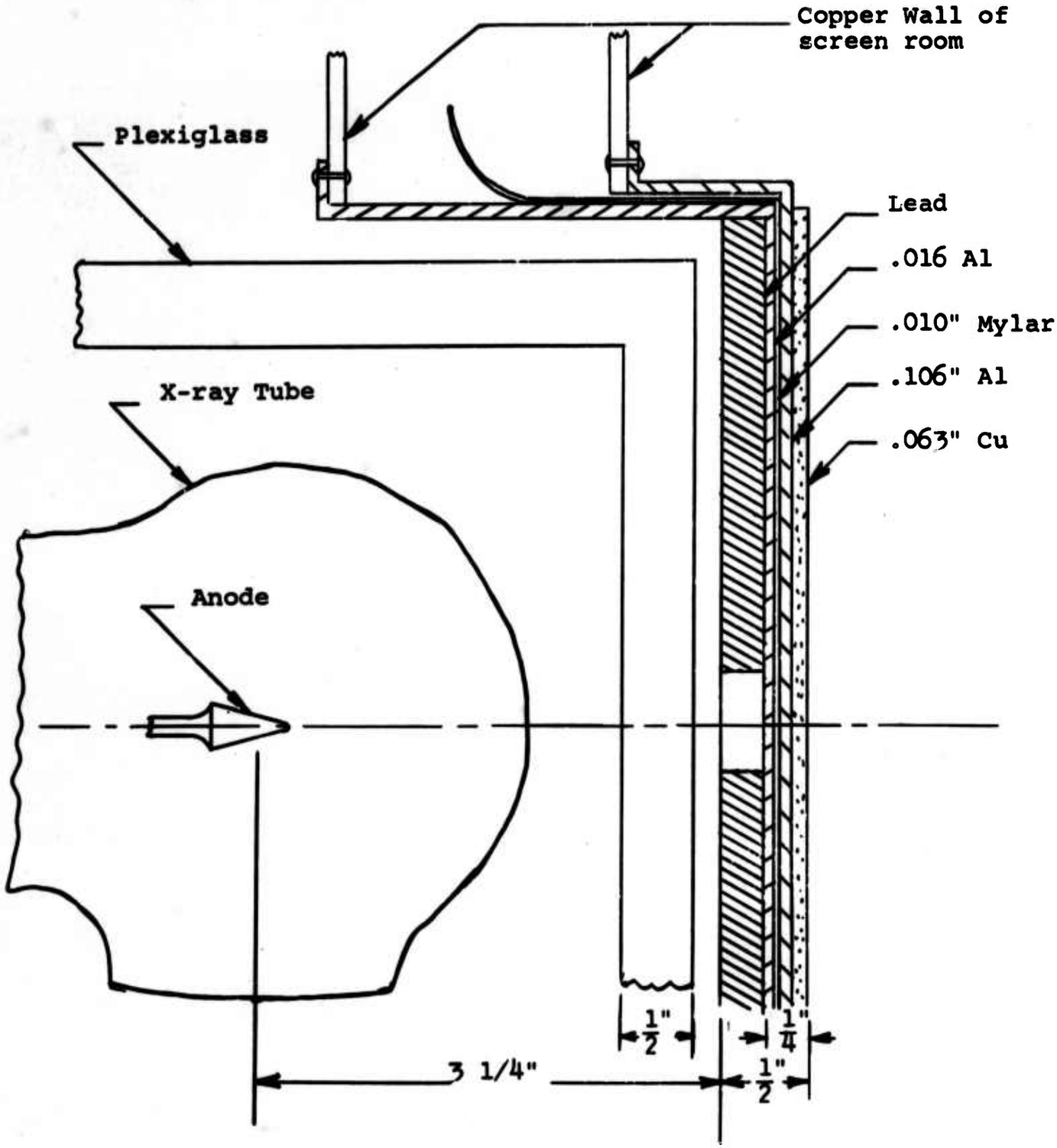

Figure 37. X-Ray Tube and Window in the Screen Room

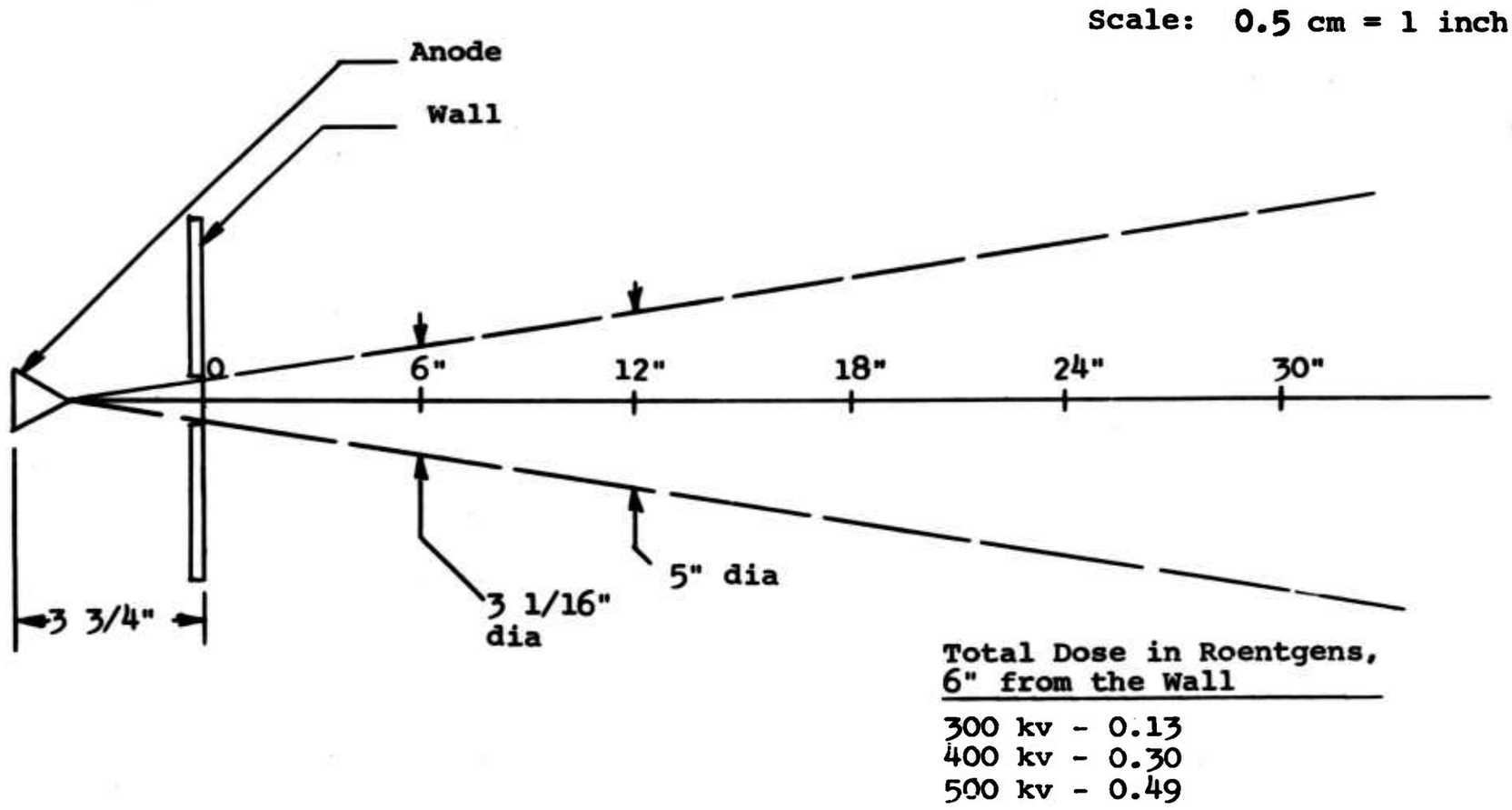

Figure 38. Collimated Radiation Beam of AFWL 600-KV Flash X-Ray System

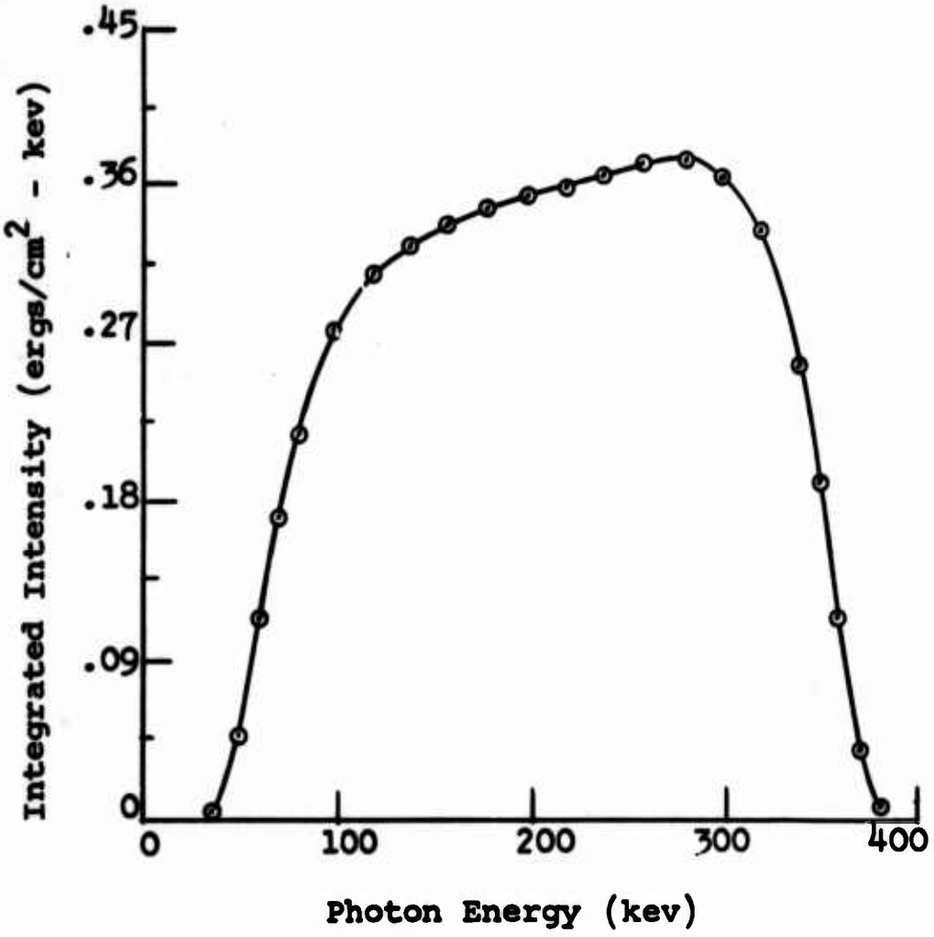

Figure 39. Energy Spectrum of a 400 kvp Flash X-Ray Pulse

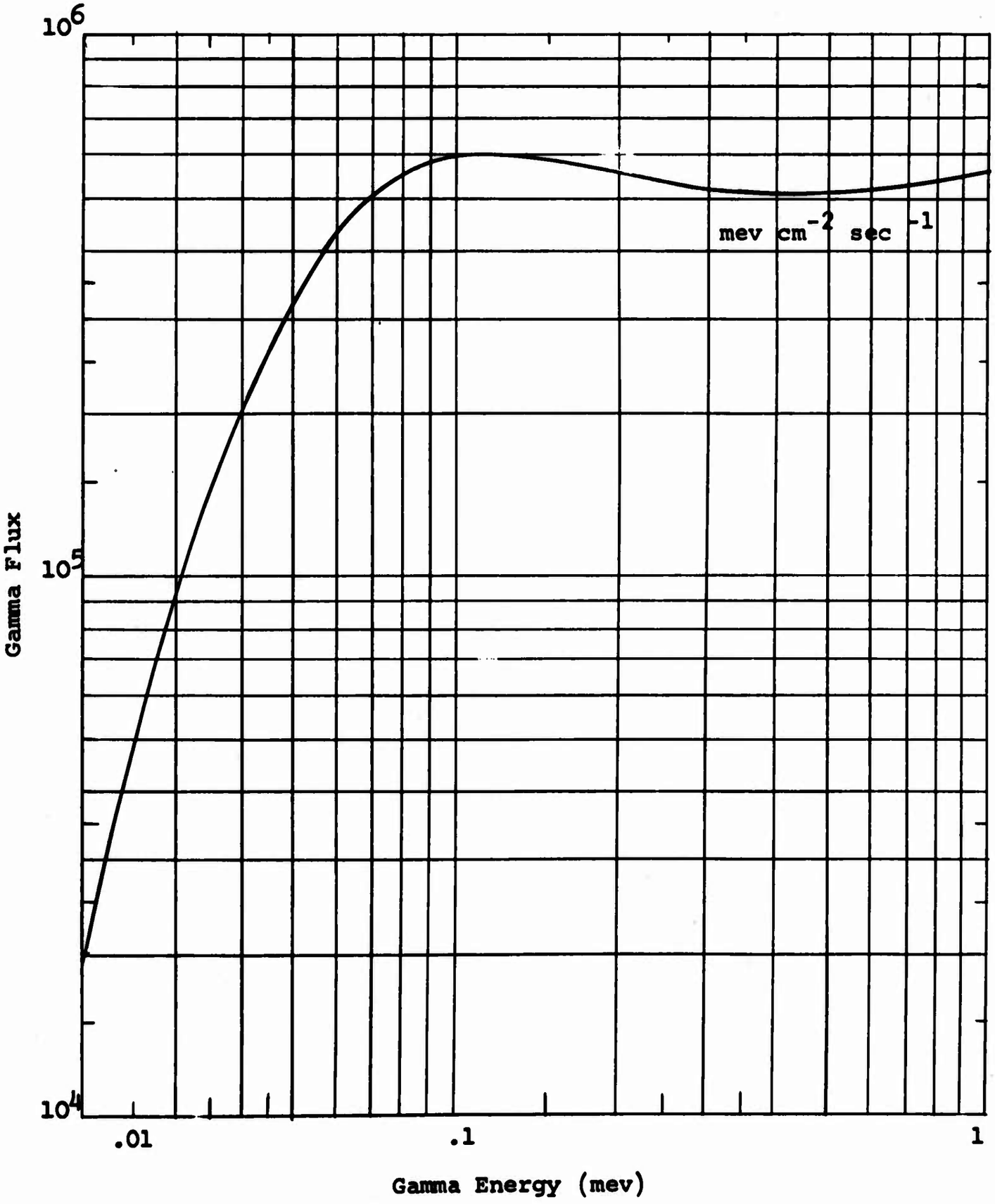

Figure 40. Gamma Flux Equivalent to 1 Roentgen-Hour as a Function of Gamma Energy

THIS PAGE INTENTIONALLY LEFT BLANK.

APPENDIX IV

THE EFFECT OF TRANSIENT RADIATION ON A GaAs LIGHT-EMITTING DIODE

The effect of transient ionizing radiation on a General Electric LED-10, infrared, light-emitting, gallium arsenide diode was experimentally investigated. The infrared light from the diode was monitored using a newly developed EG&G SD-100 silicon photodiode. The photodiode has a spectral response from 3500 to 11,300 angstroms with typical rise and fall times of 4×10^{-9} and 15×10^{-9} sec, respectively. The typical sensitivity of the photodiode operating at 9000 angstroms was 0.25 μa/μw. The infrared light-emitting diode had a spectrum which peaked at approximately 8,970 angstroms at 25° C. The diode output light power is typically 0.3 mw when operated at a continuous forward current of 100 ma.

The GE diode was positioned in a 1-inch diameter collimated X-ray beam. It was connected in a circuit as shown in figure 41. A 51-ohm resistor and a maximum coaxial cable length of twelve inches were used to minimize the viewing circuit time constant.

The photodiode was aligned with the output beam of the light-emitting diode at a distance of approximately 0.375 inch. The alignment was achieved by biasing the light-emitting diode with 100 ma DC. Then the photodiode was moved until a maximum voltage was 250 microvolts.

An attempt was made to shield the photodiode from all direct and reflected X rays. To do this, a hole, large enough to accept a TO-18 size transistor can, was drilled most of the way through a 2-inch thick lead brick. The remaining 0.1 inch was drilled to the same size as the lens in the photodiode can. The photodiode was then placed in the hole. The brick was then placed behind another 2-inch thick lead block. The end result was that the photodiode was shielded from direct X rays by 5 inches of lead, and from reflected X rays by 2 inches of lead. See figure 42 for the physical layout.

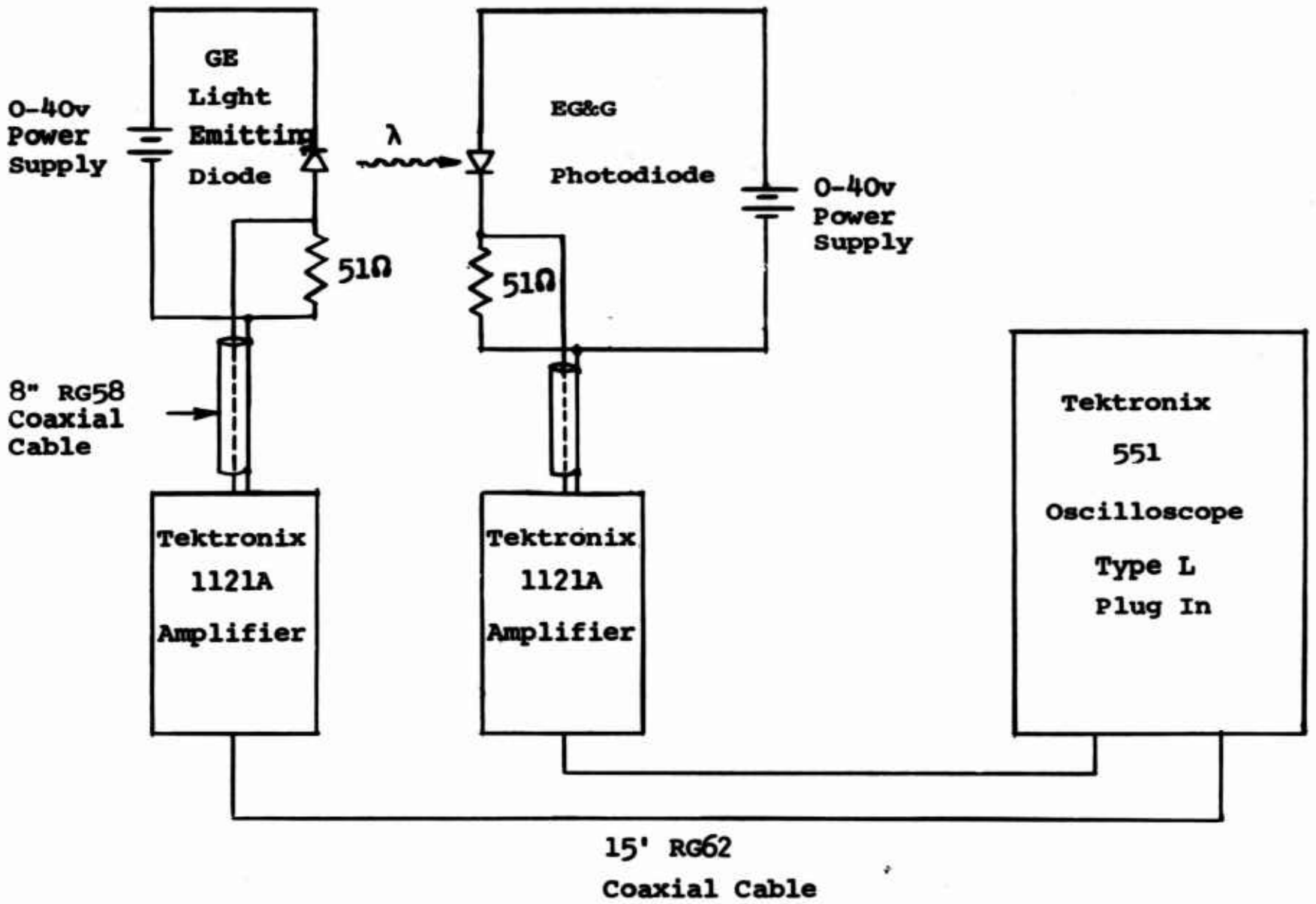

Figure 41. Schematic Diagram of Light Emitting Diode Test Circuit

Figure 41. Schematic Diagram of Light Emitting Diode Test Circuit

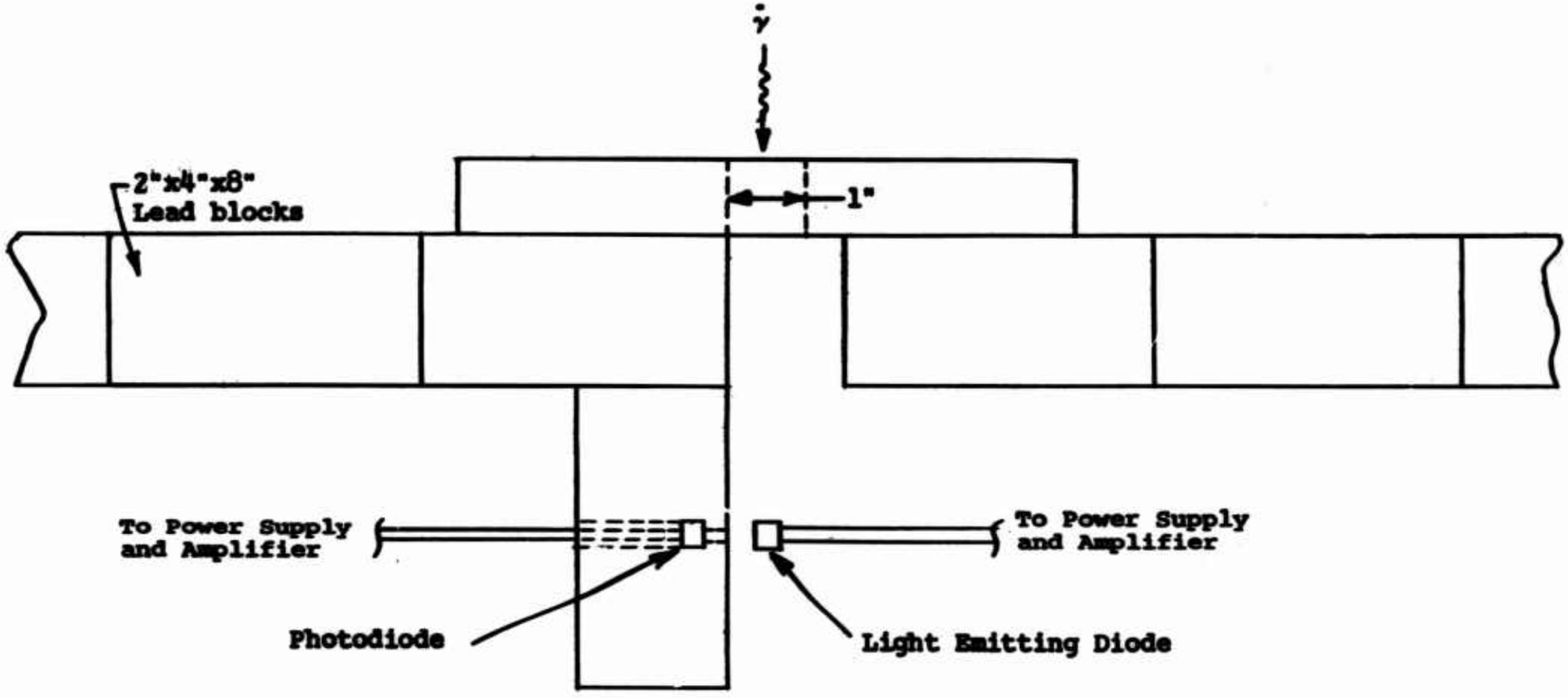

Figure 42. Shielding Layout for Light Emitting Diode Tests

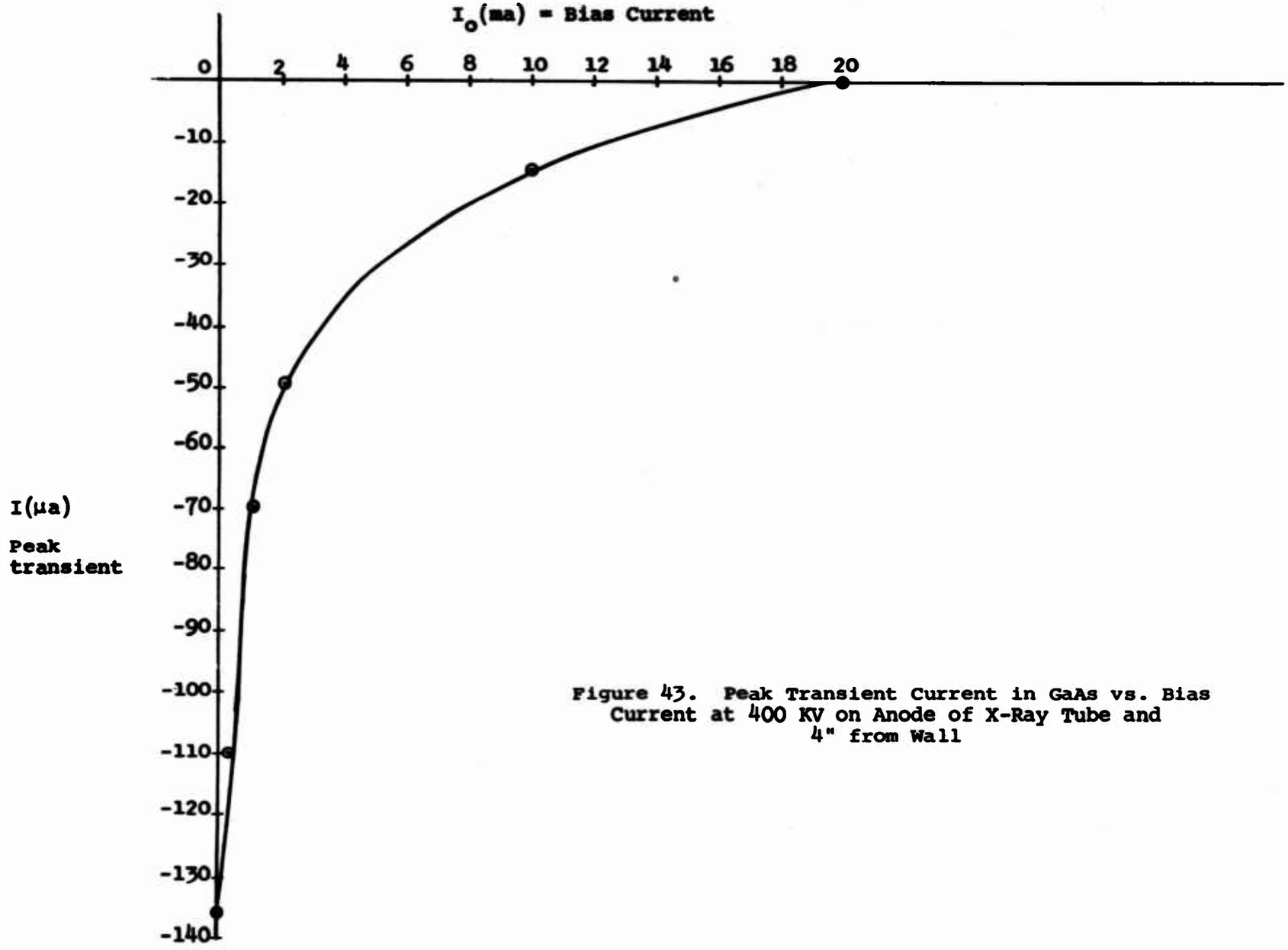

Figure 43. Peak Transient Current in GaAs vs. Bias Current at 400 KV on Anode of X-Ray Tube and 4" from Wall

A Polaroid camera attached to a Tektronix Type 551 oscilloscope was used to monitor the transient current in both diodes. In order to test the shielding, a test was performed with the GaAs diode removed. The resultant picture showed a low noise level and no apparent radiation response. The light-emitting diode was then inserted in the X-ray beam and aligned.

Tests were run to determine the effect of varying bias voltage on the response to transient radiation. As the forward bias was decreased, the transient current in the light-emitting diode increased as shown in figure 43. This increased transient current with decreasing forward bias also occurs in silicon diodes. Therefore, the GaAs diode seems to respond electrically to ionizing radiation in a manner similar to that of other diodes.

The increasing transient current should indicate a change in light emitted by the diode; however, a corresponding increase was not detected in the transient current of the photodiode. The light-emitting diode was then moved slightly out of alignment with the X-ray beam. The transient response of the photodiode remained the same as it was during the previous tests. The GaAs diode was replaced by a transistor in a TO-18 can and the results were still the same as before. Only when the transistor was removed completely was the transient current in the photodiode eliminated. These tests indicated that the transient current in the photodiode was due entirely to reflections from the packaging material that surrounds the light-emitting diode. Tests were made to determine the effect of varying radiation intensity on the transient current in the GaAs diode. Figure 44 shows the results which were as expected. The peak transient current increased with an increase of radiation intensity.

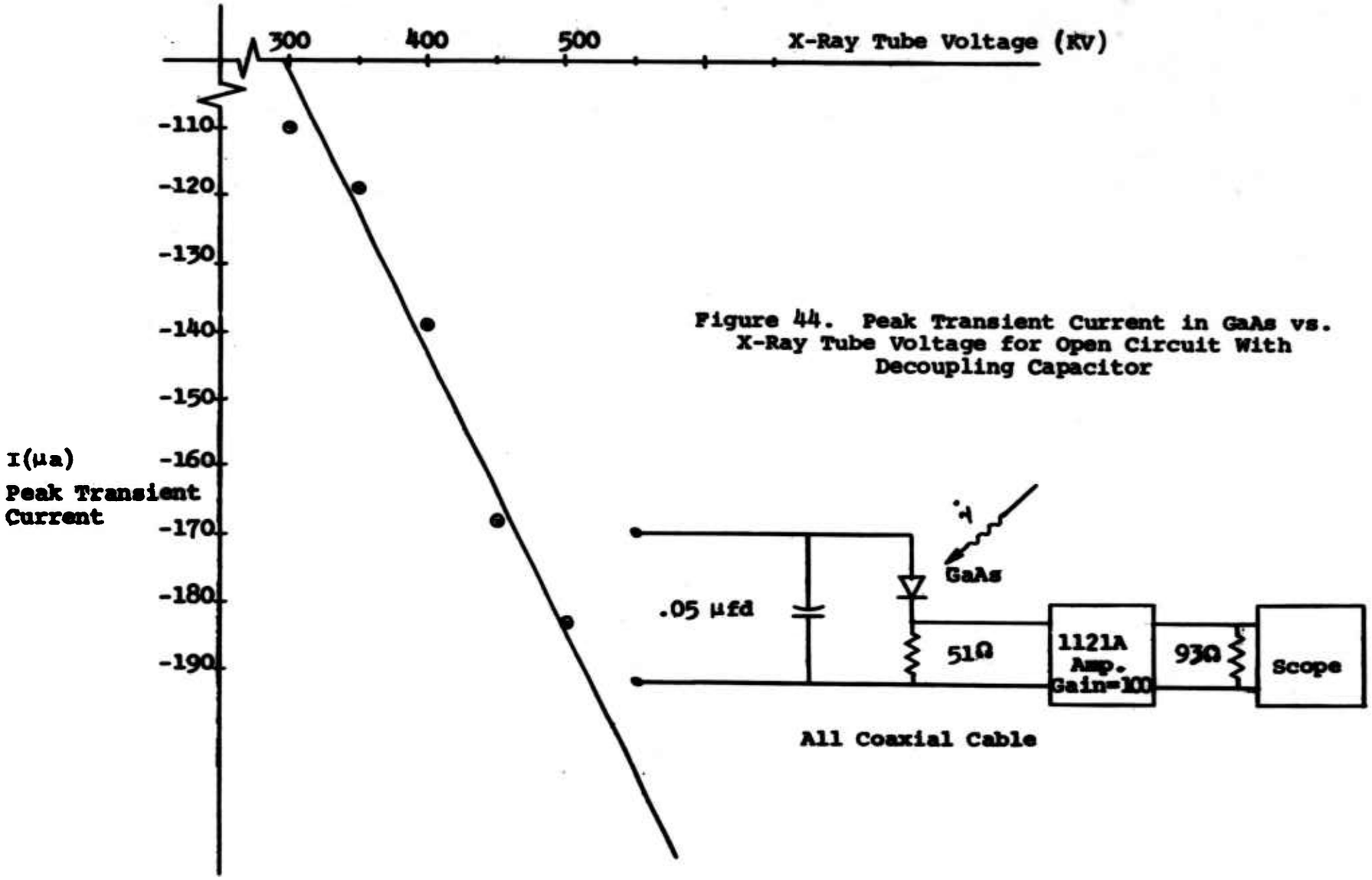

Figure 44. Peak Transient Current in GaAs vs. X-Ray Tube Voltage for Open Circuit With Decoupling Capacitor

As a result of the above investigation the following conclusions were reached:

(1) The GE diode is relatively insensitive to dose rates of less than 10^6 r/sec.

(2) A more sensitive photodiode or higher dose rate is needed to observe any possible change in light power output.

(3) Operating the GE diode at higher forward current levels will make the diode more radiation hardened to ionizing radiation.

These results compared favorably to those obtained by other investigators (references 18 and 19).

THIS PAGE INTENTIONALLY LEFT BLANK.

REFERENCES

1. V. A. J. van Lint, Mechanisms of Transient Radiation Effects, GA-4320, General Atomics, San Diego, (1963).

2. Battelle Memorial Institute TREES Handbook, ed. D. C. Jones. Prepared for DASA, (February 28, 1964).

3. William Shockley, Electrons and Holes in Semiconductors, D. Van Nostrand Company, Inc.: New York, (1963).

4. William J. Byatt and Harold T. Cates, Transient Gamma Radiation Effects on Resistive and Insulating Materials, Report EE-112, The University of New Mexico Engineering Experiment Station, (1964).

5. Harold T. Cates, Transient Radiation Effects on Resistors, Report EE-118, The University of New Mexico Engineering Experiment Station, (November 1964).

6. R. D. Middlebrook, An Introduction to Junction Transistor Theory, John Wiley & Sons, Inc.: New York, (1961).

7. S. C. Rogers and J. L. Wirth, The Transient Response of Transistors and Diodes to Ionizing Radiation, SC-R-64-194, Sandia Corporation, (July 1964).

8. W. L. Brown, Nuclear Electronic Effects Program Fifth Tri-annual Report, Bell Telephone Laboratories, Inc., (November 1960).

9. V. A. J. van Lint, et al. The Effects of Pulsed Gamma Radiation on Dynamic Electronic Components, RTD TDR-63-3110, General Atomics, San Diego, (1964).

10. R. S. Caldwell, D. S. Gage, and G. H. Hanson, The Transient Behavior of Transistors Due to Ionizing Radiation Pulses, D2-90171, The Boeing Company, (1962).

11. G. L. Keister, et al., Manual for Circuit Analysis and Design, TRE WL-TDR-64-60, Volume I, The Boeing Company, (July 1964).

12. Integrated Circuits, eds. R. M. Warner, Jr., and J. N. Fordemwalt, McGraw-Hill Book Company: New York (1965).

13. Radiation Effects Staff, Pulsed Radiation Effects on Aerospace Digital Computers, RTD-TDR-63-3051, International Business Machines Corporation, (October 1963).

14. Gladys White Grodstein, X-Ray Attenuation Coefficients from 10 Kev to 100 Mev, N.B.S. Circular 583, (April 1957).

15. H. Goldstein, Fundamental Aspects of Reactor Shielding, Tables V-X, Addison-Wesley, (1959), 236-241.

16. G. L. Keister, et al, Analytic Methods for Predicting Transient Nuclear Radiation Effects on Electronic Circuits and Devices, RTD TDR-63-3007, The Boeing Company, (July 1963).

17. R. J. Belardi, et al., Transistor Design Effects on Radiation Resistance, Final Report for Contract No. DA 36-039 AMC-02352(E), Hughes Aircraft Company, (June 1964).

18. J. E. Bell, et al., Radiation Effects on Guided Missile Electronic Equipment, Report No. FR 63-17-173, Hughes Aircraft Company, (July 1963).

19. J. E. Bell, et al., Radiation Effects on Guided Missile Electronic Equipment, Report No. FR-64-17-41, Hughes Aircraft Company, (January 1964).

20. A. H. Wilson, The Theory of Metals, 2nd ed., Cambridge Univ. Press: London, (1953).

21. F. Seitz, The Modern Theory of Solids, McGraw-Hill: New York, (1940).

22. R. A. Smith, Wave Mechanics of Crystalline Solids, John Wiley & Sons, Inc.: New York, (1961).

23. F. J. Blatt, "Theory of Mobility of Electrons in Solids," Solid State Physics, Vol. 4, (1957), 199-366.

24. A. C. Beer, "Galvanomagnetic Effects in Semiconductors," Supplement No. 4 to Solid State Physics, (1963), 278-289.

25. J. M. Ziman, Electrons and Phonons, Oxford Press: London, (1960), 264-267.

26. A. M. Weinberg and E. P. Wigner, The Physical Theory of Neutron Chain Reactors, Univ. of Chicago Press: Chicago, (1958), 190-197.

27. G. H. Wannier, Elements of Solid State Theory, Cambridge Univ. Press: London, (1959), 206-211.

28. V. A. J. van Lint, J. Alexander, and D. K. Nichols, Short-Picked Gamma Radiation Effects on Dynamic Electronic Components, Technical Documentary Report Nv. AFWL TR-65-44, Air Force Weapons Laboratory, Kirtland Air Force Base, New Mexico.

29. J. L. Wirth and S. C. Rogers, The Transient Response of Transistors and Diodes to Ionizing Radiation, Special Technical Conference on Nuclear Radiation Effects, Seattle, Washington, (July 1964). Available as a Sandia Corporation Reprint #SC-R-64-194.

30. W. W. Gartner, Transistors Principles, Design and Application, D. Van Nostrand Co., Inc.: New York, (1960).

31. R. D. Middlebrook, An Introduction to Junction Transistor Theory, John Wiley & Sons, Inc.: New York, (1961).

32. D. J. Hamilton, F. A. Lindholm, and J. A. Narud, "Comparison of Large Signal Models for Junction Transistors," Proceedings of the IEEE, Vol. 52, No. 4, (March 1964), 239-248.

33. J. P. McKelvey and R. L. Longini, "Volume and Surface Recombination Rates for Injected Carriers in Germanium," Journal of Applied Physics, Vol. 25, No. 4, (May 1954), 634-641.

34. J. P. McKelvey and R. L. Longini, "Recombination of Injected Carriers at Dislocation Edges in Semiconductor," Physical Review, Vol. 99, No. 4, (August 1955), 1227-1232.

35. J. P. McKelvey, "Experimental Determination of Injected Recombination Rates at Dislocations in Semiconductors," Physical Review, Vol. 106, No. 5, (June 1957), 910-917.

36. J. P. McKelvey, R. L. Longini, and Z. P. Brody, "Alternative Approach to the Solution of Added Carrier Transport Problems in Semiconductors," Physical Review, Vol. 123, No. 1, (July 1961), 51-57.

37. J. Coltman, E. G. Ebbigshausen, and W. Alter, "Physical Properties of Calcium Lungstate X-Ray Screens," Journal of Applied Physics, Vol. 18, (1947), 536-537.

38. J. P. McKelvey, "Analysis of Semiconductor p-n Junctions and Junction Devices by a Flux Method," Journal of Applied Physics, Vol. 33, No. 3, (March 1962), 985-991.

39. J. P. McKelvey and J. C. Balogh, "Flux Methods for the Analysis of Transport Problems in Semiconductors in the Presence of Electric Fields," Physical Review, Vol. 137, No. 5A, (March 1965), A1555-A1561.

40. R. Bellman, R. Kalaba, and G. M. Wing, "Invariant Imbedding and Mathematical Physics, 1. Particle Processes," Journal of Mathematical Physics, Vol. 1, No. 4, (1960), 280-308.

41. G. M. Wing, An Introduction to Transport Theory, John Wiley & Sons, Inc., New York, (1962).

Unclassified
Security Classification

DOCUMENT CONTROL DATA - R&D

(Security classification of title, body of abstract and indexing annotation must be entered when the overall report is classified)

1. ORIGINATING ACTIVITY (Corporate author) University of New Mexico Bureau of Engineering Research Albuquerque, New Mexico	2a. REPORT SECURITY CLASSIFICATION Unclassified 2b. GROUP

3. REPORT TITLE
LABORATORY TESTING AND THEORETICAL STUDIES IN TRANSIENT RADIATION EFFECTS ON MICROELECTRONICS

4. DESCRIPTIVE NOTES (Type of report and inclusive dates)
1 September 1964 to 31 July 1965

5. AUTHOR(S) (Last name, first name, initial)
Grannemann, W. W.; et al.

6. REPORT DATE May 1966	7a. TOTAL NO. OF PAGES 160	7b. NO. OF REFS 41
8a. CONTRACT OR GRANT NO. AF29(601)-6637 b. PROJECT NO 5710 c. Subtask No. 16.015 d.	9a. ORIGINATOR'S REPORT NUMBER(S) AFWL-TR-65-175 9b. OTHER REPORT NO(S) (Any other numbers that may be assigned this report)	

10. AVAILABILITY/LIMITATION NOTICES
Distribution of this document is unlimited.

11. SUPPLEMENTARY NOTES	12. SPONSORING MILITARY ACTIVITY Air Force Weapons Laboratory (WLRE) Kirtland Air Force Base, New Mexico 87117

13. ABSTRACT A series of experimental studies has been conducted on transistor elements suitable for microcircuits. A relationship of transient radiation effects to active volume and other parameters has been made. The experimental and theoretical method developed offers a way of obtaining minority carrier lifetimes, depletion layer width, junction area, diffusion length, and active volume when the absorbed dose and the ionization efficiency are known in the transistor element of a microcircuit. Conversely, given the above parameters it is possible to determine the primary photocurrent of the microcircuit junction under a variety of radiation conditions. Developments have been made on the Boltzmann equation. It has been shown that the fundamental Boltzmann equation describing charge transport in semiconductors can be used to modify the usual continuity equation to obtain a more accurate circuit model for transistor elements in microcircuits. This should result in changes in the Ebers-Moll model, charge control model, and the Linvill model to take into account the thin layers used in microcircuit diffusion processes. The oxide-isolated microcircuits have been tested and compared with the usual back-biased isolation junction diode type. Circuits used were the same except for the type of isolation. Several mock-up circuits were used, and it was determined that the mock-up technique was reasonably accurate for radiation effects studies. Proper elements must be included for the parasitic elements that are inherent in microcircuits.

DD FORM 1 JAN 64 1473

Unclassified
Security Classification

14. KEY WORDS	LINK A		LINK B		LINK C	
	ROLE	WT	ROLE	WT	ROLE	WT
TREE (Transient Radiation Effects on Electronics)						
TRE on microelectronics						
TRE on transistors						
Charge transport in thin-layered semiconductors						

INSTRUCTIONS

1. **ORIGINATING ACTIVITY:** Enter the name and address of the contractor, subcontractor, grantee, Department of Defense activity or other organization *(corporate author)* issuing the report.

2a. **REPORT SECURITY CLASSIFICATION:** Enter the overall security classification of the report. Indicate whether "Restricted Data" is included. Marking is to be in accordance with appropriate security regulations.

2b. **GROUP:** Automatic downgrading is specified in DoD Directive 5200.10 and Armed Forces Industrial Manual. Enter the group number. Also, when applicable, show that optional markings have been used for Group 3 and Group 4 as authorized.

3. **REPORT TITLE:** Enter the complete report title in all capital letters. Titles in all cases should be unclassified. If a meaningful title cannot be selected without classification, show title classification in all capitals in parenthesis immediately following the title.

4. **DESCRIPTIVE NOTES:** If appropriate, enter the type of report, e.g., interim, progress, summary, annual, or final. Give the inclusive dates when a specific reporting period is covered.

5. **AUTHOR(S):** Enter the name(s) of author(s) as shown on or in the report. Enter last name, first name, middle initial. If military, show rank and branch of service. The name of the principal author is an absolute minimum requirement.

6. **REPORT DATE:** Enter the date of the report as day, month, year; or month, year. If more than one date appears on the report, use date of publication.

7a. **TOTAL NUMBER OF PAGES:** The total page count should follow normal pagination procedures, i.e., enter the number of pages containing information.

7b. **NUMBER OF REFERENCES:** Enter the total number of references cited in the report.

8a. **CONTRACT OR GRANT NUMBER:** If appropriate, enter the applicable number of the contract or grant under which the report was written.

8b, 8c, & 8d. **PROJECT NUMBER:** Enter the appropriate military department identification, such as project number, subproject number, system numbers, task number, etc.

9a. **ORIGINATOR'S REPORT NUMBER(S):** Enter the official report number by which the document will be identified and controlled by the originating activity. This number must be unique to this report.

9b. **OTHER REPORT NUMBER(S):** If the report has been assigned any other report numbers *(either by the originator or by the sponsor)*, also enter this number(s).

10. **AVAILABILITY/LIMITATION NOTICES:** Enter any limitations on further dissemination of the report, other than those imposed by security classification, using standard statements such as:

(1) "Qualified requesters may obtain copies of this report from DDC."

(2) "Foreign announcement and dissemination of this report by DDC is not authorized."

(3) "U. S. Government agencies may obtain copies of this report directly from DDC. Other qualified DDC users shall request through _____."

(4) "U. S. military agencies may obtain copies of this report directly from DDC. Other qualified users shall request through _____."

(5) "All distribution of this report is controlled. Qualified DDC users shall request through _____."

If the report has been furnished to the Office of Technical Services, Department of Commerce, for sale to the public, indicate this fact and enter the price, if known.

11. **SUPPLEMENTARY NOTES:** Use for additional explanatory notes.

12. **SPONSORING MILITARY ACTIVITY:** Enter the name of the departmental project office or laboratory sponsoring *(paying for)* the research and development. Include address.

13. **ABSTRACT:** Enter an abstract giving a brief and factual summary of the document indicative of the report, even though it may also appear elsewhere in the body of the technical report. If additional space is required, a continuation sheet shall be attached.

It is highly desirable that the abstract of classified reports be unclassified. Each paragraph of the abstract shall end with an indication of the military security classification of the information in the paragraph, represented as *(TS), (S), (C), or (U)*.

There is no limitation on the length of the abstract. However, the suggested length is from 150 to 225 words.

14. **KEY WORDS:** Key words are technically meaningful terms or short phrases that characterize a report and may be used as index entries for cataloging the report. Key words must be selected so that no security classification is required. Identifiers, such as equipment model designation, trade name, military project code name, geographic location, may be used as key words but will be followed by an indication of technical context. The assignment of links, rules, and weights is optional.